Dissertation

Theoretical Studies on Redox Potential of Metalloproteins

Graduate School of
Natural Science & Technology
Kanazawa University

Division of Mathematical and Physical Science

Student ID No. 1524012010
Name Isman Kurniawan
Chief Advisor Prof. Hidemi Nagao
28 June 2018

博士論文

金属タンパク質の酸化還元電位に関する理論的研究

金沢大学大学院自然科学研究科
数物科学専攻
計算バイオ科学研究科

学籍番号　1524012010
氏名　Isman Kurniawan
主任指導教員氏名　長尾秀実

"..., Allah will raise those who have believed among you and those who were given knowledge, by degrees. And Allah is Acquainted with what you do."

(Al-Mujadila: 11)

Acknowledgements

First of all, I would like to express my deepest gratitude to the God of universe, Allah subhaanahu wata'aala, for giving me a strength, patience and ability to finish my Ph.D. study.

I would like to express my sincere gratitude to my supervisor, Prof. Hidemi Nagao, for the incredible support during my Ph.D study, and also for his patience, motivation, and enthusiasm. His supervision helped me in all the time of my research and writing of this thesis. I would also like to express my sincere gratitude to my co-supervisor, Prof. Yasuteru Shigeta, for introducing me another side of my research topics, and also for the fruitful discussion during manuscript preparation. I am also grateful to Prof. Kazutomo Kawaguchi and Prof. Kimikazu Sugimori, for an invaluable discussion and suggestion during my Ph.D. study, and also his supports to strenghten my knowledge in molecular dynamics and quantum mechanics.

I would also like to thank Prof. Mitsuo Shoji, Prof. Takeshi Sakurai and Prof. Toru Matsui for the great discussion and suggestion during manuscript preparation. My sincere thanks also goes to Prof. Mineo Saito, Prof. Tatsuki Oda and Prof. Hiroshi Iwasaki for the motivation and support during my Ph.D. study.

I thank my fellow labmates in Computational Biophysics Laboratory: Nakagawa, Kodama, Arwansyah, Habibi, Mutiara, Wada, Takagi, Matsuura, Kataoka and Maeda for the nice talk and discussion we had in the last three years. Also I thank my friends in Kanazawa University: Nurul Ikhsan, Yudha Arman, Teguh Budi, Reza Rendian and all Indonesian student in this university.

I would also like to express my appreciation to Ministry of Education, Culture, Sports, Science and Technology (MEXT) of Japan via Global Human Resource (GHR) program of Kanazawa University for the financial support during my study and life in Kanazawa.

Last but not the least, I would like to thank my parents for supporting me spiritually throughout my life. Most importantly, I wish to thank my loving and supportive wife, Siti Robiah, and my wonderful son, Muhammad Ilyas, who provide unending inspiration.

Contents

List of Figures

List of Tables

Chapter 1

General Introduction

1.1 Introduction to The Thesis

This doctoral thesis is a summary of my research interest in theoretical studies on electronic properties, in particular redox potential, of metalloprotein, i.e. copper protein and iron-sulfur protein. As for the copper protein, I investigated the electronic structure and properties of type I copper center in copper protein and the contribution of axial ligand to redox potential of type I copper center. As for the iron-sulfur protein, I investigated the redox properties and pK_a of iron-sulfur cluster in the protein with respect to possible spin structure of coupled irons. The outline of my research studies at Graduate School of Natural Science and Technology from October 2015 to June 2018 can be presented in the following steps:

The Electronical Structure and Properties of Type 1 Copper Center

We have investigated the electronic structure and properties of type 1 copper center in several copper proteins, i.e. Plastocyanin, Azurin, Stellacyanin, and Multicopper Oxidases (MCOs). Several properties, such as molecular orbital, atomic partial charge, atomic partial spin, bond constant, etc. were calculated by using two typical density functional theory (DFT) functionals, i.e. B3LYP and M06. We discussed the dependence of those properties to DFT functional, especially in relation to copper-axial ligand interaction.

Isman Kurniawan, Takahiro Matsui, Satoshi Nakagawa, Kazutomo, Kawaguchi, Hidemi Nagao. *Theoretical studies on association/dissociation process of plastocyanin and cytochrome f in photosynthesis.* Journal of Physics: Conference Series, 2018 (Accepted)

Isman Kurniawan, Kazutomo Kawaguchi, Kimikazu Sugimori, Takeshi Sakurai, Hidemi Nagao. *Theoretical Study of the Electronic Structure of Type I Copper Center in Copper Proteins.* Science Report of Kanazawa University, 2018 (in preparation)

Quantum Chemical Study of the Axial Ligand Effect on the Electronic Properties of Type I Copper Protein

We have investigated the effect of the axial ligand on the electronic properties of type I copper protein. Several DFT functional were utilized, including pure generalized gradient approximation, hybrid DFT, and long-range corrected DFT. We discussed the contribution of the axial ligand to several properties, i.e. bond constant, redox potential and maximum absorption wavelength, of type I copper protein, We also discussed the contribution of long-range correction scheme and hybrid scheme of DFT to improve the calculation accuracy.

Isman Kurniawan, Kazutomo Kawaguchi, Kimikazu Sugimori, Takeshi Sakurai, and Hidemi Nagao. *Quantum Chemical Study of the Axial Ligand Effect on the Electronic Properties of Type I Copper Protein.* Chemistry Letters, 2018 (Accepted)

Theoretical Study on the Contribution of Spin Structure to Redox Potential of [2Fe-2S] Core Cluster from Iron-Sulfur Proteins

We have investigated the contribution of possible spin structure of coupled iron atoms to redox potential and pK_a of iron-sulfur protein. The properties were calculated by using two typical DFT functionals, i.e. B3LYP and M06. To handle the spin state of couple irons, we utilized several spin approximations, i.e. high spin, low spin, approximated spin projected, and J spin coupling. We discussed the contribution of DFT functional, basis set, and spin approximation to the accuracy of calculation.

Isman Kurniawan, Kazutomo Kawaguchi, Mitsuo Shoji, Toru Matsui, Yasuteru Shigeta, and Hidemi Nagao. *A Theoretical Study on Redox Potential and pKa of [2Fe-2S] Cluster Model from Iron-Sulfur Proteins.* Bulletin of the Chemical Society of Japan, 2018 (Accepted)

1.2 Introduction to Copper Protein

Copper protein is a metalloprotein containing one or more copper ions in their active sites, and can be isolated from animal, plant, fungal, and bacterial sources.[4] This proteins involve in reduction-oxidation reactions as oxidoreductase proteins or electron carrier proteins, and also take a part in oxygen transport processes. Copper protein can be classified into three groups according to their properties under spectroscopic and magnetic measurement, i.e. type 1 copper (T1Cu), type 2 copper (T2Cu), and type 3 copper (T3Cu). T1Cu present a strong absorption at around 600 nm and narrow hyperfine splitting in the electronic paramagnetic resonance (EPR) spectrum. T2Cu does not produce intense absorption at 600-700 nm and also present hyperfine splitting of EPR spectrum in normal magnitude. Different with T1Cu and T2Cu, T3Cu can not be detected by EPR spectrum due to strong antiferromagnetic interaction.

Copper protein containing a T1Cu only is called cupredoxin or blue copper protein. There are several blue copper proteins such as Azurin, Plastocyanin, Stellacyanin, etc. This proteins have unusually high reduction potential and take a part in various electron transfer processes.[5–7] For example, Azurin takes a role in multi-step denitrification processes in some bacterias by transferring an electron to heme-containing nitrite reductase and cytochrome c551.[8] Meanwhile, during photosynthesis processes of plant and algae, Plastocyanin has a role as electron carrier between cytochrome f and P700+. Plastocyanin is also involved in electron transfer process from cytochrome f (photosystem II) to chlorophyll (photosystem I). In T1Cu of blue copper protein, the copper ion (Cu) is coordinated to three ligands in trigonal plane, i.e. two histidines (His), one cysteine (Cys), and an axial ligand at a longer distance. Methionine (Met) residue is usually bound to the copper as axial ligand in many blue copper protein, except for Stellacyanin and related proteins. In those proteins, the copper ion coordinated to glutamine (Gln) as axial ligand, instead of methionine. As for Azurin, the axial ligand found in T1CC is not only methionine, but also glycine (Gly) residue as additional axial ligand to generate a five-coordinate site. One of His, Cys and Met ligands come from C-terminal loop of the protein, while the other His ligand located in β-sheet backbone.[7, 9–11] The secondary structure of blue copper protein is presented in Figure 1.1.

The existence of sulfur atoms of cysteine ligand in T1CC have been revealed by X-ray photoelectron experiments[12], while the presence of two histidine ligands have been unveiled by recent nuclear magnetic resonance (NMR) study.[13] In T1Cu of blue copper protein, a highly covalent π bond was formed between Cu and Cys where p orbital from sulfur atom overlap with d orbital of Cu.[14] Regarding the study of copper(II) substitution by cobalt(II) in several blue proteins, the high intense 600 nm absorption of T1Cu is originated from ligand-to-metal charge-transfer (LMCT) transition between

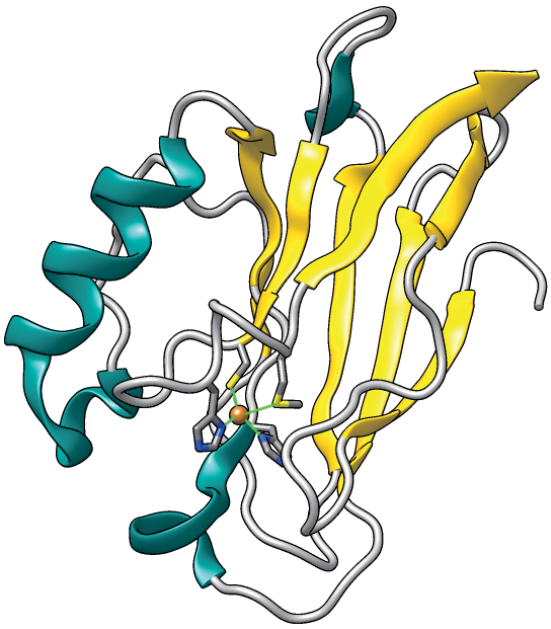

FIGURE 1.1: The secondary structure of Azurin protein (PDB ID: 4AZU[1]) where Gly ligand is neglected.

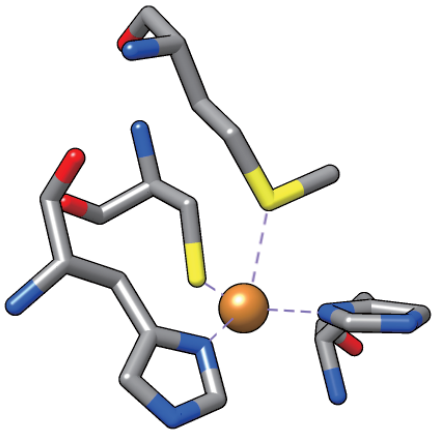

FIGURE 1.2: Ball and stick structure of T1Cu in Azurin protein.

copper(II) and sulfur atom of cysteine.[15–17] The study by Resonance Raman spectra point outs the coupling of LMCT excitation with vibrational motions around the active site in the region of 350-450 cm^{-2}.[18, 19]

Meanwhile, the existence of T1Cu not only found in blue copper protein, but also in Multicopper Oxidases (MCOs). According to spectroscopic characterization, MCOs containing all type of copper center, i.e. T1Cu, T2Cu, and T3Cu. As found in other copper protein, T1Cu in MCOs is comprised of Cu coordinated to one Cys and two His residues in trigonal plane, and coordinated to Met as axial ligand. A strong absorption around 600 nm is also observed from this copper center that arises from Cu to Cys charge-transfer excitation, and lead to the intense blue color. T1Cu in MCOs located at

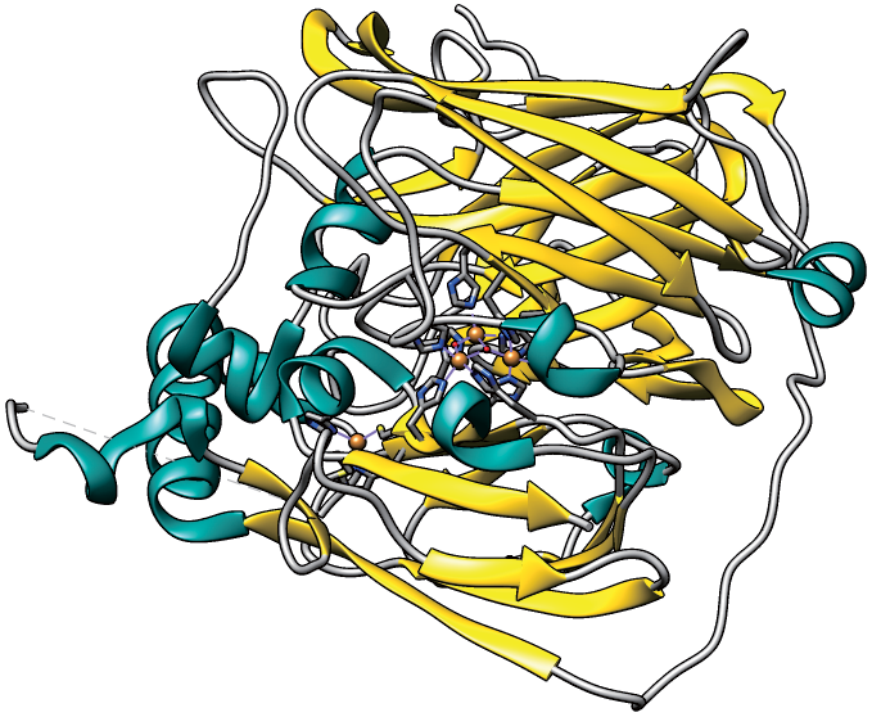

FIGURE 1.3: The secondary structure of Multicopper Oxidase protein (PDB ID: 4NER[2])

the substrate binding site and can interact with other substrates as electron acceptor. Unlike T1Cu, T2Cu and T3Cu in MCOs located at a same site and the combination of both copper center is known as tri-nuclear copper (TNC) center.[20] T2Cu located at one side of TNC center and bound to two His residues and a water molecule. This copper center is depicted by a typical EPR signal, but not detectable in the UV – visible region. Meanwhile, each T3Cu ion bound to three His ligands and also bound to a hydroxide molecule as bridging atom. A coupled pair of this copper center lead to antiferromagnetic state that characterized by 330 nm absorption band, which arising from a charge-transfer transition between Cu and hydroxide ion.[21] The distance between T1Cu site and TNC site is found around 13 and linked by a His-Cys-His peptide chain. This link is known as the pathway of electron-transfer process between those sites. The secondary structure of MCOs is presented in Figure 1.3.

Depending upon the substrate specificity, MCOs can be classified into two classes. The first class oxidize organic substrate and transition metal ions, e.g. Laccase, Ascorbate Oxidase,[22, 23], while another class only oxidize transition metal ions, e.g. Fet3p, Ceruloplasmin, CueO.[24, 25] The catalysis processes in both classes occurred by an outer-sphere electron transfer mechanism, wherein chemical bridge between substrate and enzyme do not necessary to be established.[26] MCOs utilize four electrons obtain from one-electron oxidations of a substrate to reduce dioxygen molecule to water by

reductive cleavage of O-O bonding as follows[20]

$$O_2 + 4e^- + 4H^+ \xrightarrow{4Cu2+} 2H_2O$$

In this redox process, T1Cu center takes a role in catching electrons from other substrate and transfer the electron to TNC center, while TNC center will use the electrons to reduce dioxygen molecule to water.[27] According to the reaction mechanism that is presently accepted, the reaction begin by the oxidation of substrate by T1Cu and followed by electron transfer process from T1Cu to TNC site, where the reduction of oxygen takes place.[20] The reduction of Cu(II) ion to Cu(I) in T1Cu causes a minimal change of protein structure and resulting a low activation energy and thus a fast electron transfer.[28]

1.3 Introduction to Iron-Sulfur Protein

Iron-sulfur proteins are almost the oldest metalloproteins that existed on the earth. They are found in many kinds of living organisms and take a role in a variety biological processes such as photosynthesis and respiration. Iron-sulfur proteins have a wide range of redox potential and allow them to interact with many kinds of substrates by acting as electron carriers.[29, 30] In 1960, this proteins were discovered regarding on their unique $g = 1.9$ of electron paramagnetic resonance (EPR) signal, which is not observed in the measurement of other metalloproteins.[31–33] Despite their function as electron carriers, iron-sulfur clusters are also involved in several processes such as reduction of disulfide bonds and initiation or stabilization of radical chain reactions,[34] or act as Lewis acids.[35] Furthermore, iron-sulfur clusters can also stabilize the structure of protein[34, 36] and used to store sulfur or iron atoms.[36, 37]

Iron-sulfur proteins contain a core structure or cluster that is composed by iron atoms bound to sulfide ion, the so-called acid- sulfur. This cluster connects to the chain of polypeptide through thiolate side chain of cysteine residues. Iron-sulfur clusters are classified with respect to the number of iron and sulfur atoms found in the cluster.[38] Besides, the clusters are also classified on the basis of protein type, such as structural motifs and spectroscopic and electrochemical properties. According to this classification, iron-sulfur proteins are divided into several major groups, i.e. rubredoxin ([1Fe-4S]), ferredoxins ([2Fe-2S], [4Fe-4S], [3Fe-4S], [3Fe-4S][4Fe-4S], and [4Fe-4S][4Fe-4S]), Rieske proteins ([2Fe-2S]), and high-potential iron-sulfur proteins (HiPIPs, [4Fe-4S]). Despite the structure difference of iron-sulfur proteins, the cluster geometries are found to be quite similar between each others, especially within the cluster class. The cluster presents a distorted tetrahedral geometry in all iron-sulfur proteins.

Ferredoxin is one of sub-class of iron-sulfur protein that refer to a wide range of small, low molar mass iron sulfur protein. This protein involves in several biological processes and takes a role as electron carriers in different biological pathways including photosynthesis and respiration.[39] Ferredoxin is highly acidic protein that contain iron and inorganic or acid-labile sulfurs.[39] The cluster of this protein is found to present spin-coupled structure.[40] In the oxidized state, iron-sulfur cluster in ferredoxin contains two ferric ions bound to sulfur ligand in almost tetrahedral structure, which the ferric ions are found in high spin and five unpaired d-electrons.

The optical properties of iron-sulfur cluster are confirmed by the Mössbauer analysis and EPR spectra. A broad absorption bands are observed in visible region for measurement of ferredoxin in oxidized state, which indicate a charge-transfer transitions from both sulfide ions and thiolate ligands to ferric ions. As for infrared analysis, there are some weaker absorptions bands observed in the region between 700 and 1200 nm that arise from $d - d$ transitions of high spin ferric ions. In both oxidized and reduced state, ferredoxin exhibits very intense natural circular dichroism (CD) in the visible region, which present the distinctive feature of two iron proteins.[41]

Ferredoxin has a low redox potential with the average of -400 mV and cover a range of 800 mV, The value of redox potential correspond to the cluster type, H-bonding network, protein structure, and water solubility. The broad range of redox potential allow them to act as redox partners for a variety of substrate in a number of important biological reactions. According to CD and optical rotatory dispersion studies, the environment of polar active site around the cluster in all ferredoxins is found to be very similar, which is correspond to ligand charge transfer and similar electronic structure of the iron center.[42] Furthermore, ferredoxins are classified on the basis of the number of iron atom contain in the cluster, in which one of the class is [2Fe-2S] ferredoxins. The secondary structure of [2Fe-2S] ferredoxin is presented in Figure 1.4, while [2Fe-2S] cluster is presented in Figure 1.5.

The [2Fe-2S] cluster contain two iron atoms coordinated to two inorganic sulfurs and four cysteine thiolates from the protein. This cluster is not fully planar but there is any tilt in the plane of the first and second irons. The cluster of [2Fe-2S] ferredoxin located close to the surface of protein and surrounded by hydrophobic residues. The surface of [2Fe-2S] ferredoxins is known to be highly acidic, except the vicinity of the cluster.

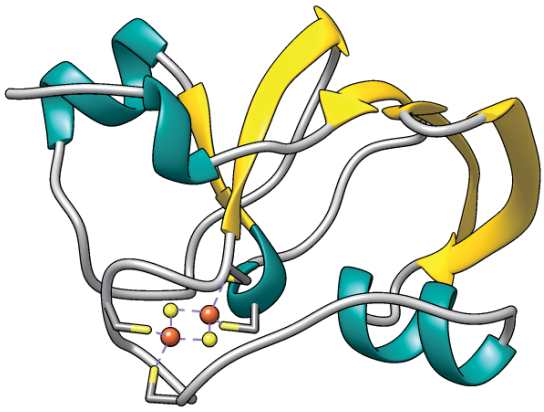

FIGURE 1.4: The secondary structure of ferredoxin protein (PDBID 1A70).

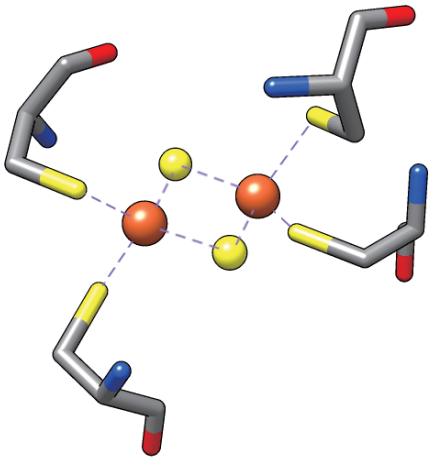

FIGURE 1.5: The iron-sulfur cluster obtained from ferredoxin protein.

1.4 Introduction to Density Functional Theory

Fifty years ago, a theorem has been proved by Hohenberg and Kohn[43] as a solution of Schrödinger equation.[44] Since the publication in 1926, the Schrödinger equation has been a challenge to be solved. Two years later, Dirac said in his paper on the quantum theory of the electron:[45]

> The underlying physical laws necessary for the mathematical theory of a large part of physics and the whole of chemistry are thus completely known, and the difficulty is only that the exact application of these laws leads to equations much too complicated to be soluble.

In spite of this somewhat discouraging comment, an effort to solve the Schrödinger equation for real condition has opened a new discipline of chemistry, which is called ab initio theory. The rapid increase of computational resource and software applications

has encouraged the study of molecular system with exceptionally high accuracy. One of main goals of quantum chemistry is obtain the calculation results with high accuracy compare to experimental measurement.

Schrödinger Equation

The schrödinger equation for a molecular system with N-electrons and M nuclei can be written as

$$\hat{H}\Psi = E\Psi \tag{1.1}$$

where the Hamiltonian operator $\hat{H}$ is expressed as

$$\hat{H} = \hat{V}_{\text{ext}} + \hat{T} + \hat{V}_{\text{ee}} \tag{1.2}$$

and the wave function Ψ is formulated as

$$\Psi = \Psi(\mathbf{r}_1, \mathbf{r}_2, \mathbf{r}_3, ..., \mathbf{r}_N). \tag{1.3}$$

The kinetic energy operator $\hat{T}$ is expressed as

$$\hat{T} = -\frac{1}{2}\sum_{i=1}^{N}\nabla_i^2, \tag{1.4}$$

the electron-electron repulsion operator is given by

$$\hat{V}_{\text{ee}} = \sum\sum_{i<j}\frac{1}{r_{ij}}, \tag{1.5}$$

and the external potential owing to the M nuclei as

$$\hat{V}_{\text{ext}} = -\sum_{i=1}^{N}\sum_{A=1}^{M}\frac{Z_A}{|\mathbf{R}_A - \mathbf{r}_i|}. \tag{1.6}$$

In the equation 1.6, r_i and R_A represent electron coordinate and nucleus coordinate, respectively, and Z_A represent the charge of nucleus R_A. To obtain the energies, equation 1.1 is solved for a set of Ψ subject. The lowest energy, E_0, is defined as the ground state energy and the probability density to find an electron with any particular set of coordinates is symbolized as $|\Psi_0|^2$.

The average total energy for a certain state is specified by a particular Ψ and expressed as

$$E|\Psi| = \int \Psi^* \hat{H}\Psi dr \equiv \left\langle \Psi|\hat{H}|\Psi \right\rangle \tag{1.7}$$

The notation of $|\Psi|$ stressed the point that the energy is a functional of the wavefunction. The calculated energy is always higher than that of the ground state unless Ψ equivalent to Ψ_0. This theorem is called the variational theorem and expressed as

$$E|\Psi| \geq E_0 \tag{1.8}$$

To obtain the energy that is close to ground state one, all possible wavefunction is used to minimize the total energy. Instead of use random wavefunction, an ansatz for the structure of Ψ is provided by Hartree Fock theory. In this theory, Ψ is assumed as antisymmetric product of of functions (ϕ) that depends on the coordinate of a single electron, which expressed as

$$\Psi_{HF} = \frac{1}{\sqrt{N!}}\det[\phi_1\phi_2\phi_3...\phi_N] \tag{1.9}$$

where "det" means a matrix determinant.[46]

The substitution of this ansatz into Ψ in Schrödinger equation resulting Hartree Fock energy that is expressed as

$$\begin{aligned} E_{\mathrm{HF}} = & \int \phi_i^*(\mathbf{r}) \left(-\frac{1}{2}\sum_i^N \nabla_i^N + V_{ext} \right) \phi_i(\mathbf{r}) d\mathbf{r} \\ & + \frac{1}{2}\sum_{i,j}^N \int \frac{\phi_i^*(\mathbf{r}_1)\phi_i(\mathbf{r}_1)\phi_j^*(\mathbf{r}_2)\phi_j(\mathbf{r}_2)}{|\mathbf{r}_i - \mathbf{r}_j|} d\mathbf{r}_1 d\mathbf{r}_2 \\ & - \frac{1}{2}\sum_{i,j}^N \int \frac{\phi_i^*(\mathbf{r}_1)\phi_j(\mathbf{r}_1)\phi_i(\mathbf{r}_2)\phi_j^*(\mathbf{r}_2)}{|\mathbf{r}_i - \mathbf{r}_j|} d\mathbf{r}_1 d\mathbf{r}_2 \end{aligned} \tag{1.10}$$

The second and third term represent the classical Coulomb energy written in terms of the orbitals and the exchange energy, respectively.

The determination of ground state orbitals are performed by utilizing the variation theorem to this energy expression with the constraint of orthonormal orbitals, which lead to Self Consistent Field equation as

$$\left[-\frac{1}{2}\nabla^2 + v_{ext}(\mathbf{r}) + \int \frac{\rho(\mathbf{r}')}{|\mathbf{r} - \mathbf{r}'|} d\mathbf{r}' \right] \phi_i(\mathbf{r}) + \int v_x(\mathbf{r}, \mathbf{r}')\phi_i(\mathbf{r}')d\mathbf{r}' = \varepsilon_i \phi_i(\mathbf{r}) \tag{1.11}$$

where the non-local exchange potential (v_x) is expressed as

$$\int v_x(\mathbf{r}, \mathbf{r}')\phi_i(\mathbf{r}')d\mathbf{r}' = -\sum_j^N \int \frac{\phi_j(\mathbf{r})\phi_j^*(\mathbf{r}')}{|\mathbf{r} - \mathbf{r}'|}\phi_i(\mathbf{r}')d\mathbf{r}'. \tag{1.12}$$

The Hartree-Fock equations explain non-interacting electrons that is affected by a mean

field potential consisting of the classical Coulomb potential and a non-local exchange potential. From this point, several methods have been developed to approximate the value of Ψ and E_0, which directly proportional to the required computational cost. Moreover, to obtain an accurate solutions, the flexibility of wavefunction's spatial variation should be also considered, e.g. increasing the basis set.

Density Functional Theory

In 1964, two theorems have been proved by Hohenberg and Kohn and lead to the fundamental of density functional theory, which is expressed as

$$\delta \left[E[\rho] - \mu(\int \rho(\mathbf{r}) d\mathbf{r} - N) \right] = 0. \tag{1.13}$$

According to equation 1.2, the energy functional that consists of three term, i.e. the kinetic energy, the interaction with the external potential and the electron-electron interaction, can be re-written as

$$E[\rho] = T[\rho] + V_{ext}[\rho] + V_{ee}[\rho], \tag{1.14}$$

with the interaction with the external potential is trivially derived from

$$V_{ext}[\rho] = \int \hat{V}_{ext} \rho(\mathbf{r}) d\mathbf{r}. \tag{1.15}$$

Kohn and Sham suggested an approach to approximate the functional of kinetic energy and electron-electron interaction.[47] They introduced N-non-interacting electrons system that is represented by a single determinant wavefunction. The kinetic energy and electron density of this system are obtained directly from the orbitals as

$$T_s[\rho] = -\frac{1}{2} \sum_{i}^{N} \left\langle \phi_i | \nabla^2 | \phi_i \right\rangle . \tag{1.16}$$

The density of a non-interacting electrons system will reproduce the true ground state density as

$$\rho(\mathbf{r}) = \sum_{i}^{N} |\phi_i|^2. \tag{1.17}$$

By introducing the exchange-correlation functional, the energy functional can be rearranged as

$$E[\rho] = T_s[\rho] + V_{ext}[\rho] + V_H[\rho] + E_{xc}[\rho] \tag{1.18}$$

where $V_H[\rho]$ is classical Coulomb interaction or Hartree energy that is formulated as

$$V_H[\rho] = \frac{1}{2}\int \frac{\rho(\mathbf{r}_1)\rho(\mathbf{r}_2)}{|\mathbf{r}_1 - \mathbf{r}_2|} d\mathbf{r}_1 d\mathbf{r}_2 \tag{1.19}$$

and $E_{xc}[\rho]$ is exchange-correlation functional that is expressed as

$$E_{xc}[\rho] = (T[\rho] - T_s[\rho]) + (V_{ee}[\rho] - V_H[\rho]). \tag{1.20}$$

Simply, $E_{xc}[\rho]$ represents the accumulation of error from the approximation of a non-interacting kinetic energy and classical electron-electron interaction. By applying the variational theorem (Equation 1.13) to the explicit term of energy functional (Equation 1.18) in terms of the density constructed from non-interacting orbitals, the orbitals that minimize the energy will be obtained and satisfied the following set of equations

$$\left[-\frac{1}{2}\nabla^2 + v_{ext}(\mathbf{r}) + \int \frac{\rho(\mathbf{r}')}{|\mathbf{r} - \mathbf{r}'|} d\mathbf{r}' + v_{xc}(\mathbf{r})\right] \phi_i(\mathbf{r}) = \varepsilon_i \phi_i(\mathbf{r}). \tag{1.21}$$

A local multiplicative potential is introduced as the functional derivative of the exchange correlation energy regarding the density, which is formulated as

$$v_{xc}(\mathbf{r}) = \frac{\delta E_{xc}[\rho]}{\delta \rho}. \tag{1.22}$$

The set of non-linear equations describe how non-interacting electrons behave under an effective local potential. For the exact functional, the orbitals will produce an exact ground state density and exact ground state energy by applying Equation 1.17 and 1.18, respectively. The Kohn-Sham equations show a similar form with the Hartree-Fock equation (Equation 1.11) where the non-local exchange potential is substituted by the local exchange-correlation potential. For practical reasons, the exchange correlation energy can be partitioned into exchange and correlation energy as

$$E_{xc}[\rho] = E_x[\rho] + E_c[\rho]. \tag{1.23}$$

Local Density Approximation (LDA) Functionals

The development of method to approximate E_{xc} has accelerated the expansion of research field. So far, several functional has been developed, which are more or less suitable to be used for any specific study. In judging a calculation results, a direct comparison with experimental data is required. However, it is important to understand the derivation and structure of functionals when choosing a functional for certain study. The early phase of the development is the implementation of a functional to one particular

system in which closely exact results could be obtained, i.e. homogeneous electron gas. In this system, the electrons suppose to have a constant external potential and, as the consequnce, the charge density will be constant.

In the early of 1920, Thomas and Fermi investigated the homogeneous electron gas.[48, 49] They assumed that the orbitals of the system are plane waves by symmetry. The total energy functional can be readily calculated if the electron-electron interaction is estimated as classical Hartree potential, in which the exchange and correlation effects are neglected.[48, 49] By applying these conditions, the dependence of the kinetic energy and exchange energy in Equation 1.10 can be expressed in the terms of a local functions of the density. In the homogeneous electron gas, the exchange energy can be approximated by using local density approximation (LDA), which is expressed as

$$E_x^{\mathrm{LDA}}[\rho] = -\int \frac{3}{4}\left(\frac{3}{\pi}\right)^{\frac{1}{3}} \rho^{\frac{4}{3}} d(\mathbf{r}) \tag{1.24}$$

with the corresponding exchange potential is

$$v_x^{\mathrm{LDA}}(\mathbf{r}) = -\left(\frac{3}{\pi}\rho(\mathbf{r})\right)^{\frac{1}{3}}. \tag{1.25}$$

A parameter r_s, which is known as the Wigner-Seitz radius, is often used to express the above formula, and formulated as

$$r_s = \left(\frac{4\pi\rho}{3}\right)^{-\frac{1}{3}}. \tag{1.26}$$

Hence, the v_x^{LDA} can be rewritten as

$$v_x^{\mathrm{LDA}} = -\left(\frac{3}{2\pi}\right)^{\frac{2}{3}} \frac{1}{r_s}. \tag{1.27}$$

The first approximation for E_{xc} is given by the uniform electron gas model as

$$E_{xc}^{\mathrm{LDA}} = \int \varepsilon_{xc}^{\mathrm{LDA}}[\rho(\mathbf{r})]\rho(\mathbf{r})d\mathbf{r} \tag{1.28}$$

where $\varepsilon_{xc}^{\mathrm{LDA}}$ represent the exchange-correlation energy distribution per unit volume. In this formula, the value of $\varepsilon_{xc}^{\mathrm{LDA}}$ only depends on the density at the point where it is estimated.

Basically, a uniform positive charge of equal density without exchange effects is needed by the ideal electron gas of uniform density. Hence, by considering the interaction of the positive charge with itself and with the electron distribution, Equation 1.18 can be

reduced as

$$E[\rho] = T_s + E_{xc}[\rho]. \tag{1.29}$$

By performing a random-phase analysis, von Barth and Hedin (vBH) have suggested a correlation functional that is spin dependent.[50] For the case of spin independent, the correlation function suggested by von Barth and Hedin can be expressed as

$$\varepsilon_c^{\mathrm{vBH}} = -\frac{1}{2}c_o\left[(1+Z^3)\ln\left(1+\frac{1}{Z}\right)+\frac{Z}{2}-Z^2-\frac{1}{3}\right] \tag{1.30}$$

where $Z = rs/30$. Afterwards, other correlation function was proposed by Vosko, Wilk and Nusair (VWN).[51] The VWN correlation function was acquired by using Padé approximation interpolation of numerical calculations, which is formulated as

$$\varepsilon_c^{\mathrm{VWN}} = \frac{A}{2}\left[\ln\frac{x}{X(x)}+\frac{2b}{Q}\tan^{-1}\frac{Q}{2x-b}-\frac{bx_o}{X(x_o)}\left(\ln\frac{(x-x_o)^2}{X(x)}+\frac{2(b+2x_o)}{Q}\tan^{-1}\frac{Q}{2x+b}\right)\right] \tag{1.31}$$

where the functions of x, X, and Q are respectively expressed as

$$x = r_s^{1/2}, \quad X(x) = x^2+bx+c, \quad \text{and} \quad Q = (4c-b^2)^{1/2}. \tag{1.32}$$

The local correlation functional has also been proposed by Perdew and Wang (PW92), which is formulated as[52]

$$\varepsilon_c^{\mathrm{PW92}} = -2a\rho(1+\alpha_1 r_s)\ln\left[1+\frac{1}{2a\left(\beta_1 r_s^{1/2}+\beta_2 r_s+\beta_3 r_s^{3/2}+\beta_4 r_s^2\right)}\right]. \tag{1.33}$$

Generalized Gradient Approximation (GGA) Functionals

The implementation of LDA in a calculation produce an energy that is not as good as those produce by correlated *ab initio* method. The produced errors were observed directly proportional to the size of the system. The local approximation used in LDA seems to fail in reproduce the effects of the creation or rupture of chemical bonds. One of the factor is the behavior of molecule that is not analogous to the system with uniform electron gas distribution. To adjust the non-uniformity of the electron density, gradients term are added into exchange and correlation functionals. The addition of gradients term of the density introduced a non-local or semilocal functionals.

The first approximation to included the gradient was not satisfied because it did not achieve several requirements of the exchange-correlation functionals. Indeed, the results is worse than that of the local approximation. To solve this problem, generalized gradient

approximation (GGA) was proposed, which is formulated as:

$$E_{xc}^{\mathrm{GGA}}[\rho] = \int d\mathbf{r}\varepsilon_{xc}[\rho, |\nabla\rho|, \nabla^2\rho] \tag{1.34}$$

By using GGA, Perdew and Wang proposed the exchange and correlation functional (PW86) that is widely applied in several density functional programs, which is formulated as[53]

$$\varepsilon_x^{\mathrm{PW86}} = \varepsilon_x^{\mathrm{LDA}}[\rho]\left(1 + 0.0864\frac{s^2}{m} + bs^4 + cs^6\right)^m \tag{1.35}$$

where s is express as

$$s = \frac{|\nabla\rho|}{(24\pi^2)^{1/3}\rho^{4/3}}. \tag{1.36}$$

The correlation functional of PW86 is formulated as[53, 54]

$$\varepsilon_c^{\mathrm{P86}} = \varepsilon_c^{\mathrm{LDA}}[\rho] + e^{-\Phi}C_c[\rho]\frac{|\nabla\rho|^2}{\rho^{4/3}}. \tag{1.37}$$

One of the popular exchange functionals is proposed by Becke (B88) that is formulated as[55]

$$\varepsilon_x^{\mathrm{B88}} = \varepsilon_x^{\mathrm{LDA}}[\rho]\left[1 - \frac{\beta}{2^{1/3}A_x}\frac{x^2}{1 + 6\beta x\sinh^{-1(x)}}\right] \tag{1.38}$$

where

$$x = 2^{1/3}\frac{|\nabla\rho|}{\rho^{4/3}}, \quad A_x = (3/4)(3/\pi)^{1/3}, \quad \text{and} \quad \beta = 0.0042. \tag{1.39}$$

Meanwhile, the correlation functional proposed by Lee, Yang and Parr is also widely used, which the functional is given by[56]

$$\varepsilon_c^{\mathrm{LYP}} = -a\frac{1}{1 + d\rho^{-1/3}}\left\{\rho + b\rho^{-2/3}\left[C_F\rho^{5/3} - 2t_w + \frac{1}{9}\left(t_w + \frac{1}{2}\nabla^2\rho\right)\right]e^{-c\rho^{-1/3}}\right\} \tag{1.40}$$

where

$$t_w = \frac{1}{8}\left(\frac{|\nabla\rho|^2}{\rho} - \nabla^2\rho\right). \tag{1.41}$$

Meta-Generalized Gradient Approximation Functionals

To improve the accuracy, GGA functionals have been developed by introducing kinetic energy density term into exchange-correlation energy formula. This new approximation, which is called meta-GGA, yield new form of the functionality as

$$E_{xc} = \int \rho(r)\varepsilon_{xc}(\rho, |\nabla\rho|, \nabla^2\rho, \tau)d\mathbf{r} \tag{1.42}$$

where the kinetic energy density τ is defined as

$$\tau = \frac{1}{2}\sum_i |\nabla\varphi_i|^2. \tag{1.43}$$

Hybrid Exchange Functionals

The hybrid exchange functional proposes a different approximation in calculating exchange-correlation functional. This functional combines the value of Hartree-Fock (HF) energy and the result of the calculation by LDA (or GGA) functional. Coupling constant (λ) is introduced to adjust the proportion between HF energy and LDA (or GGA) energy. At $\lambda = 0$, the non-interacting system is identical with Hartree-Fock ansatz, while at $\lambda = 1$, the systems are fully interacting and LDA (or GGA) functionals will produce an excellent approximation. Hence, coefficients are used to determine the portion of HF and LDA/GGA energy given by

$$E_{xc} \approx aE_{\mathrm{HF}} + bE_{xc}^{\mathrm{GGA}} \tag{1.44}$$

with the coefficients are established with respect to a system with known exact result.

This approach has been adopted by Becke to define a new functional, in which the coefficients are determined by fitting the calculation data to the experimental data of ionization energies, proton affinities, atomization energies, and total atomic energies for a series of small molecule.[57] The results of the functional proposed by Becke is formulated as

$$E_{xc} = E_{xc}^{\mathrm{LDA}} + 0.2(E_x^{\mathrm{HF}} - E_x^{\mathrm{LDA}}) + 0.72\Delta E_x^{\mathrm{B88}} + 0.81\Delta E_c^{\mathrm{PW91}} \tag{1.45}$$

Here, the functional of $\Delta E_x^{\mathrm{B88}}$ and E_c^{PW91} are GGA functional that is widely used to correct the LDA exchange and correlation energies, respectively.[52, 58] Recently, this type of hybrid functionals are widely used for chemical systems, which B3LYP functional is the most popular one.[56] The hybrid exchange functional produce a more reliable results than GGA functional in the calculation of binding energies, geometries, and frequency.

Hybrid Meta-GGA Exchange Functionals

Hybrid meta-GGA exchange functionals utilized meta-GGA functional, instead of GGA functional, in the formulation of functional. M06 is one of popular hybrid meta-GGA functional that is widely used for either organic or inorganic system. The local parts of

of M06 functional rely on three variables, i.e. spin density (ρ_σ), reduced spin density gradient (x_σ), and spin kinetic energy density (τ_σ).[59] The expression of x_σ and τ_σ are respectively formulated as

$$x_\sigma = \frac{|\nabla\rho_\sigma|}{\rho_\sigma^{4/3}} \tag{1.46}$$

$$\tau_\sigma = \frac{1}{2}\sum_{i}^{\text{occup}} |\nabla\Psi_{i\sigma}|^2. \tag{1.47}$$

The exchange functional of M06 is written as

$$E_x^{\text{M06}} = \sum_\sigma \int \left[F_{X\sigma}^{\text{PBE}}(\rho_\sigma, \nabla\rho_\sigma) f(w_\sigma) + \varepsilon_{X\sigma}^{\text{LSDA}} hX(x_\sigma, z_\sigma)\right] d\mathbf{r} \tag{1.48}$$

where $F_{X\sigma}^{\text{PBE}}(\rho_\sigma, \nabla\rho_\sigma)$ is the the exchange energy density of PBE exchange model,[60] and $\varepsilon_{X\sigma}^{\text{LSDA}}$ is the local spin density approximation for exchange functional.[47] As for correlation functional, M06 treat the opposite-spin and parallel spin differently. The opposite spin of M06 correlation energy is formulated as

$$E_c^{\alpha\beta} = \int e_{\alpha\beta}^{\text{UEG}}[g_{\alpha\beta}(x_\alpha, x_\beta) + h_{\alpha\beta}(x_{\alpha\beta}, z_{\alpha\beta})] d\mathbf{r} \tag{1.49}$$

while for parallel spins is

$$E_c^{\sigma\sigma} = \int e_{\sigma\sigma}^{\text{UEG}}[g_{\sigma\sigma}(x_\sigma) + h_{\sigma\sigma}(x_\sigma, z_\sigma)] D_\sigma d\mathbf{r}. \tag{1.50}$$

The total energy of correlation part of M06 is given by

$$E_c = E_c^{\alpha\beta} + E_c^{\alpha\alpha} + E_c^{\beta\beta}. \tag{1.51}$$

Finally, the hybrid exchange-correlation energy can be formulated as

$$E_{xc}^{\text{hyb}} = \frac{X}{100} E_x^{\text{HF}} + \left(1 - \frac{X}{100}\right) E_x^{\text{DFT}} + E_c^{\text{DFT}} \tag{1.52}$$

where E_x^{HF}, E_x^{DFT}, and E_c^{DFT} are the non-local Hartree-Fock (HF) exchange energy, the local DFT exchange energy, and the local DFT correlation energy, respectively.

Chapter 2

Theoretical Study on the Electronic Structure of Type 1 Copper Center

2.1 Introduction

Copper proteins play a fundamental rote in a wide range of biomolecular processes such as electron transfer, oxygen transportation, and so on. One or more coper ions can be found in the active site of this protein. The copper protein containing one copper ion is called type 1 copper (T1Cu) proteins. There are several copper protein classified as T1Cu protein such as Azurin, Plastocyanin, Stellacyanin, etc. Meanwhile, copper protein can also contain more than one copper ions like found in Multicopper Oxidases (MCOs). MCOs contain two copper center, i.e. type I copper (T1Cu) and tri-nuclear copper (TNC), that located at different active sites. T1Cu is composed by a copper ion coordinated to two histidines and a cysteine in a trigonal planar structure, and an axial ligand such as methionine and so on.[61–63] During the reaction, T1Cu accepts an electron from other substrates with higher redox potential and transfer the electron to TNC.[16, 64, 65] In the end of one cycle reaction, dioxygen molecules are reduced to yield two water molecules in TNC.[27]

There are several properties of T1Cu related to electronic structure and reaction that have been investigated experimentally by many groups.[27, 66–70] The structure of T1Cu has been identified by a strong absorption at around 600 nm and narrow hyperfine splittings in the electron paramagnetic resonance (EPR) spectroscopy.[27, 67] Related to the kinetic aspect of electron transfer, Holwerda and coworkers have investigated the rate of electron transfer in T1Cu and found the dependence of the transfer rate to

pH.[66] Solomon and co-workers have also studied the characteristic of room temperature circular dichroism and magnetic circular dichroism spectra of several T1Cu proteins, such as Stellacyanin, Plastocyanin, and Azurin.[67] From the comparison of the absorption and circular dichroism intensities, they found that the characteristics of band absorption represent transition of energy level.

Not only properties of T1Cu, several properties of MCOs have been also investigated by many groups.[2, 20, 23, 25, 27, 71–82] In detail, Solomon and coworkers have published a review of reported physical properties of MCOs, such as EPR and redox potential.[20] The mechanism of oxygen binding followed by a reduction reaction on TNC site have also been suggested according to spectroscopic and quantum mechanical study.[20, 71, 75, 80] The intermolecular and intramolecular electron transfer in MCOs have been investigated by Roberts and coworkers by using laser flash photolysis.[25] Shleev and coworkers have also investigated the probability of direct electron transfer from electrode to MCOs.[73] Related to the active site structure, Augustine and coworkers have investigated the contribution of the structure in supporting the efficiency of reduction reaction on TNC.[81] They found that the efficiency of reduction reaction correspond to the asymmetrical structure of TNC.

From the viewpoint of theoretical and computational study, T1Cu has attracted many interest in relation to the electronic structure.[7, 16, 28, 83, 84] Solomon and co-workers have investigated the interaction of copper ion and ligands by using quantum method.[7, 16] Corni and co-workers have utilized density functional theory (DFT) method to study the electronic properties of Azurin's active site and their contribution to electron transfer reaction.[84] Their results point out that the energy spectrums of Azurin in two different oxidation states is different.

In the term of quantum calculations, DFT methods have been expanded into the consideration of long-range interaction in the calculation, such as van der Waals interactions. Regarding the long-range interaction, M06 suite of DFT has proposed by Zhao and Truhlar.[59, 85] This functional shows a better performance compare to B3LYP due to the implementation of meta-GGA exchange functional. M06 has been applied in many calculations of molecular properties for both organic and inorganic molecule with a promising results.[86–88]

In the previous study, we have studied the electronic structure of Azurin in oxidized state and have found the dependence of the partial charge and partial spin on the distance of metal-ligand bond.[89] We have also investigated two stable structure of Azurin obtained from jump motion in molecular dynamics (MD) simulation.[90] The solvent effects on the electronic structure of Azurin's active site have also been investigated by using polarizable continuum model (PCM).[91] This study aim to investigate the dependency

of the electronic structure and properties of T1Cu on DFT functional. We prepared T1Cu cluster model from several T1Cu proteins, i.e. Azurin, Plastocyanin, Stellacyanin, and MCOs. Two typical DFT functionals, i.e. M06 and B3LYP, are utilized with 6-31G(d) basis set to calculate several properties, such as ionization potential, electron affinity and maximum absorption wavelength. The force field parameters, i.e. bond constant and angle constant, around T1Cu are also presented and discussed.

2.2 Computational Methods

In this section, we present the calculation procedure of the electronic properties and force field parameters of T1Cu. T1Cu clusters are prepared from X-ray crystal structure followed by optimization by using quantum method. Then, the electronic properties of the optimized structures are calculated. The optimization and calculation were performed by using Gaussian 09 package.[92]

2.2.1 Cluster Model for the Type I Copper Center

T1Cu clusters was extracted from the series of X-ray crystal structure of copper proteins. In the case of oxidized state, the cluster of Azurin, Plastocyanin, Stellacyanin, and MCOs were extracted from X-ray crystal structure with PDB ID are 4AZU, 1PLC, 1X9R and 4NER, respectively. Meanwhile, the cluster of Azurin, Plastocyanin, Stellacyanin, and MCOs in reduced state were extracted from X-ray crystal structure with PDB ID are 1E5Y, 5PCY, 1X9U and 4E9T, respectively. In this model, all T1Cu clusters composed by a copper ion coordinated to two histidines and a cysteine in trigonal plane, and a methionine as axial ligand, except for Stellacyanin. In Stellacyanin, the copper bound to glumatine, instead of methionine, at axial ligand position. The schematic diagram of T1Cu model cluster is presented in Figure 2.1. The preparation of the structures is finalized by adding hydrogen atoms and optimizing the hydrogens position with B3LYP/6-31G(d) method.[89]

2.2.2 Electronic Properties

Several properties of T1Cu were calculated and discussed in relation to DFT functional dependency. The calculated properties consist of molecular orbital, atomic partial charges and partial spin, ionization potential (IP) of reduced T1Cu and electron affinity (EA) of oxidized T1Cu. Atomic partial charges are calculated by using Merz-Singh-Kollman scheme.[93] In addition, we also calculate maximum absorption wavelength by

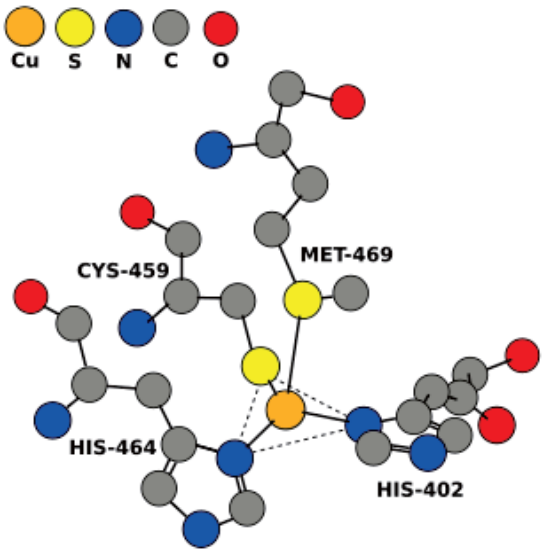

FIGURE 2.1: The schematic diagram of Type I copper model cluster.

using time-dependent DFT. The solvation effect is approximated by using conductor-like polarizable continuum model with $\varepsilon = 10$.[94, 95]

2.2.3 Force Field Parameters

Force fields of bond and angle around T1Cu are approximated by calculating potential energy surface (PES) with B3LYP and M06 methods. PES is constructed by calculating total energies of T1Cu structure with respect to varied bond and angle. Bond distance was varied in the range of ± 0.1 Å from equilibrium distance with increment 0.02 Å, while angle distance was varied in the range of $\pm 5°$ from equilibrium angle with increment $1°$.[96] The force fields are obtained from fitting analysis of PES by using a harmonic potential function, which the potential given by[89]

$$V(r, K_r) = K_r(r - r_c)^2 \tag{2.1}$$

$$V(\theta, K_\theta) = K_\theta(\theta - \theta_c)^2 \tag{2.2}$$

where K_r and K_θ represent the bond and angle constants, respectively, while r_c and θ_c represent the equilibrium bond and angle, respectively.

2.3 Results and Discussion

In this section, we present the result of the electronic structure and properties of T1Cu. The calculated properties consists of atomic partial charge, partial spin densities, ionization potential, electron affinity, maximum absorption wavelength, bond and angle

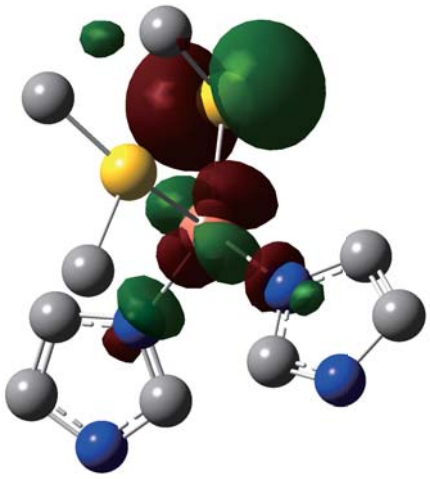

FIGURE 2.2: SOMO orbital of T1Cu calculated by using M06.

constants. We discussed the dependency of those properties on DFT functional.

2.3.1 Electronic Properties

At the first, we present a SOMO orbital calculated by using M06, as shown in Figure 2.2. The shape of SOMO correspond to $d_{x^2-y^2}$ orbital of the copper ion, p orbitals of the sulfur and σ orbital of two nitrogen atoms. On the interaction between copper ion and ligands, we found an antibonding orbital between copper ion and a cysteine and two histidines in trigonal plane. The orbital of methionine's sulfur did not present in SOMO indicate that the interaction between copper and methionine is relatively weak. Our calculation produce SOMO that the shape is in agreement with the reference.[16, 90]

Regarding spin analysis, we present the surface of spin density calculated by using M06 in Fig. 2.3. The shape of the surface is found to be similar to SOMO orbital shown in Fig. 2.2, which is also similar with our previous results.[90] The distribution of spin density around T1Cu is represented by atomic partial spin provided in Tab. 2.1. We found that atomic partial spin of copper ion in all T1Cu cluster obtained from M06 calculation is smaller than those obtained from B3LYP calculation. This results show that spin distribution calculated by M06 is more delocalized around the copper ion. In relation to simple Hubbard model, spin distribution could be correspond to two parameters, i.e. transfer integral (t) and on-site repulsion (U), and commonly represented by t/U ratio. In this case, spin delocalization around copper ion is related to transfer integral between d orbital of copper ion and p orbital of cysteine's sulfur atom. The higher value of atomic partial spin on copper ion by M06 indicate that M06 calculation produce a higher value of transfer integral and, as the consequence, lower value of t/U ratio. According to this results, charge transfer between copper ion and cysteine's sulfur is likely more favorable

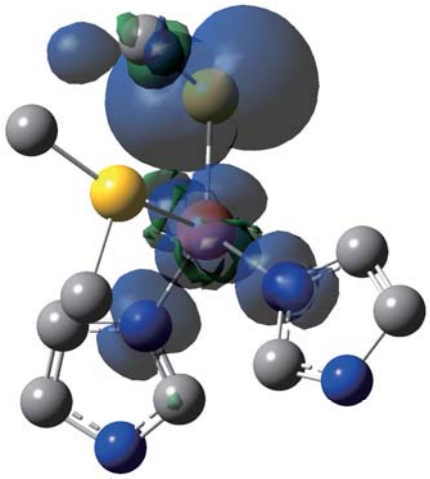

FIGURE 2.3: Spin density surface of T1Cu calculated by using M06.

TABLE 2.1: Atomic spin distribution of T1Cu in oxidized state calculated by using B3LYP (M06).

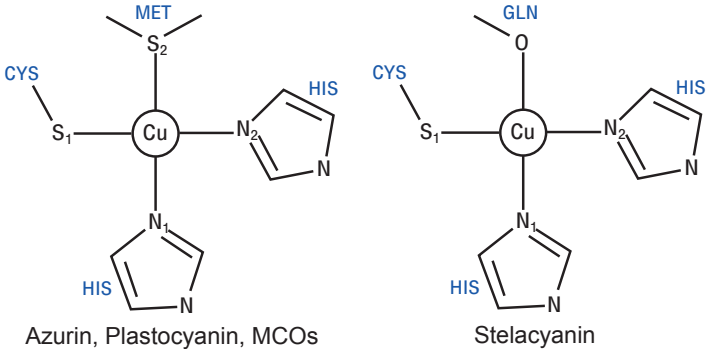

Atom	Atomic Spin Distribution			
	Azurin	Plastocyanin	Stellacyanin	MCOs
Cu	0.49 (0.46)	0.51 (0.48)	0.57 (0.54)	0.53 (0.49)
S_1	0.43 (0.47)	0.39 (0.42)	0.33 (0.35)	0.38 (0.41)
S_2/O	0 (0)	0.00 (0.00)	0 (0)	0 (0)
N_1	0.03 (0.03)	0.04 (0.04)	0.05 (0.05)	0.04 (0.04)
N_2	0.03 (0.03)	0.04 (0.05)	0.04 (0.05)	0.19 (0.16)

to occurs by M06 calculation. Atomic partial spin on methionine's sulfur is found to be zero in all T1Cu cluster. This indicate that the probability of the unpaired electron of copper to distribute onto methionine's sulfur is zero because the distance between of both atoms is relatively larger than the other copper-ligand bond.

Atomic partial charges of T1Cu calculated by B3LYP and M06 are presented in Table 2.2. We found that the partial charge of copper ion calculated by M06 is less positive than that calculated by B3LYP. In contrary, as for cysteine's sulfur atom, the partial charge obtained from M06 calculation is less negative than that obtained from B3LYP calculation. This indicate that, in M06 calculation, the negative charge of cysteine's

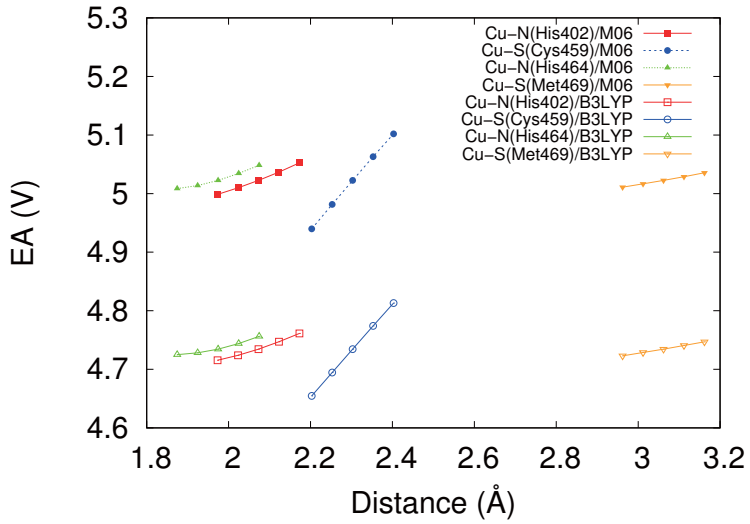

FIGURE 2.4: EA of T1Cu in MCOs as a function of bond distance. The equilibrium distance lie on a middle point and increment point is 0.05 Å.

sulfur is more distributed onto the copper ion. The tendency of atomic partial charge is found consistently in all T1Cu cluster, which means the dependency of atomic partial charge on DFT functional is similar for all T1Cu cluster. According to atomic partial spin and atomic partial charge analysis, we found that M06 calculation yield the distribution of either unpaired electron of copper ion or the negative charge of cysteines's sulfur that is more distributed onto the other atom.

The results of ionization potential (IP), electron affinity (EA), and maximum absorption wavelength (λ) of T1Cu are presented in Table 2.3. We found that IP and EA obtained from M06 calculation is consistently larger than those obtained from B3LYP calculation, which indicate the dependency of IP and EA on DFT functional. We also present the plot of EA along with the distance of Cu-ligand bond, as shown in Figure 2.4. From the figure, we found that the change of bond distance affect to EA value, in which EA is directly proportional to the distance. We found that the dependency of EA on Cu-Cys bond distance is relatively larger than the other bond. This finding indicates that Cu-Cys bond present a largest contribution in assisting the electron transfer process, which is in agreement with experimental data.[97]

Regarding MAW, we found that M06 calculation produce the wavelengths that is larger than those produced by B3LYP calculation. In this T1Cu case, MAW depict a transition energy between σ orbital of Cys sulfur and $d_{x^2-y^2}$ orbital Cu.[67] Energy involve in this transition is known as band-gap energy of electron transition and the value is inversely proportional to the wavelength. This indicate that the larger wavelength correspond to the smaller energy required for the transition. Hence, the larger MAW of M06 calculation imply that electron transition is more favorable to occur.

TABLE 2.2: Atomic partial charge of T1Cu calculated by using B3LYP (M06).

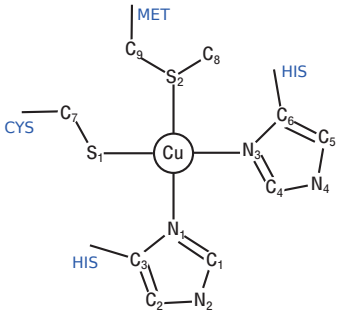

Azurin, Plastocyanin, MCOs

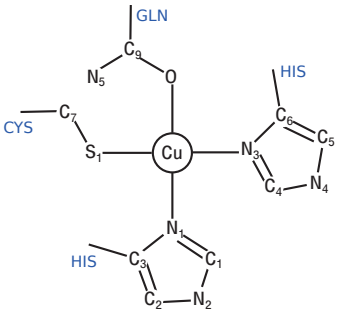

Stelacyanin

Atom	Atomic Partial Charge			
	Azurin		Plastocyanin	
	Ox	Red	Ox	Red
Cu	+0.63 (+0.59)	+0.36 (+0.31)	+0.65 (+0.58)	+0.35 (+0.30)
S_1	-0.49 (-0.45)	-0.78 (-0.75)	-0.53 (-0.48)	-0.73 (-0.69)
S_2/O	-0.40 (-0.38)	-0.34 (-0.32)	-0.32 (-0.30)	-0.26 (-0.24)
N_1	-0.26 (-0.28)	-0.22 (-0.22)	-0.27 (-0.25)	-0.32 (-0.32)
N_2	+0.24 (+0.20)	+0.21 (+0.19)	+0.19 (+0.18)	+0.20 (+0.18)
N_3	-0.29 (-0.26)	-0.26 (-0.23)	-0.24 (-0.23)	-0.20 (-0.18)
N_4	+0.19 (+0.16)	+0.18 (+0.16)	+0.14 (+0.12)	+0.15 (+0.14)
C_1	+0.12 (+0.16)	+0.08 (+0.10)	+0.18 (+0.19)	+0.13 (+0.15)
C_2	-0.07 (-0.04)	-0.10 (-0.09)	-0.03 -0.03	-0.21 (-0.20)
C_3	+0.37 (+0.36)	+0.24 (+0.24)	+0.22 (+0.21)	+0.49 (+0.49)
C_4	+0.09 (+0.11)	+0.08 (+0.09)	+0.15 (+0.16)	+0.09 (+0.10)
C_5	-0.01 (+0.02)	-0.13 (-0.12)	+0.01 (+0.02)	-0.11 (-0.10)
C_6	+0.40 (+0.37)	+0.43 (+0.41)	+0.20 (+0.20)	+0.25 (+0.25)
C_7	+0.18 (+0.14)	+0.14 (+0.10)	+0.24 (+0.22)	+0.05 (+0.01)
C_8/N_5	+0.11 (+0.09)	+0.11 (+0.09)	+0.12 (+0.11)	+0.09 (+0.09)
C_9	+0.27 (+0.26)	+0.11 (+0.10)	+0.11 (+0.09)	-0.04 (-0.06)
Atom	Stellacyanin		MCOs	
	Ox	Red	Ox	Red
Cu	+0.54 (+0.50)	+0.33 (+0.28)	+0.55 (+0.54)	+0.36 (+0.33)
S_1	-0.58 (-0.55)	-0.79 (-0.75)	-0.45 (-0.41)	-0.71 (-0.68)
S_2/O	-0.61 (-0.61)	-0.60 (-0.60)	-0.22 (-0.23)	-0.21 (-0.22)
N_1	-0.03 (-0.03)	-0.07 (-0.07)	-0.35 (-0.37)	-0.20 (-0.21)
N_2	+0.23 (+0.22)	+0.18 (+0.17)	+0.19 (+0.16)	-0.06 (-0.05)
N_3	-0.26 (-0.27)	-0.31 (-0.30)	-0.17 (-0.18)	-0.36 (-0.36)
N_4	+0.18 (+0.17)	+0.12 (+0.10)	+0.10 (+0.10)	+0.15 (+0.14)
C_1	+0.05 (+0.06)	+0.04 (+0.06)	+0.16 (+0.18)	+0.19 (+0.21)
C_2	-0.04 (-0.04)	-0.11 (-0.11)	-0.09 (-0.08)	-0.01 (-0.01)
C_3	+0.15 (+0.16)	+0.17 (+0.18)	+0.58 (+0.58)	+0.19 (+0.20)
C_4	+0.10 (+0.11)	+0.10 (+0.12)	+0.19 (+0.20)	+0.12 (+0.14)
C_5	-0.05 (-0.05)	-0.11 (-0.11)	+0.03 (+0.02)	-0.17 (-0.16)
C_6	+0.44 (+0.45)	+0.55 (+0.56)	+0.19 (+0.21)	+0.55 (+0.56)
C_7	+0.11 (+0.08)	+0.01 (-0.02)	+0.17 (+0.14)	+0.12 (+0.09)
C_8/N_5	-0.14 (-0.15)	-0.15 (-0.15)	+0.08 (+0.08)	0.06 (+0.06)
C_9	+0.94 (+0.96)	+0.89 (+0.91)	+0.05 (+0.04)	+0.01 (-0.01)

Ox: Oxidized state, Red: Reduced state.

TABLE 2.3: The results of ionization potential (IP), electron affinity (EA), and maximum absorption wavelength (λ) of T1Cu in various copper protein

Protein	Method	IP/eV	EA/eV	λ/nm	
				calc.	exp.[a]
Azurin	B3LYP	5.04	4.84	683.94	631
	M06	5.32	5.12	694.90	
Plastocyanin	B3LYP	4.93	4.46	502.94	597
	M06	5.23	4.72	527.96	
Stellacyanin	B3LYP	4.87	4.44	576.85	609
	M06	5.16	4.71	579.87	
Multicopper oxidase	B3LYP	4.86	4.77	660.59	610
	M06	5.18	5.02	671.73	

[a] Ref. [16]

2.3.2 Force Field Parameter

We approximate the bond constant around T1Cu of Azurin, Plastocyanin, Stellacyanin, and MCOs from a series of PES obtained from M06 calculation shown in Figure 2.5, 2.6, 2.7, and 2.8, respectively. Meanwhile, a series of PES of Azurin, Plastocyanin, Stellacyanin, and MCOs obtained from B3LYP calculation are shown in Figure 2.9, 2.10, 2.11, and 2.12, respectively. The value of the bond constants are summarized in Table 2.4, 2.5, 2.6, and 2.7. From the results, we found the dependency of bond constant on DFT functional. Bond constant obtained from M06 calculation is consistently larger than those obtained from B3LYP calculation for all T1Cu cluster. Particularly, we found that the most significant dependency of bond constant is found on the interaction of Cu and axial ligand. For example, as for T1Cu in Azurin, the bond constant of Cu-Met bond obtained from B3LYP and M06 calculation are 7.02 and 27.93 kcal/mol·Å^2, respectively. As for T1Cu in Plastocyanin, the bond constant of Cu-Met bond obtained from B3LYP and M06 calculation are 18.50 and 45.35 kcal/mol·Å^2, respectively. As for T1Cu in Stellacyanin, the bond constant of Cu-Glu bond obtained from B3LYP and M06 calculation are 9.55 and 36.03 kcal/mol·Å^2, respectively. As for T1Cu in MCOs, the bond constant of Cu-Met bond obtained from B3LYP and M06 calculation are 6.24 and 34.62 kcal/mol·Å^2, respectively.

As we know, the larger the bond constant value, the stronger the interaction between both atoms. Hence, the larger bond constant obtained from M06 calculation indicate that M06 calculation tends to represent the bond interaction between copper and ligand in a stronger way than B3LYP. In particular, the contribution of M06 is more significant in the case of Cu and axial ligand. The distance of the bond between Cu and axial ligand is significantly larger than the other bond. As consequence, Cu interact with axial ligand interact with long-range interaction that is much weaker than the others. Thus,

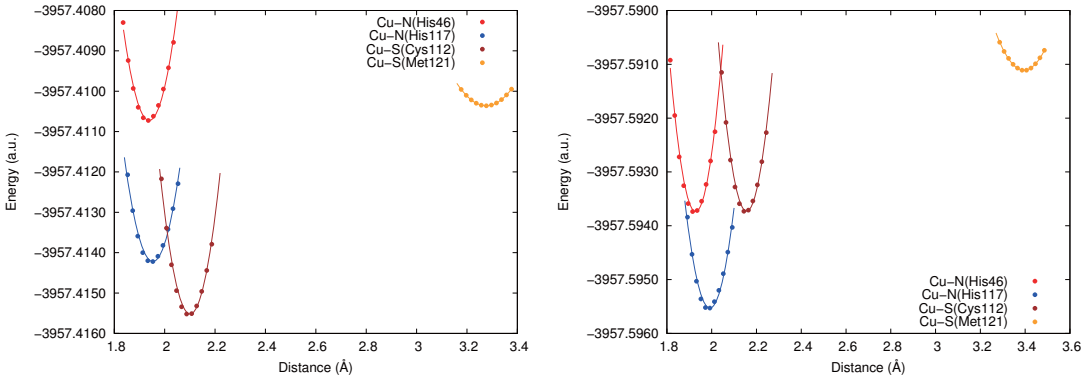

(a) (b)

FIGURE 2.5: Potential energy surface for bond distance around T1Cu of Azurin in (a) oxidized and (b) reduced state calculated by M06.

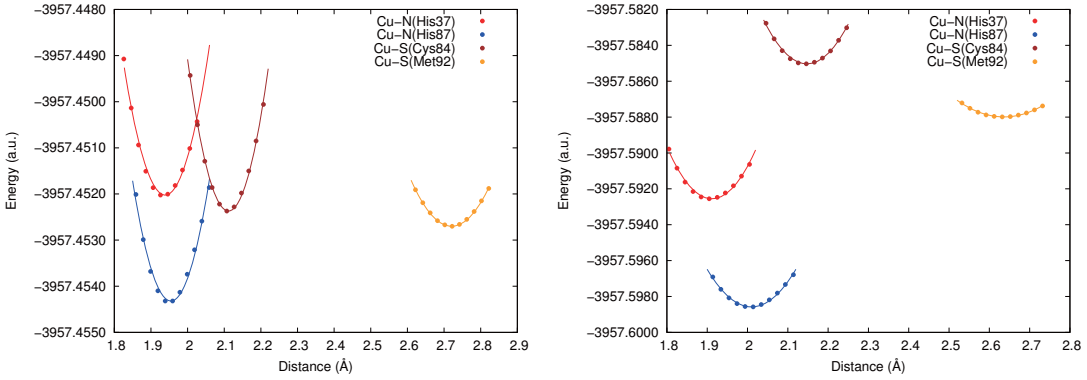

(a) (b)

FIGURE 2.6: Potential energy surface for bond distance around T1Cu of Plastocyanin in (a) oxidized and (b) reduced state calculated by M06.

TABLE 2.4: Fitting parameter for bond distance around T1Cu of Azurin calculated by B3LYP (M06).

Bond	Reduced State			Oxidized State		
	r_{PDB}	r_c	K_r	r_{PDB}	r_c	K_r
Cu-N(His46)	2.00	1.97 (1.94)	109.39 (136.66)	2.06	1.96 (1.93)	107.82 (131.11)
Cu-N(His117)	2.11	2.00 (1.95)	106.04 (127.09)	2.19	2.05 (1.99)	72.16 (99.98)
Cu-S(Cys112)	2.27	2.14 (2.10)	135.11 (154.38)	2.28	2.20 (2.16)	96.67 (123.98)
Cu-S(Met121)	3.18	3.56 (3.28)	9.69 (25.80)	3.33	3.79 (3.39)	7.02 (27.93)

The unit of distance (r) and force constant (K_r) are Å and kcal $\mathrm{mol}^{-1}\mathrm{Å}^{-2}$, respectively.

according to this results, we found that M06 treats the long-range interaction better than B3LYP does due to the type of exchange functional. M06 utilize meta-GGA exchange functional, instead of pure GGA exchange functional, by considering spin kinetic energy density parameter. By coupling with HF exchange functional in a proper ratio, meta-GGA exchange functional can improve the performance of DFT calculation, especially in the case of long-range interaction.

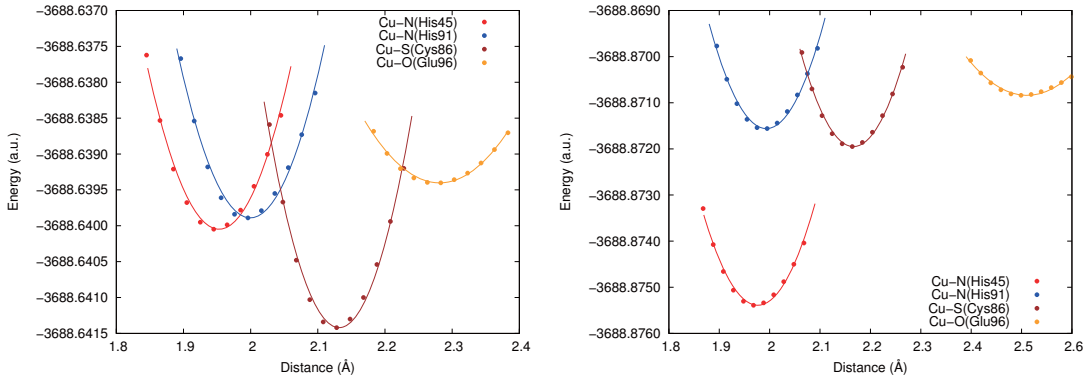

FIGURE 2.7: Potential energy surface for bond distance around T1Cu of Stellacyanin in (a) oxidized and (b) reduced state calculated by M06.

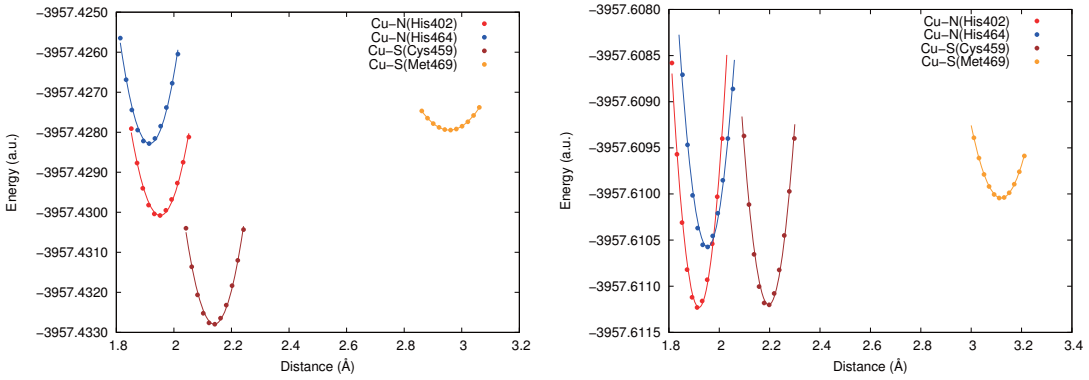

FIGURE 2.8: Potential energy surface for bond distance around T1Cu of MCOs in (a) oxidized and (b) reduced state calculated by M06.

TABLE 2.5: Fitting parameter for bond distance around T1Cu of Plastocyanin calculated by B3LYP (M06).

Bond	Reduced State			Oxidized State		
	r_{PDB}	r_c	K_r	r_{PDB}	r_c	K_r
Cu-N(His37)	2.13	1.94 (1.91)	96.63 (115.17)	1.91	1.97 (1.94)	126.52 (132.22)
Cu-N(His87)	2.39	2.09 (2.00)	54.52 (93.60)	2.06	2.00 (1.95)	89.24 (127.45)
Cu-S(Cys84)	2.17	2.19 (2.15)	87.18 (123.90)	2.07	2.15 (2.11)	152.73 (165.42)
Cu-S(Met92)	2.87	2.86 (2.63)	18.02 (40.90)	2.82	2.93 (2.72)	18.50 (45.35)

The unit of distance (r) and force constant (K_r) are Å and kcal mol^{-1}Å^{-2}, respectively.

The angle constants around T1Cu of Azurin, Plastocyanin, Stellacyanin, and MCOs are approximated from a series of PES obtained from M06 calculation shown in Figure 2.13, 2.14, 2.15, and 2.16, respectively. Meanwhile, a series of PES of Azurin, Plastocyanin, Stellacyanin, and MCOs obtained from B3LYP calculation are shown in Figure 2.17, 2.18, 2.19, and 2.20, respectively. The value of the angle constants are summarized in Table 2.8, 2.9, 2.10, and 2.11. In the matter of angle constant, we did not found any

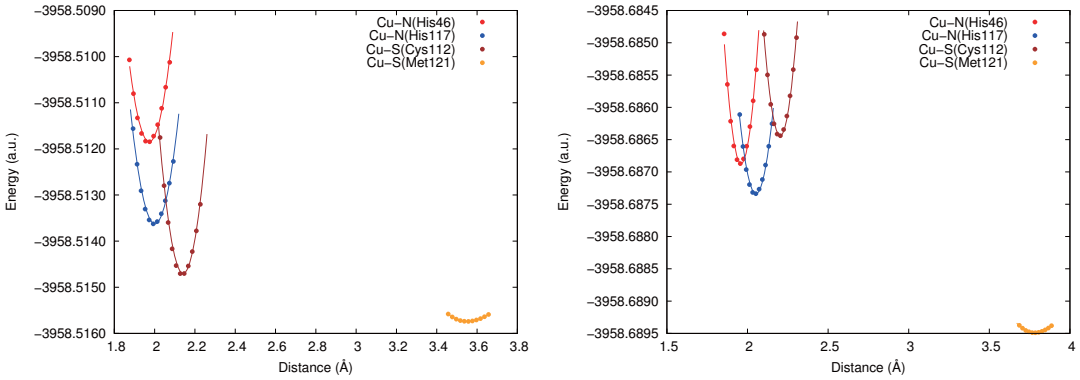

(a) (b)

FIGURE 2.9: Potential energy surface for bond distance around T1Cu of Azurin in (a) oxidized and (b) reduced state calculated by B3LYP.

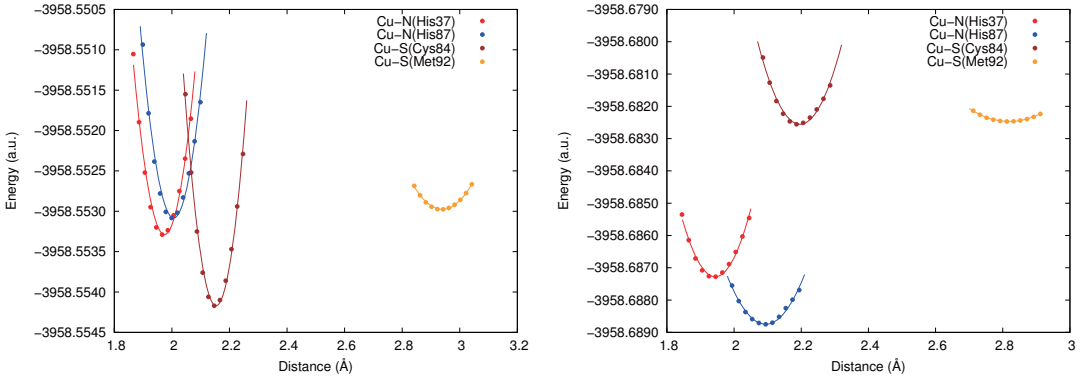

(a) (b)

FIGURE 2.10: Potential energy surface for bond distance around T1Cu of Plastocyanin in (a) oxidized and (b) reduced state calculated by B3LYP.

TABLE 2.6: Fitting parameter for bond distance around T1Cu of Stellacyanin calculated by B3LYP (M06).

Bond	Reduced State			Oxidized State		
	r_{PDB}	r_c	K_r	r_{PDB}	r_c	K_r
Cu-N(His45)	1.89	1.99 (1.95)	101.46 (124.55)	2.17	2.02 (1.98)	83.15 (107.09)
Cu-N(His91)	2.06	2.05 (2.00)	99.84 (123.56)	2.06	2.05 (1.99)	85.78 (110.74)
Cu-S(Cys86)	2.23	2.18 (2.13)	128.73 (158.12)	2.24	2.22 (2.17)	92.33 (117.53)
Cu-O(Gln96)	2.22	2.41 (2.28)	29.21 (43.68)	2.52	2.83 (2.51)	9.55 (36.03)

The unit of distance (r) and force constant (K_r) are Å and kcal mol^{-1}Å^{-2}, respectively.

dependency of angle constant on DFT functional. In some case, M06 produce angle constant that is larger than B3LYP does, while in another case, M06 produce angle constant that is smaller than B3LYP does. This finding correspond to the complexity of angle constant, in which the approximation for an angle is still depend on another angle. Hence, a bias raised by the other angle can be involved in the calculation.

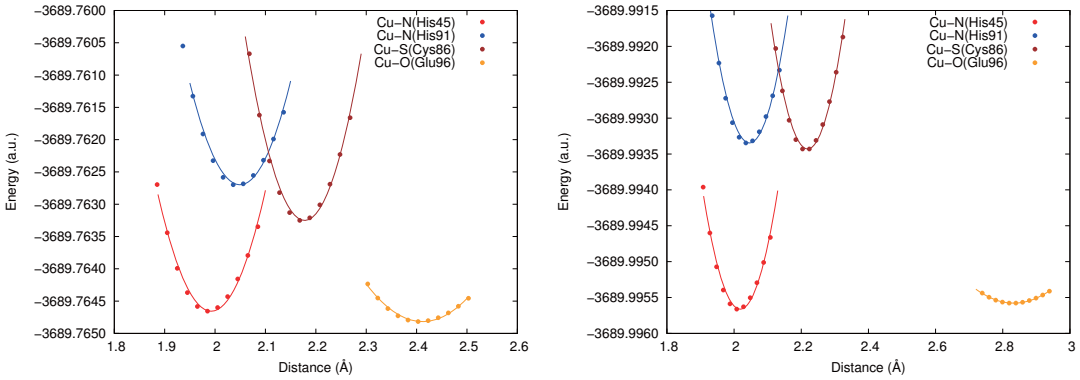

(a) (b)

FIGURE 2.11: Potential energy surface for bond distance around T1Cu of Stellacyanin in (a) oxidized and (b) reduced state calculated by B3LYP.

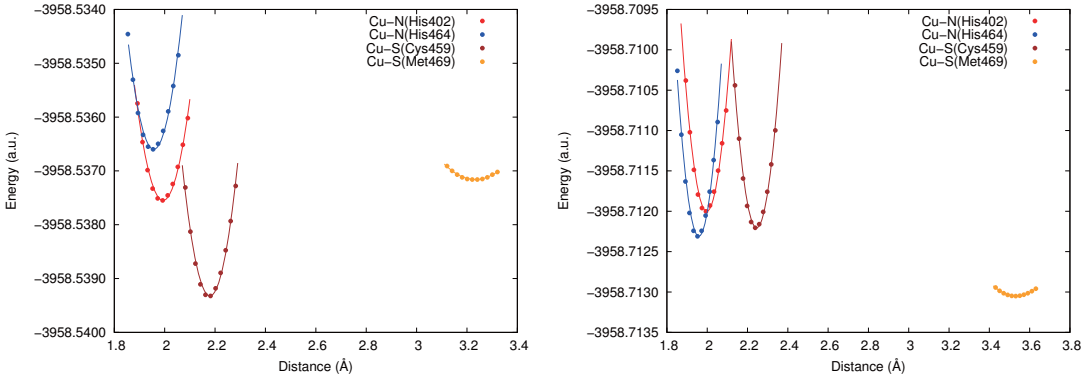

(a) (b)

FIGURE 2.12: Potential energy surface for bond distance around T1Cu of MCOs in (a) oxidized and (b) reduced state calculated by B3LYP.

TABLE 2.7: Fitting parameter for bond distance around T1Cu of MCOs calculated by B3LYP (M06).

Bond	Reduced State			Oxidized State		
	r_{PDB}	r_c	K_r	r_{PDB}	r_c	K_r
Cu-N(His402)	2.072	1.99 (1.95)	104.28 (129.56)	2.01	2.00 (1.92)	89.57 (139.47)
Cu-N(His464)	1.974	1.96 (1.92)	121.49 (152.54)	2.03	1.96 (1.95)	107.79 (112.10)
Cu-S(Cys459)	2.302	2.18 (2.14)	126.97 (149.02)	2.30	2.25 (2.20)	92.3 (113.79)
Cu-S(Met469)	3.061	3.23 (2.96)	11.88 (32.57)	3.23	3.53 (3.12)	6.24 (34.62)

The unit of distance (r) and force constant (K_r) are Å and kcal $\mathrm{mol}^{-1}\mathrm{Å}^{-2}$, respectively.

2.4 Conclusion

We have presented a model cluster of T1Cu obtained from several copper protein, i.e. Azurin, Plastocyanin, Stellacyanin, and MCOs. Several properties, such as atomic partial charge, atomic partial spin, ionization potential (IP) of reduced T1Cu, electron affinity (EA) of oxidized T1Cu, bond and angle constants, etc. have been discussed in

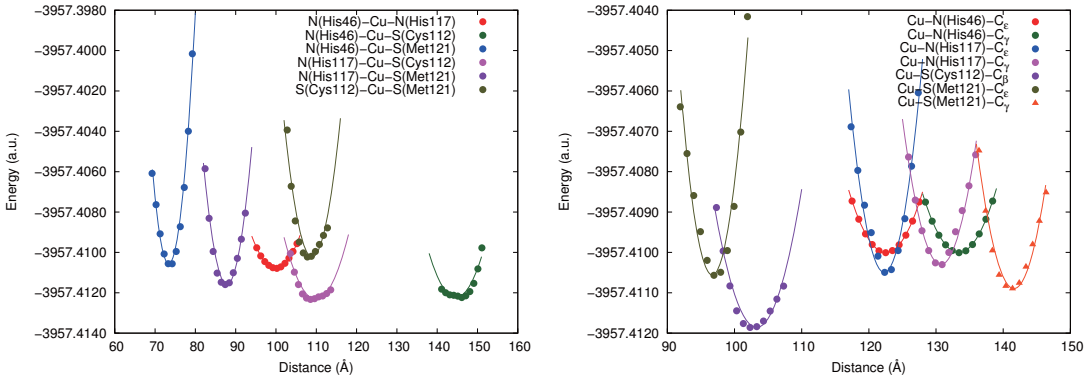

(a)

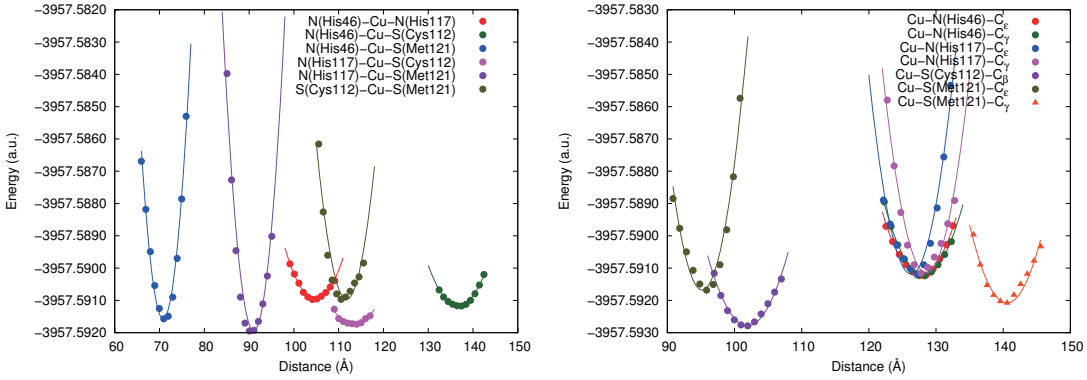

(b)

FIGURE 2.13: Potential energy surface for bond angle around T1Cu of Azurin in (a) oxidized and (b) reduced state calculated by M06.

TABLE 2.8: Fitting parameter for bond angle around T1Cu of Azurin calculated by B3LYP (M06).

Angle	Reduced State			Oxidized State		
	θ_{PDB}	θ_c	K_θ	θ_{PDB}	θ_c	K_θ
N(His46)-Cu-N(His117)	104	105 (100)	64 (93)	103	103 (105)	68 (70)
N(His46)-Cu-S(Cys112)	132	139 (145)	54 (103)	133	139 (137)	43 (58)
N(His46)-Cu-S(Met121)	75	73 (73)	558 (589)	73	70 (71)	478 (457)
N(His117)-Cu-S(Cys112)	124	116 (110)	44 (101)	123	115 (113)	34 (44)
N(His117)-Cu-S(Met121)	84	88 (88)	406 (367)	88	91 (91)	387 (413)
S(Cys112)-Cu-S(Met121)	110	110 (109)	208 (287)	112	113 (112)	155 (218)
Cu-N(His46)-C_ε	124	121 (123)	103 (104)	126	125 (128)	105 (128)
Cu-N(His46)-C_γ	132	135 (133)	103 (104)	130	131 (128)	104 (132)
Cu-N(His117)-C_ε	124	121 (122)	217 (334)	128	124 (126)	215 (322)
Cu-N(His117)-C_γ	129	133 (131)	188 (227)	127	131 (129)	205 (304)
Cu-S(Cys112)-C_β	109	107 (103)	88 (157)	108	106 (102)	75 (128)
Cu-S(Met121)-C_ε	99	97 (97)	425 (430)	98	95 (95)	342 (349)
Cu-S(Met121)-C_γ	138	142 (142)	245 (236)	137	142 (141)	134 (161)

The unit of angle (θ) and force constant (K_θ) are (°) and kcal mol^{-1}rad^{-2}, respectively.

relation to DFT functionals. We have found that DFT functional affect to the properties of atomic partial charge and atomic partial spin. In M06 calculation, negative charge

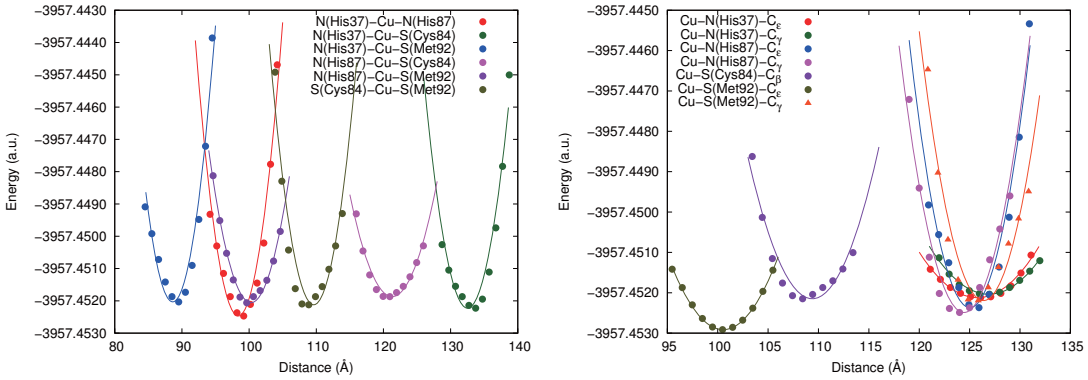

(a)

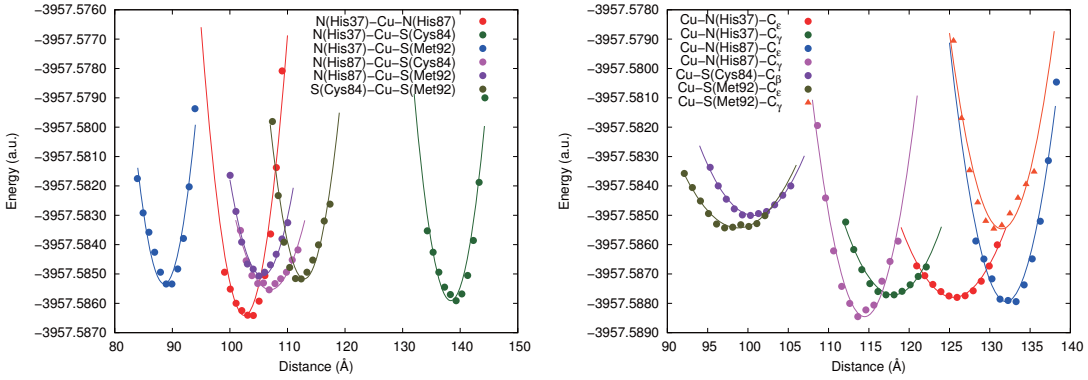

(b)

FIGURE 2.14: Potential energy surface for bond angle around T1Cu of Plastocyanin in (a) oxidized and (b) reduced state calculated by M06.

TABLE 2.9: Fitting parameter for bond angle around T1Cu of Plastocyanin calculated by B3LYP (M06).

Angle	Reduced State			Oxidized State		
	θ_{PDB}	θ_c	K_θ	θ_{PDB}	θ_c	K_θ
N(His37)-Cu-N(His87)	99	101 (104)	75 (82)	97	97 (99)	219 (229)
N(His37)-Cu-S(Cys84)	136	137 (139)	92 (112)	132	131 (134)	140 (123)
N(His37)-Cu-S(Met92)	88	88 (89)	181 (181)	89	88 (90)	225 (201)
N(His87)-Cu-S(Cys84)	110	108 (107)	57 (57)	121	122 (121)	106 (98)
N(His87)-Cu-S(Met92)	106	106 (105)	221 (188)	101	100 (100)	228 (240)
S(Cys84)-Cu-S(Met92)	113	113 (112)	148 (148)	110	111 (109)	152 (133)
Cu-N(His37)-C_ε	117	123 (126)	64 (80)	123	123 (126)	76 (62)
Cu-N(His37)-C_γ	126	120 (117)	53 (73)	129	130 (127)	75 (66)
Cu-N(His87)-C_ε	127	129 (133)	82 (105)	124	123 (126)	149 (171)
Cu-N(His87)-C_γ	120	117 (114)	71 (130)	126	127 (124)	135 (179)
Cu-S(Cys84)-C_β	101	106 (100)	38 (44)	110	111 (108)	53 (70)
Cu-S(Met92)-C_ε	95	99 (97)	99 (81)	96	100 (100)	113 (102)
Cu-S(Met92)-C_γ	133	133 (131)	62 (82)	127	127 (126)	79 (106)

The unit of angle (θ) and force constant (K_θ) are (°) and kcal $\mathrm{mol}^{-1}\mathrm{rad}^{-2}$, respectively.

of Cys sulfur atom is more distributed onto the other atom, especially Cu atom. Also, the distribution of unpaired electron of Cu calculated by M06 is more delocalized, which

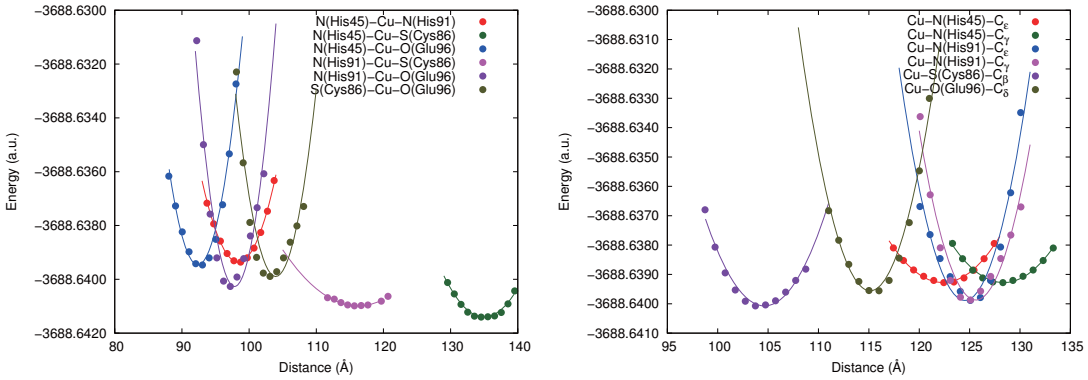

(a)

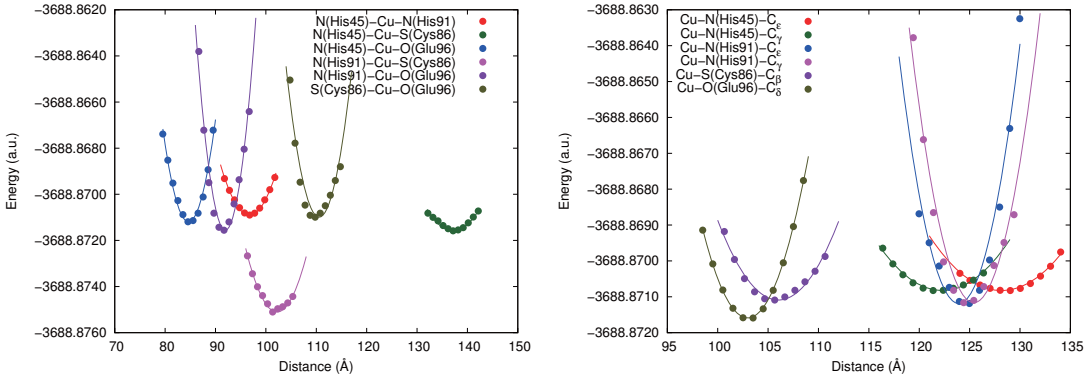

(b)

FIGURE 2.15: Potential energy surface for bond angle around T1Cu of Stellacyanin in (a) oxidized and (b) reduced state calculated by M06.

TABLE 2.10: Fitting parameter for bond angle around T1Cu of Stellacyanin calculated by B3LYP (M06).

Angle	Reduced State			Oxidized State		
	θ_{PDB}	θ_c	K_θ	θ_{PDB}	θ_c	K_θ
N(His45)-Cu-N(His91)	100	97 (98)	212 (213)	98	95 (97)	130 (136)
N(His45)-Cu-S(Cys86)	128	131 (135)	84 (88)	132	134 (137)	63 (72)
N(His45)-Cu-S(Met96)	94	91 (92)	367 (400)	87	83 (85)	290 (319)
N(His91)-Cu-S(Cys86)	126	116 (116)	39 (34)	125	118 (102)	26 (148)
N(His91)-Cu-O(Gln96)	95	98 (98)	513 (529)	90	92 (92)	522 (518)
S(Cys86)-Cu-O(Gln96)	105	105 (104)	295 (394)	111	112 (111)	184 (313)
Cu-N(His45)-C_ε	121	121 (122)	95 (102)	128	125 (128)	52 (61)
Cu-N(His45)-C_γ	129	130 (128)	95 (102)	122	126 (122)	54 (65)
Cu-N(His91)-C_ε	127	123 (125)	297 (383)	126	122 (124)	257 (404)
Cu-N(His91)-C_γ	123	127 (126)	294 (376)	123	127 (125)	248 (384)
Cu-S(Cys86)-C_β	108	109 (105)	77 (178)	108	110 (106)	73 (126)
Cu-O(Glu96)-C_δ	117	115 (115)	365 (364)	106	104 (103)	260 (256)

The unit of angle (θ) and force constant (K_θ) are (°) and kcal $\mathrm{mol}^{-1}\mathrm{rad}^{-2}$, respectively.

is indicated by low value of atomic partial spin of Cu. Bearing on bond constant, M06 produce this parameter around T1Cu in all clusters that is larger than those calculated

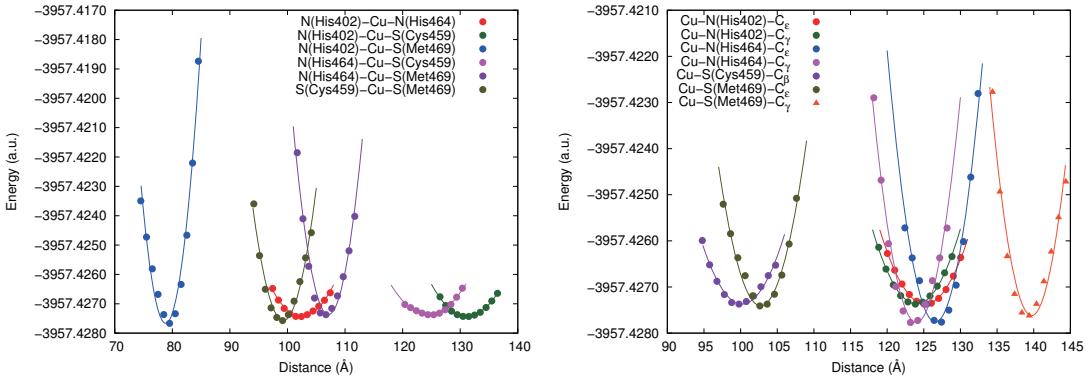

(a)

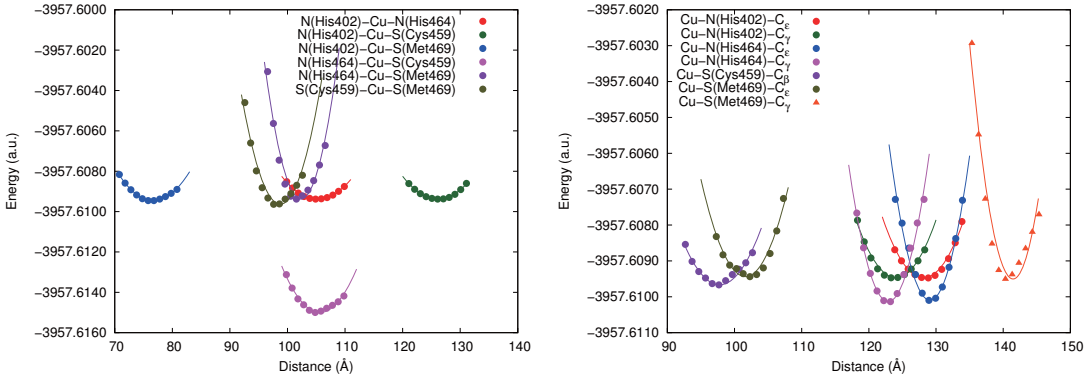

(b)

FIGURE 2.16: Potential energy surface for bond angle around T1Cu of MCOs in (a) oxidized and (b) reduced state calculated by M06.

TABLE 2.11: Fitting parameter for bond angle around T1Cu of MCOs calculated by B3LYP (M06).

Angle	Reduced State			Oxidized State		
	θ_{PDB}	θ_c	K_θ	θ_{PDB}	θ_c	K_θ
N(His402)-Cu-N(His464)	103	102 (102)	93 (72)	105	105 (105)	78 (60)
N(His402)-Cu-S(Cys459)	129	131 (131)	93 (59)	126	130 (126)	69 (62)
N(His402)-Cu-S(Met469)	79	78 (79)	419 (529)	78	76 (77)	359 (74)
N(His464)-Cu-S(Cys459)	124	120 (124)	36 (50)	128	121 (106)	26 (109)
N(His464)-Cu-S(Met469)	107	107 (107)	375 (355)	102	102 (102)	370 (348)
S(Cys459)-Cu-S(Met469)	100	100 (99)	236 (284)	100	100 (99)	174 (246)
Cu-N(His402)-C_ε	125	123 (125)	94 (86)	127	125 (128)	89 (93)
Cu-N(His402)-C_γ	124	126 (124)	98 (93)	125	127 (124)	90 (94)
Cu-N(His464)-C_ε	125	125 (127)	205 (280)	127	127 (129)	210 (240)
Cu-N(His464)-C_γ	125	126 (124)	204 (278)	125	125 (123)	202 (227)
Cu-S(Cys459)-C_β	100	105 (100)	43 (92)	100	103 (98)	40 (84)
Cu-S(Met469)-C_ε	104	102 (103)	181 (188)	103	101 (102)	153 (127)
Cu-S(Met469)-C_γ	140	141 (140)	240 (314)	141	143 (141)	190 (324)

The unit of angle (θ) and force constant (K_θ) are (°) and kcal mol^{-1}rad^{-2}, respectively.

by B3LYP. In particular, the dependency on DFT functional is found to be more significant in the case of the bond between Cu and axial ligand. This indicate that M06

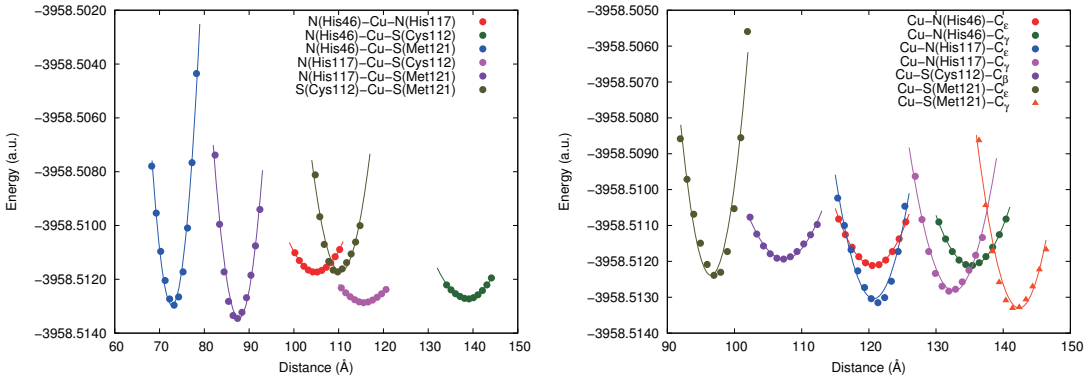

(a)

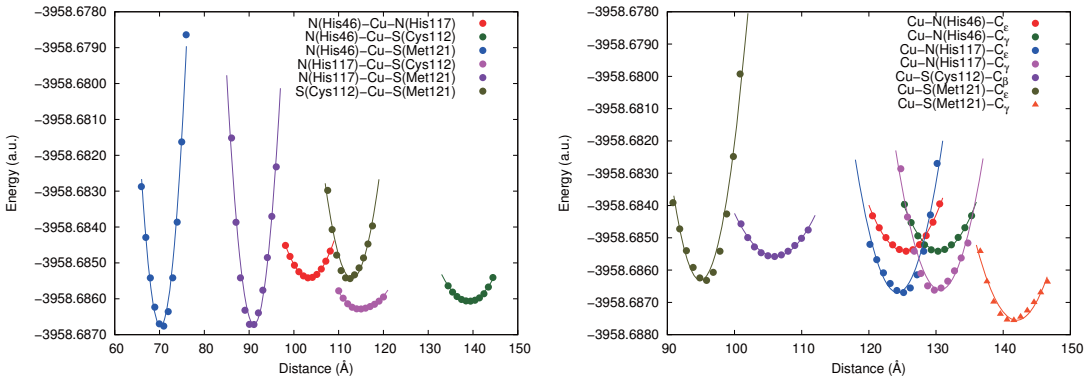

(b)

FIGURE 2.17: Potential energy surface for bond angle around T1Cu of Azurin in (a) oxidized and (b) reduced state calculated by B3LYP.

can handle long-range interaction better than B3LYP does. However, we did not find any consistent contribution of DFT function in the case of angle constant due to the complexity of the calculation.

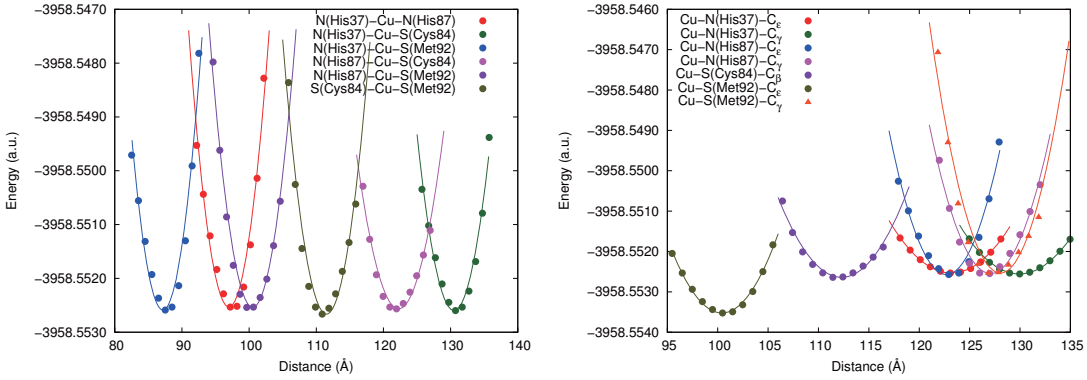

(a)

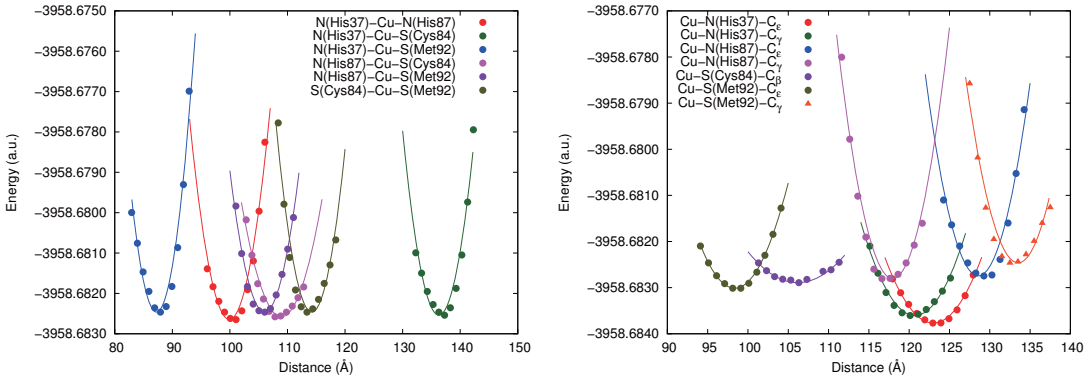

(b)

FIGURE 2.18: Potential energy surface for bond angle around T1Cu of Plastocyanin in (a) oxidized and (b) reduced state calculated by B3LYP.

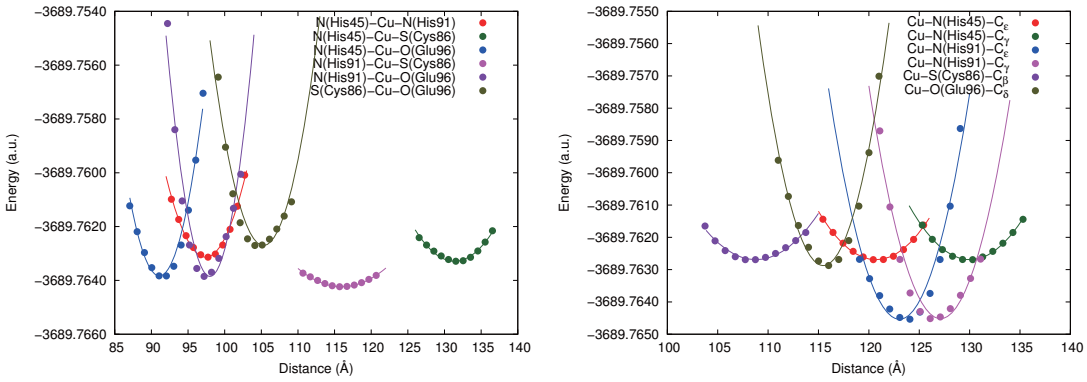

(a)

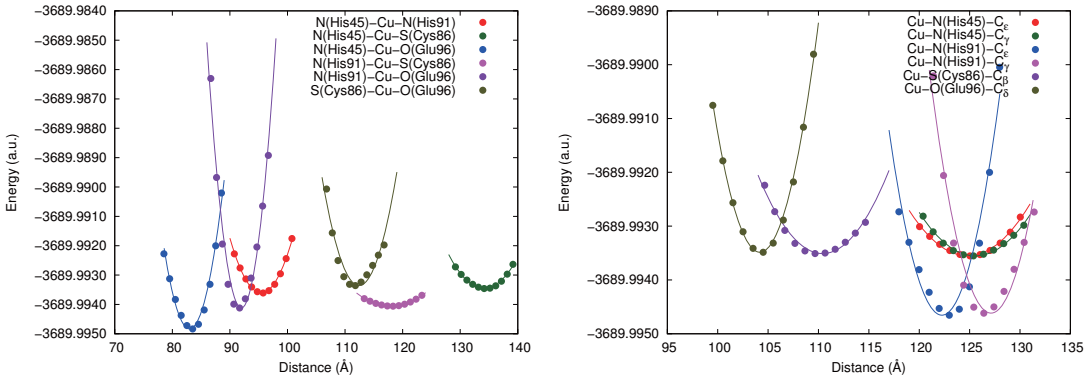

(b)

FIGURE 2.19: Potential energy surface for bond angle around T1Cu of Stellacyanin in (a) oxidized and (b) reduced state calculated by B3LYP.

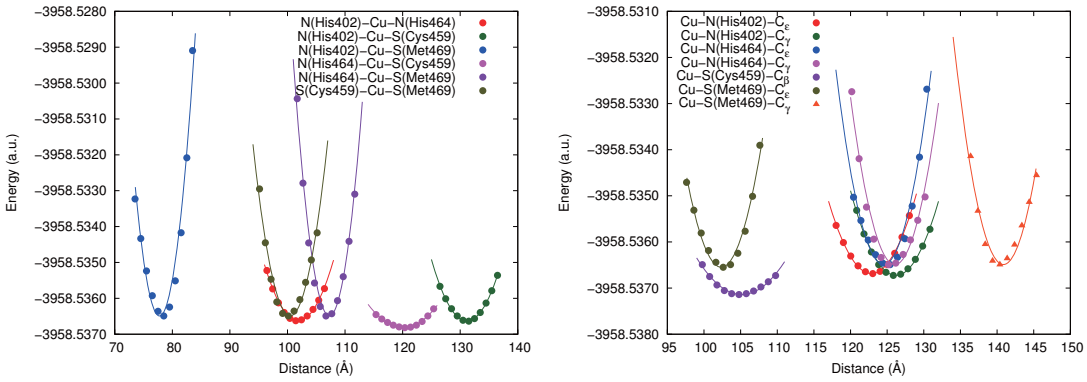

(a)

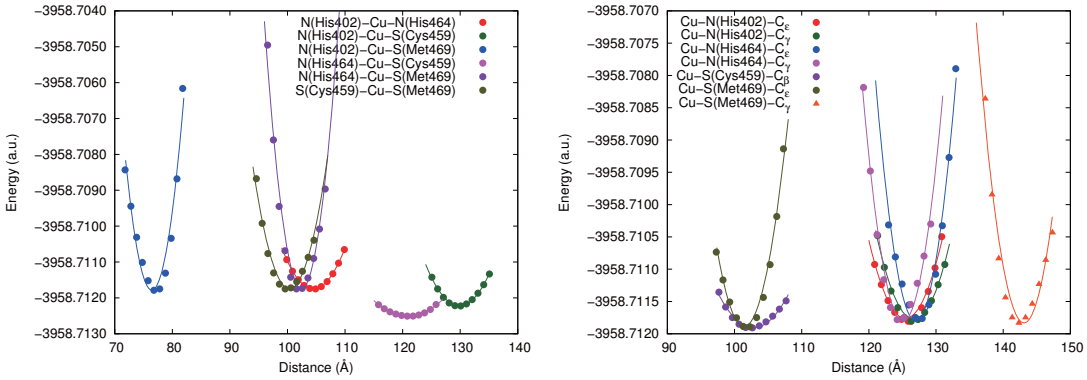

(b)

FIGURE 2.20: Potential energy surface for bond angle around T1Cu of MCOs in (a) oxidized and (b) reduced state calculated by B3LYP.

Chapter 3

Quantum Chemical Study of the Axial Ligand Effect on the Electronic Properties of Type I Copper Protein

3.1 Introduction

Type I copper (T1Cu) proteins, such as Azurin, Plastocyanin, Stellacyanin, etc., play an important role in a various biomolecular processes involving electron transfer.[10, 11, 98] This proteins receive an electron from other proteins with higher redox potential and transfer the electron to other protein with lower redox potential.[16, 64, 65] T1Cu protein is recognized by an intense blue color arising from a charge transfer from ligand to metal, which the band is observed around 600 nm, and a narrow hyperfine splitting of spectrum analysis using electron paramagnetic resonance.[5] This proteins present relatively high value of redox potential and the secondary structure is quite similar between the structure in oxidized and reduced state.[99] T1Cu protein contains a copper cluster, the so-called type I copper center (T1CC), which the geometrical structure is closely to trigonal bypyramidal. Generally, copper ion (Cu) in T1CC bound to a cysteine (Cys) and two histidines (His) in equatorial position, and also bound to methionine (Met) in axial position. A short bond distance between Cu and Cys is known to be highly covalent and thus arise an intense of charge-transfer band.[10]

On the contrary, Met bound to Cu with the bond distance more than 3 and interact with a long-range interaction.[10] Although the interaction between Cu and Met is

relatively weak, several groups has reported that this interaction contribute to protein function.[100–106] The contributions of axial ligand interaction have been investigated by Li and coworkers. They found that the lack of the ligand give a contribution to redox potential of T1Cu protein.[101] The study by Garner and coworkers have also revealed the contribution of axial ligand in stabilizing protein structure. The lack of the ligand lead to protein destabilization due to the change of hydrophobic or hydrogen bond interaction around T1CC.[102] Furthermore, several studies have revealed the other roles of the axial ligand, such as steric protection of Cu ion and geometric control.[104, 105]

Several groups have investigated some properties of T1CC, such as absorption wavelength, EPR spectra, and redox potential.[66–70, 75] The absorption wavelength and EPR spectra of T1CC have been investigated by Somolon and coworkers.[67] They have also investigated the other properties, such as room temperature circular dichroism and magnetic circular dichroism spectra, of several T1Cu proteins, such as Azurin, Plastocyanin, and Stellacyanin. Meanwhile, the electronic structure and properties of T1CC have also been studied by using computational method. For example, the interactions between Cu and ligand have been investigated by using quantum mechanical method by Solomon and coworkers. The results of their studies have been discussed in relation to the electronic structure.[16, 95]

This study aimed to investigate the effect of axial ligand (Met) on the properties of T1Cu protein by using density functional theory (DFT) with long-range correction (LC) scheme. For typical example, we prepared T1CC extracted from X-ray crystal structure of Azurin protein (PDB ID 4AZU).[22] As shown in Figure 3.1, we prepared T1CC model cluster that consists of a copper ion, a cysteine, two histidines, and a methionine. In the term of axial ligand, we neglect Glycine (Gly) axial ligand of T1CC in Azurin because the contribution is much less effective than Met ligand.[100]

3.2 Computational Methods

3.2.1 The Model of Type 1 Copper Center

The calculations of electronic structure and properties of T1CC cluster are conducted by utilizing eight density functional theory (DFT) functionals. Those functionals is chosen with respect to several classes of DFT functionals, i.e. (i) pure generalized gradient approximation (GGA) (PBE and BLYP), (ii) hybrid (B3LYP and M06), (iii) long-range corrected (LC)-GGA (LC-BLYP and LC-ωPBE), and (iv) LC hybrid (ωB97X and CAM-B3LYP). We investigated the long-range interaction of axial Met ligand by calculating equilibrium bond distance and bond constant of Cu-Met bond, redox potential, and

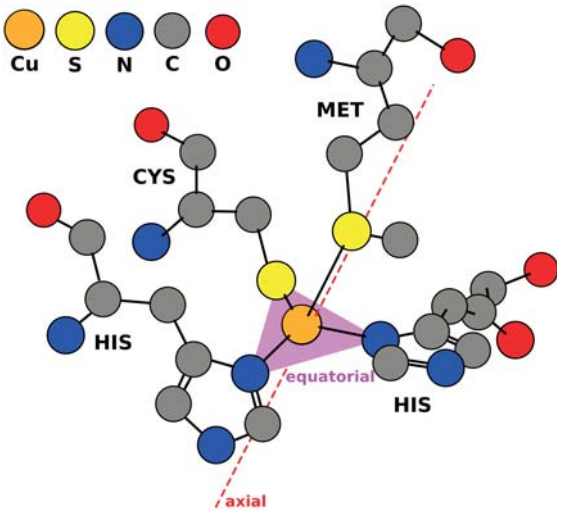

FIGURE 3.1: A schematic diagram of T1CC model cluster.

maximum absorption wavelength (MAW). In the case of redox potential and MAW, the calculations are performed by utilizing several T1CC model cluster with varied distance of Cu-Met bond. Thus, we prepared five T1CC clusters with Cu-Met bond distances are 3.18, 3.28, 3.38, 3.48, and 3.58 .

3.2.2 Force Field and Electronical Properties

We calculated equlibrium bond distances and bond constants by approximating potential energy surface (PES) along with Cu-Met bond distance. Then, equlibrium bond distances and bond constants are calculated from fitting analysis of PES using a harmonic potential function as[89]

$$V(r, K_r) = K_r(r - r_c)^2 \tag{3.1}$$

which K_r and r_c means bond constant and equilibrium bond constant, respectively. Meanwhile, redox potential (E_{redox}) of T1CC is calculated by using Nernst's equation

$$E_{\text{redox}} = \frac{\Delta G_{\text{redox}}}{nF} - E_{\text{NHE}} \tag{3.2}$$

which ΔG_{redox} represents the Gibbs free energy for redox reaction, E_{NHE} represents reference potential (4.44 V),[107], n and F are the number of electron involve in reaction, and Faraday constant (96.485 kJ/mol.V), respectively. In the meantime, MAW is approximated by using time-dependent DFT method with polarizable continuum solvation model ($\varepsilon = 10$).[108] In the term of redox potential and MAW, relative values of those properties is calculated instead of absolute value. The calculation of relative values is performed by subtracting the absolute values with the minimum values. However, the

TABLE 3.1: The absolute value of minimum energy, redox potential, and absorption wavelength.

Method	Relative Minimum Energy (kcal/mol)	Redox Potential (mV)	Maximum Absorption Wavelength (nm)
BLYP	356.42	822	579
PBE	1553.75	616	580
B3LYP	0.00	552	603
M06	696.42	224	604
LC-BLYP	3065.50	191	758
LC-ωPBE	929.15	229	724
ωB97X	244.79	353	682
CAM-B3LYP	434.19	449	678
Exp.	-	341[a]	631[b]

[a] Ref. [69]
[b] Ref. [70]

absolute values of those properties are presented in Table 3.1. The accuracy of calculation is estimated by calculating relative error from the comparison between calculated results and experimental data, which the relative error given by

$$\text{Error}_{\text{relative}} = \frac{|P_{\text{calc}} - P_{\text{exp}}|}{P_{\text{exp}}} \tag{3.3}$$

where P_{calc} and P_{exp} mean the value of the properties obtained from calculation and experiment, respectively. All of the calculations are conducted by using Gaussian 09 package.[92]

3.3 Results and Discussions

3.3.1 Equilibrium Bond Distance and Bond Constant

The plot of PES along with the bond distance between Cu and Met is presented in Figure 3.2. We scaled the energies value by subtracting the value with minimum energies. From the figure, the position of curve indicates the equilibrium bond distance and the curvature indicates the bond constant. In the case of equilibrium bond distance, M06 produced the bond distance (3.24) with the value is closest to the bond distance obtained from X-ray crystal structure (3.18). In the meantime, we found that BLYP produce a poor result that indicated by a large deviation of the bond distance in comparison with the distance obtained from X-ray structure. We calculated the relative minimum energy for each DFT functional by subtracting the energies with B3LYP minimum energy. The value of relative minimum energies are presented in Table 3.1.

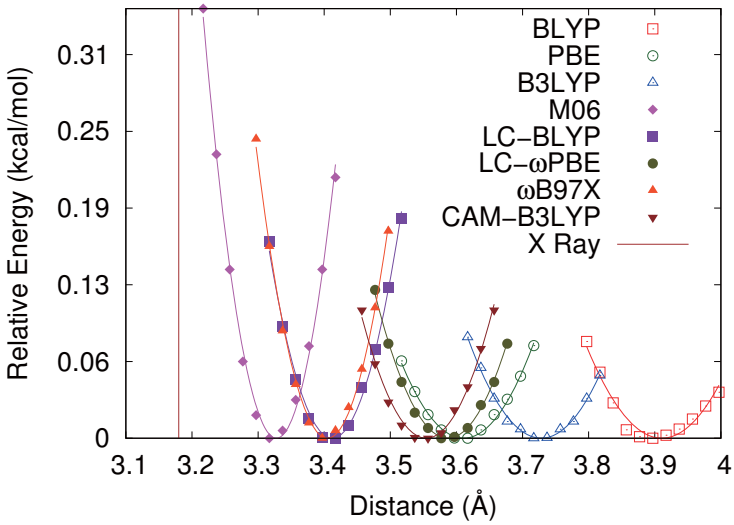

FIGURE 3.2: Potential energy surface along Cu-Met bond distance calculated by using various type of DFT functional.

The bond constants of Cu-Met bond obtained from the approximation of fitting analysis were summarized in Table 2. The Cu-Met bond constants obtained from the fitting procedure were summarized in Table 2. We found that M06 produce the highest value of bond constants. Indeed, the bond constant obtained from M06 calculation (43.64 kcal/-mol) is almost two times higher than those obtained from ωB97X (20.46 kcal/mol), as the second higher. This suggest that long-range interaction of Cu-Met bond is presented by M06 calculation in the stronger way. Although the expression of explicit long-range correction does not involved in M06 functional, but this functional utilizes a mixing scheme of meta-GGA exchange functional with non-local HF exchange functional in a proper way. For the case of bond constant, the mixing scheme in hybrid M06 is found to be more dominant than the contribution of explicit LC scheme in LC-DFT. By comparing to another hybrid functional, the bond constant obtained from M06 calculation is almost seven times higher than those obtained from B3LYP calculation (6.67 kcal/mol). This is related to the fact that M06 utilize meta-GGA exchange functional instead of pure GGA functional, as used in B3LYP.[59] As we expected, BLYP present the weakest long-range interaction of Cu-Met bond due to the lack of LC scheme.

3.3.2 Redox Potential and Maximum Absorption Wavelength

The plot of relative redox potential as a function of Cu-Met bond distance is presented in Figure 3.3. From the Figure, we confirms the contribution of the interaction between Cu and axial Met ligand to redox potential. The value of redox potential is found to be decreased along with the increasing of the bond distance. In this calculation, we found that the series of LC-DFT is more sensitive to the change of the bond distance than

TABLE 3.2: Fitting parameter for bond distance of Cu-Met.

Method	$r_c()$	K_r (kcal/mol)
BLYP	3.91	5.79
PBE	3.61	6.95
B3LYP	3.73	6.67
M06	3.24	43.63
LC-BLYP	3.41	16.91
LC-ωPBE	3.59	9.73
ωB97X	3.40	20.46
CAM-B3LYP	3.55	10.43
X-ray structure	3.18	-

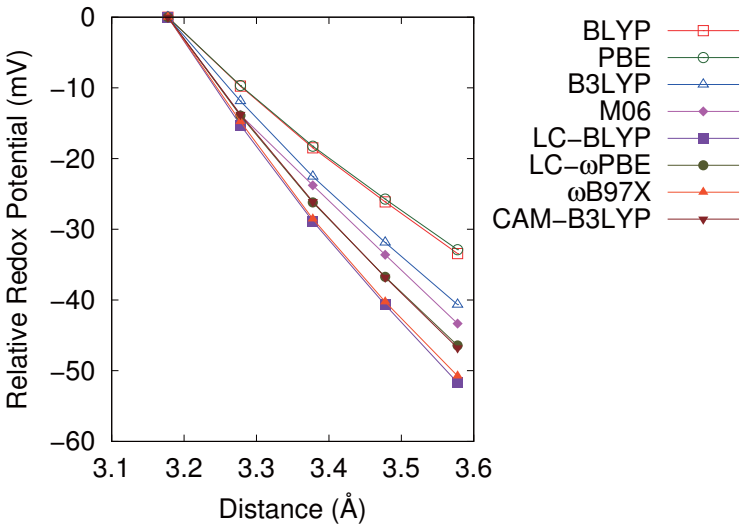

FIGURE 3.3: Relative redox potential as a function of Cu-Met bond distance.

non-LC-DFT. Amongst LC-DFT, LC-BLYP present the most sensitive functional with the tendency is close to ωB97X functional. Meanwhile, PBE and BLYP functional is much less sensitive to the change of the bond distance, which correspond to similar LC scheme deficiency. This results indicate the effect of LC scheme on the bond distance sensitivity of DFT functional for redox potential calculation.

Bearing on accuracy, the relative error of redox potential is calculated and shown in Figure 3.4 We found poor results produced from pure GGA calculation that is indicated by high value of the error. We also found that the accuracy of LC-DFT calculation is better than non-LC-DFT calculation, except for M06. The accuracy of M06 is relatively similar to LC-DFT calculation. In this case, the performance of mixing scheme of exchange functional in M06 is quite similar to the contribution of LC scheme in LC-DFT. The ωB97X functional produce the best result indicate that the LC scheme implemented in this functional is better than others. We present the contribution of LC scheme explicitly by comparing between BLYP with LC-BLYP, and B3LYP and CAM-B3LYP.

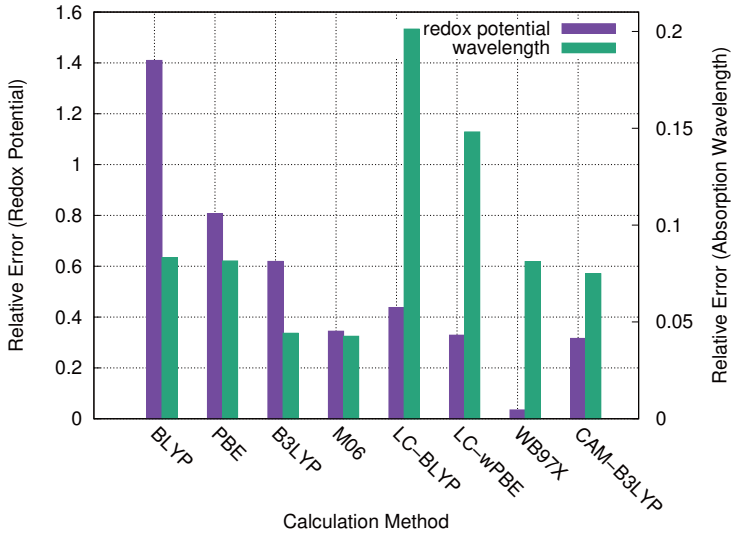

FIGURE 3.4: The relative error in the calculation of redox potential and absorption wavelength.

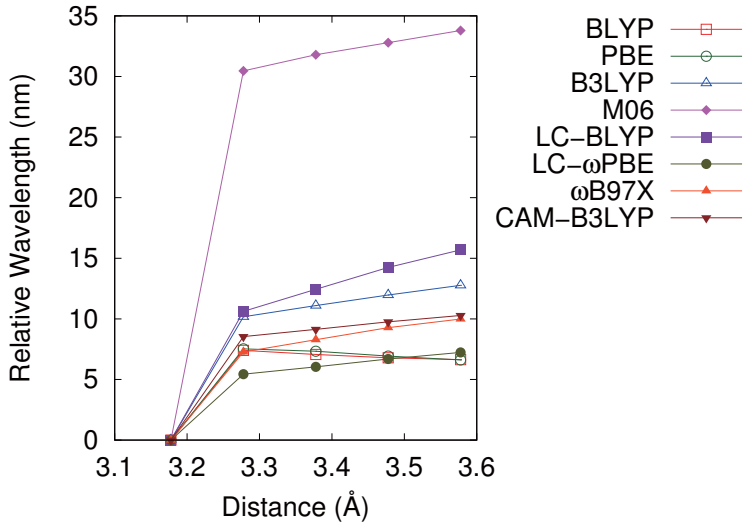

FIGURE 3.5: The relative absorption wavelength as a function of Cu-Met bond distance.

The utilization of LC scheme in BLYP and B3LYP reduce the error by 0.97 (from 1.40 to 0.43) and 0.30 (from 0.61 to 0.31), respectively. This results suggest the contribution of the LC scheme to improve the accuracy of redox potential.

We present the plot of relative MAW as a function of Cu-Met bond distance in Figure 3.5. From the figure, we confirm that the bond distance of Cu-Met bond give a contribution to MAW. The wavelength is found to be increased along with the increasing of the bond distance. The tendency of BLYP and PBE functional are found to be similar as the consequence of similar type of pure GGA DFT functional. In the term of MAW, M06 is found to be the most sensitive to the change of bond distance. However, any significant contribution of LC scheme is not found in the sensitivity of the bond distance to MAW.

In the term of the accuracy of MAW, we found that pure GGAs calculation produce the result that is more accurate than LC pure GGAs. This results correspond to the fact that MAW of T1Cu mainly raised by electron transition from $d_{x^2-y^2}$ orbital of Cu to π orbital of Cys sulfur. In this transition, Met orbital has no contribution and thus the short-range interaction of Cu-Cys is more dominant than long-range interaction of Cu-Met. Meanwhile, the most accurate result was obtained from M06 calculation, in which the accuracy is almost similar to B3LYP's. This finding point out the contribution of mixing scheme in hybrid functional in enhancing the ability to handle both short and long-range interaction.

3.4 Conclusion

In summary, we have investigated and confirmed the contribution of axial ligand on the properties of T1Cu protein, i.e. bond constant, redox potential and MAW. To perform the calculation, several type of DFT functional that represent some class of DFT functional were chosen, i.e. (i) pure generalized gradient approximation (GGA) (PBE and BLYP), (ii) hybrid (B3LYP and M06), (iii) long-range corrected (LC)-GGA (LC-BLYP and LC-PBE), and (iv) LC hybrid (B97X and CAM-B3LYP). Regarding on long-range interaction of Cu-Met bond, we confirmed the contribution of LC scheme and hybrid scheme of DFT in improving the accuracy of redox potential calculation. This result correspond to the ability of those LC-DFT and hybrid DFT in accounting the long-range interaction. However, as for MAW calculation, we found that LC scheme do not perform well because short-range interaction is more dominant than long-range interaction in this calculation.

Chapter 4

Theoretical Study on the Contribution of Spin Structure to Redox Potential of [2Fe-2S] Core Cluster from Iron-Sulfur Proteins

4.1 Introduction

Iron sulfur proteins are usually exist in living organism and take a role in variety processes in biological systems, such as nitrogen fixation, photosynthesis, and respiration.[36, 109, 110] This proteins present a broad range of redox potential and thus allow them to interact with many types of redox substrates by acting as electron carriers.[29, 30] This proteins contain one or more iron-sulfur clusters that comprised by one to eight iron atoms, cysteine's sulfur atoms, and inorganic acid labile sulfurs that connect the cluster with peptides. In supporting biological processes, this clusters present an important role in several functions such as radical chain stabilization,[36] redox reaction,[29, 30] and Lewis acids.[35] The classification of iron-sulfur clusters are suggested in the basis of the number of iron and sulfur atoms, structural motif, and its electrochemical and spectroscopic properties.[109] Despite the similarity of iron-sulfur clusters in several iron-sulfur proteins, the residues of those proteins are found to interact with the cluster in different way. Hence, in order to know the function of this protein, it is necessary to know the environmental effect in the vicinity of the cluster.

Iron-sulfur proteins are classified into several classes. Ferredoxins is one of those classes that present low molar mass and also support several biological pathways of electron

transfer by acting as electron carriers.[39] This proteins are recognized from the feature of EPR signal as that from a nonheme iron.[111, 112] Similar to the other iron-sulfur protein, ferredoxins have also a broad range of redox potential that allow them to interact with a various type of redox substrate in several important processes in biological systems.[29, 30, 109, 113]

Furthermore, ferredoxins are classified into several classes. [2Fe-2S] ferredoxin is one of ferredoxins classes that contain a complex cluster of two iron atoms, two inorganic sulfur atoms, and four cysteine thiolates. [2Fe-2S] Ferredoxins have attracted much interest for their function in supporting many biological processes, and thus the number of studies to explore structure-function relationships of this protein have also been increased. [33, 113–115] In 1962, Tagawa and Arnon have obtained the first crystal structure of a clostridium ferredoxin by using X-ray studies. They continue their study with the measurement of redox potential of the protein.[115] Regarding iron-sulfur cluster, Buchanan et.al. confirmed the existence of inorganic sulfur atom in the cluster, in which the amount of sulfur is equimolar with non-heme iron protein.[33] Furthermore, Tagawa and Arnon reinvestigated the redox potential and stoichiometry of electron transfer process of ferredoxin.[115] According to their studies, the value of redox potential of spinach ferredoxin is found as about -420 mV.

In order to enhance the understanding of this protein, several theoretical studies of ferredoxins have also been conducted.[116–120] Noodleman and coworkers performed X valence bond scattered wave (X-VB-SW) calculation to investigate the structure of various cluster that is mimicked the iron-sulfur cluster.[116] Their studies reveal that the bonds between iron and inorganic bridging sulfur are stronger than the bonds between iron and sulfur of thiolate. Then, Noodleman and coworkers continued their studies with the estimation of antiferromagnetic coupling constants in the cluster by using broken symmetry analysis.[117] Even though they obtain an overestimated results compare to the corresponding experimental data, but they found the tendency of the results is in agreement the experimental data, which indicate the validity of the method.

Meanwhile, Mouesca and coworkers calculated redox potential of iron-sulfur cluster by utilizing several parameters into their calculation, i.e. ground state energies, spin Hamiltonian, and resonance delocalization. They approximated the value of those parameters from the results of calculation in low spin and high spin state.[118] By using those parameters, they obtained a results that are in good agreement with experimental data. In their calculations, they also suggested the concept of spin and electron delocalization barycenter that is similar to the concept of ligand field stabilization theory. Several factors that determine the magnitude of redox potential of ferredoxins protein have been

analyzed by Banci and coworkers. They confirmed the contribution of the net charges of acidic and basic groups to the wide range of redox potential of ferredoxin proteins.

Recently, we have suggested an accurate approximation method to calculate the redox potentials of organic and inorganic compound by means of electronic structure calculations with solvation models.[121–123] Since the estimation of solvation free energies of highly charged ions by using solvation model often fail, the calculation of redox potential of transition metal complexes with +3/-3 charges by using conventional methods is over or underestimated the experimental data. Later, by adding correction terms originated from counter ion around the metal complexes, referred as a Pseudo Counter Ion Solvation Scheme (PCIS), we have succeeded in reproducing the redox potential of transition metal complexes within 0.25 V.[122] The environment of protein is usually modeled by a dielectric medium with $\varepsilon = 4-10$ and the difference of the results by using the solvation model and those by real models represent the importance of the actual protein environment. Hence, redox potential of metalloproteins such as heme proteins, iron-sulfur proteins, and copper proteins is interesting to be estimated by using the present method and evaluate the performance of the method.

This study aim to calculate the redox potential of two [2Fe-2S] ferredoxins, i.e., spinach ferredoxin and adrenodoxin. Regarding accuracy, the relative values of redox potentials between two proteins are analyzed, instead of absolute ones to reduce systematic error. Particularly, we investigated the contribution of DFT functionals and two basis sets w/wo diffuse function to redox potential. The contribution of DFT functionals is investigated by utilizing two typical DFT functionals, i.e. B3LYP and M06. M06, that is originally proposed by Zhao and Truhlar,[59, 85] has been reported to give better results than B3LYP for the calculation of organic and inorganic molecules.[86–88] We present a cluster model containing an [2Fe-2S] iron-sulfur cluster with several possible spin states. Thus, four spin approximations are utilized related to the spin issue, as will explain below. The solvent contribution around the cluster was treated by using implicit solvation model. The combination of the methodologies and spin approximation are summarized in relation to the accuracy of the redox potential of [2Fe-2S] ferredoxins. In addition, the singly occupied natural orbital (SONO) and atomic partial charge of the cluster in reduced state are investigated to get the insight about the difference of redox potentials between two ferredoxins.

4.2 Computational Methods

4.2.1 The Model of Iron-Sulfur Cluster

The calculations were performed by using two typical DFT functionals, i.e. B3LYP and M06, combined with two basis sets, i.e. 6-31G(d) and 6-31G(d,p), w/wo diffuse functions. All calculations were conducted by using Gaussian 09 program package.[92] We investigated two iron-sulfur proteins, i.e. ferredoxin and adrenodoxin, for typical example. The models of iron-sulfur cluster were prepared from X-ray crystal structures of ferredoxin (PDBID 1A70[124]) and adrenodoxin (PDBID 2MJD[125] and 2MJE[125]). The clusters consist of two irons, two bridging sulfur atom, and four methylthiolates as a replacement of cysteine residues, as shown in Figure 4.1. The hydrogen atoms were added into the cluster and were optimized by using B3LYP/6-31G(d), while the other heavy atoms were freezed.

4.2.2 Redox Potential and pK_a

We approximated a various spin states of the clusters, raised by coupled iron, by using several spin approximations. Firstly, we calculate the energy of the cluster with the spin state defined as high spin (HS) and low spin (LS), in which the energy in LS state was approximated by using broken symmetry (BS) technique.[116] As for the LS states, other spin approximation, the so-called approximate spin projection (AP), was also utilized, which is formulated as[126–128]

$$E^{\mathrm{LS}}_{\mathrm{APBS}} = \alpha E^{\mathrm{LS}}_{\mathrm{BS}} - \beta E^{\mathrm{HS}}, \tag{4.1}$$

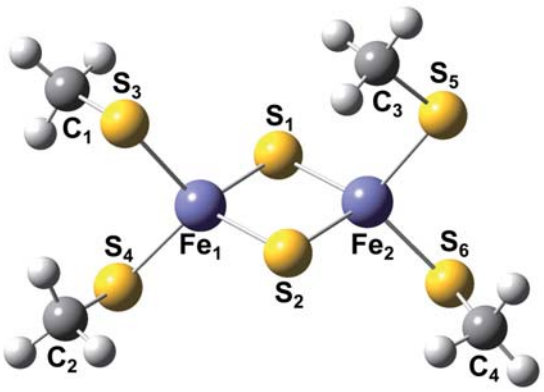

FIGURE 4.1: A structure of iron-sulfur cluster.

TABLE 4.1: The formula of coupling constant and ground state energy.

Oxidized State	Reduced State
$S_1 = S(\mathrm{Fe}^{3+}) = 5/2$	$S_1 = S(\mathrm{Fe}^{3+}) = 5/2$
$S_2 = S(\mathrm{Fe}^{3+}) = 5/2$	$S_2 = S(\mathrm{Fe}^{2+}) = 2$
	$B = 1/10\,[e(\mathrm{HS})_u - e(\mathrm{HS})_g]$
$J_{\mathrm{ox}} = 2/25\,[E_0(\mathrm{HS}) - E_0(\mathrm{BS})]$	$J_{\mathrm{red}} = 1/10\,[E_0(\mathrm{HS})_g - E_0(\mathrm{BS}) + 5B]$

$e(\mathrm{HS})_u$ and $e(\mathrm{HS})_g$ are orbital energies belong to u and g component of metal d orbitals split by resonance delocalization.

where

$$\alpha = \frac{\left\langle \hat{S}^2 \right\rangle^{\mathrm{HS}} - \left\langle \hat{S}^2 \right\rangle^{\mathrm{LS}}_{\mathrm{exact}}}{\left\langle \hat{S}^2 \right\rangle^{\mathrm{HS}} - \left\langle \hat{S}^2 \right\rangle^{\mathrm{LS}}_{\mathrm{BS}}} \tag{4.2}$$

$$\beta = \alpha - 1. \tag{4.3}$$

Meanwhile, we also used another spin approximation to estimated the energy in LS state. In this approximation, the effect of J spin coupling (JC) in Heisenberg Hamiltonian with an isotropic correction is considered, in which the ground state energy is formulated as[118, 120]

$$E_0(\mathrm{GS})_{\mathrm{ox}} = E_0(\mathrm{BS}) - 5/2J_{\mathrm{ox}} \tag{4.4}$$

$$E_0(\mathrm{GS})_{\mathrm{red}} = E_0(\mathrm{BS}) - 2J_{\mathrm{red}} \tag{4.5}$$

where J means the spin coupling parameter. We utilized the parameter of Heisenberg Hamiltonian shown in Table 4.1 that is obtained from the reference.[118, 120] From Table 4.1, S_1 and S_2 represent spin eigenvalues on two iron centers, B represents resonance delocalization parameter, and S represents total spin.

Regarding solvent contribution around the vicinity of the cluster, we used conductor-like polarizable continuum model (CPCM), with $\varepsilon = 10$, to account the contribution of solvent.[94, 95] Also, we used PCIS method as an alternative solvation model by adding a charge-dependent correction term that is derived from a Generalized Born theory.[122] The implementation of this correction scheme can reduce error in redox potential calculation of highly charged metal complexes.[122] We calculated standard redox potential (E_{redox}) by using a relationship of redox potential and the Gibbs free energy difference of oxidized and reduced states ($\Delta G_{\mathrm{redox}}$) that is written as

$$E_{\mathrm{redox}} = \frac{\Delta G_{\mathrm{redox}}}{nF} - E_{\mathrm{SHE}} \tag{4.6}$$

where n and F represent the number of electrons, and Faraday constant, respectively, while E_{SHE} represents absolute of standard hydrogen electrode, taken as 4.43 V.[129] In this calculation, the free energy difference was directly calculated, instead of using a thermodynamic cycle. We defined the free energy difference as the difference between the free energy of the cluster in oxidized and reduced states, the so-called vertical ionization potential (VIP), as given by

$$\Delta G_{\mathrm{redox}} \approx E^{\mathrm{ox}}_{(\mathrm{aq})} - E^{\mathrm{red}}_{(\mathrm{aq})}. \tag{4.7}$$

The terms of free energy correction were completely omitted due to the high computational costs of vibrational analyses. Nevertheless, our previous study revealed that this approximation can produce a good enough results for the calculation of redox potentials of metal complexes.[122]

We also calculated acid dissociation constant ($\mathrm{p}K_a$) by using free energy difference upon a deprotonation reaction (ΔG_{dep}) that is written as

$$\mathrm{p}K_a = \frac{\Delta G_{\mathrm{dep}}}{2.303RT} \tag{4.8}$$

where R and T represent gas constant and temperature, respectively. The free energy was derived from deprotonation reaction (see scheme in Figure 4.2), $\mathrm{AH} \Longleftrightarrow \mathrm{A}^- + \mathrm{H}^+$, given by

$$\Delta G_{\mathrm{dep}} = E_{\mathrm{aq}}(\mathrm{A}^-) + G_{\mathrm{aq}}(\mathrm{H}^+) - E_{\mathrm{aq}}(\mathrm{AH}) \tag{4.9}$$

where the free energy correction terms were again omitted in a similar way with redox potential calculation. Furthermore, we calculated the free energy of proton in aqueous phase as

$$G_{\mathrm{aq}}(\mathrm{H}^+) = G_{\mathrm{g}}(\mathrm{H}^+) + \Delta G_{\mathrm{aq,solv}}(\mathrm{H}^+) + \Delta G^{1\mathrm{atm}\rightarrow 1\mathrm{M}} \tag{4.10}$$

where $\Delta G_{\mathrm{aq,solv}}(\mathrm{H}^+)$ taken as -265.9 kcal/mol.[130] We defined the value of $G_{\mathrm{g}}(\mathrm{H}^+)$ as -6.28 kcal/mol at 298.15 K, according to Sackur-Tetrode equation for gas-phase monoatomic species.[131] We added $\Delta G^{1\mathrm{atm}\rightarrow 1\mathrm{M}}$, with the value is 1.89 kcal/mol,[132] to convert the standard state from 1 atm to 1 Molar. Bearing on protonation process, we calculated the difference of the cluster energy in oxidized and protonated reduced state, according to Figure 4.2. This value will indicate the protonation feasibility of the sulfur in each site. In addition, we also investigated SONO orbital of the iron-sulfur cluster in reduced state by using localized natural orbital method.[133] The atomic partial charges of the clusters were also investigated by using Merz-Singh-Kollman scheme.[93]

4.3 Results and Discussions

4.3.1 Redox Potential

Firstly, we analyze the reliability of combination of method and spin approximations in reproducing the experimental results. As for reference, we used the value of redox potential of spinach ferredoxin and adrenodoxin obtained from experimental data as -0.42V[33] and -0.27V[134], respectively. In this study, we analyze the results by utilizing the absolute error derived from relative redox potential (ΔE) between those proteins, i.e $\Delta E = E_{\text{ferredoxin}} - E_{\text{adrenodoxin}}$, instead of absolute redox potentials to eliminate systematic error. We defined the absolute errors for relative redox potential upon the experimental results as a difference of relative error produced by our calculations and experimental studies ($\Delta\Delta E = |\Delta E_{\text{calc}} - \Delta E_{\text{exp}}|$). Then, we approximated the reliability of combination of methods by evaluating the absolute error. We present the absolute value of redox potential of the cluster in Table 4.2.

We summarize the calculation results of $\Delta\Delta E$ in Table 4.3. As for the calculation by using B3LYP without PCIS scheme, the implementation of diffuse function do not yield any improvement on the value of $\Delta\Delta E$ for all spin approximations, except for JC approximation. We found the value of $\Delta\Delta E$ calculated by B3LYP with HS, BS, and AP are found to be similar whether the diffusion function is implemented or not. However, the implementation of diffuse function in JC approximation reduce the error by 0.05 V (from 0.26 to 0.21 V). This suggest that a little bit improvement may be obtained from JC approximation, though the value is not significantly closer to the corresponding experimental data. This improvement is related to the fact that the

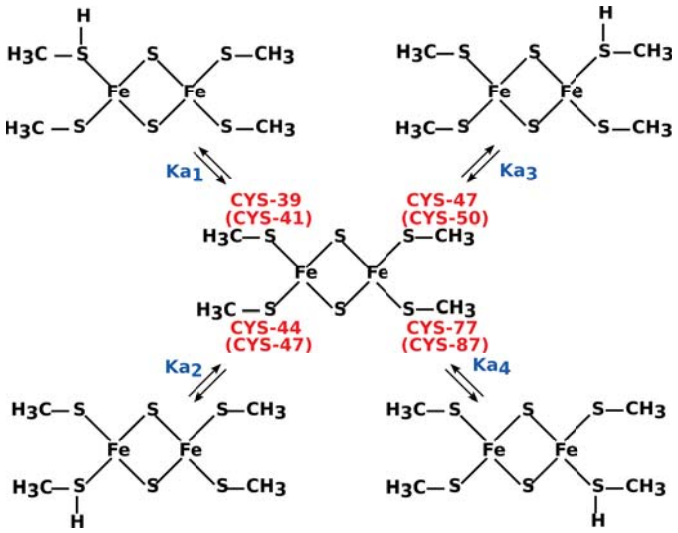

FIGURE 4.2: The protonation model of cysteine residue in iron-sulfur cluster of ferredoxin (adrenodoxin).

TABLE 4.2: The absolute redox potential of iron-sulfur cluster in ferredoxin (adrenodoxin) protein.

Method	Spin Approximation			
	HS	BS	AP	JC
VIP scheme				
1	-2.11	-2.39	-2.67	0.32
	(-2.19)	(-2.46)	(-2.72)	(0.21)
2	-1.63	-1.91	-2.19	0.64
	(-1.71)	(-1.98)	(-2.24)	(0.58)
3	-2.15	-2.90	-3.74	0.17
	(-2.23)	(-2.63)	(-3.06)	(0.49)
4	-1.69	-2.15	-2.62	0.88
	(-1.76)	(-2.13)	(-2.51)	(0.91)
VIP with PCIS scheme				
1	-1.88	-2.16	-2.45	0.55
	(-1.92)	(-2.19)	(-2.45)	(0.48)
2	-1.40	-1.68	-1.96	0.87
	(-1.44)	(-1.71)	(-1.97)	(0.85)
3	-1.92	-2.67	-3.51	0.40
	(-1.96)	(-2.36)	(-2.79)	(0.76)
4	-1.46	-1.92	-2.39	1.11
	(-1.49)	(-1.86)	(-2.24)	(1.18)

HS: High spin, BS: Broken symmetry, AP: Approximated spin projected, JC: J spin coupling
1: B3LYP/6-31G(d), 2: B3LYP/6-31++G(d), 3: M06/6-31G(d), 4: M06/6-31++G(d)

Hamiltonian for the cluster in oxidized and reduced state is defined differently in JC approximation. In contrary, a significant improvement was obtained when the diffuse function is implemented in M06 calculation with AP approximation, in which the error reduce by 0.32 V (from 0.35 to 0.03 V).

In the case of VIP with PCIS scheme, we also found a little dependency of basis set on the calculation with B3LYP. Nevertheless, the implementation of diffusion function in the calculation with BS and JC UM06 give an improvement of $\Delta\Delta E$ value. The most significant improvement with respect to the diffuse function was obtained from the calculation with AP UM06, in which the absolute error decreases by 0.30 V (from 0.31 to 0.01 V). This findings indicate that the diffuse function give a contribution to improve the calculation of redox potential with M06 functional.

Bearing on DFT exchange correlation functional, the calculation by M06 produce the results that are more accurate than those by B3LYP, except for HS and AP approximations without diffuse function. For example, in VIP with PCIS scheme and BS approximation, the value of $\Delta\Delta E$ by B3LYP and M06 with diffuse function are found as 0.17 and 0.09 V, respectively. This different corresponds to two hybrid issues, i.e. the type of exchange functional, and the ratio of the exchange functional with HF exchange

TABLE 4.3: The absolute error of redox potential difference.

Method	Spin Approximation			
	HS	BS	AP	JC
VIP scheme				
1	0.23	0.21	0.20	0.26
2	0.23	0.21	0.20	0.21
3	0.23	0.28	0.35	0.18
4	0.22	0.13	0.03	0.12
VIP with PCIS scheme				
1	0.19	0.17	0.16	0.22
2	0.19	0.17	0.16	0.17
3	0.19	0.24	0.31	0.22
4	0.18	0.09	0.01	0.08

HS: High spin, BS: Broken symmetry, AP: Approximated spin projected, JC: J spin coupling
1: B3LYP/6-31G(d), 2: B3LYP/6-31++G(d), 3: M06/6-31G(d), 4: M06/6-31++G(d)

functional. For the former issue, M06 utilize meta-GGA exchange functional coupled with exact HF exchange, while B3LYP utilize pure GGA functional. Overall, the best result was obtained from AP UM06/6-31++G(d,p) calculation with the absolute error of 0.01 V.

Since the implicit solvent model was used in this calculations, we here evaluate the correlation of the absolute error to the inverse of ε, i.e., $1/\varepsilon$. As shown in Figure 4.3, the absolute value of the redox potential was found to be inversely proportional to the dielectric constant, in which the tendencies of B3LYP and M06 were almost similar. However, we found that the calculation within a range from $\varepsilon = 1$ (vacuum) to $\varepsilon = 78$ (water) can not reproduced the experimental results for neither the spinach ferredoxin (-0.42 V) nor adrenodoxin (-0.27 V). This indicates the lacks of protein environment that in the present model.

4.3.2 Acid Constant (pK_a)

Regarding protonation process, we presented the protonation possibility of [2Fe-2S] cluster by determining pK_a values of thiol groups in cysteine (see Table 4.4). We found that all pK_a value is larger than 7 indicating the existence of those residues in deprotonated state upon the reduction in vivo. A few methodology dependence on pK_a is found in pK_a calculation of ferredoxin. On the contrary, the methodology dependency on pK_a is found to be large in pK_a calculation of adrenodoxin. The contribution of diffuse function to pK_a values is found differently in the calculation of B3LYP and M06. Generally, the implementation of diffuse function lead to the decreasing (increasing) of pK_a values

TABLE 4.4: The calculated pK_a value of ferredoxin (adrenodoxin).

Method	pK_{a1}	pK_{a2}	pK_{a3}	pK_{a4}
1	15.7	15.0	16.3	14.7
	(19.1)	(20.5)	(21.4)	(20.3)
2	15.0	15.4	16.0	14.2
	(18.1)	(20.1)	(19.0)	(18.3)
3	14.6	14.0	14.6	12.6
	(17.1)	(17.2)	(17.3)	(17.1)
4	14.2	14.1	15.3	12.9
	(17.8)	(18.7)	(17.3)	(17.1)

1: B3LYP/6-31G(d), 2: B3LYP/6-31++G(d), 3: M06/6-31G(d), 4: M06/6-31++G(d)

by B3LYP (M06) except for pK_{a2} (M06 except for pK_{a1}). We also found that pK_{a4} of ferredoxins present the lowest pK_a value compare to another sites calculated by using all methods, while the lowest pK_a value of adrenodoxin is presented by pK_{a1} for method 1 and 2. This correspond to the configurations of all protonated clusters that are closely similar each other. However [2Fe-2S] clusters are slightly deviated in both protein, which affect to the absolute redox potentials of these [2Fe-2S] proteins.

4.3.3 Singly Occupied Natural Orbital (SONO)

We presented singly occupied natural orbital (SONO) of the iron-sulfur clusters in reduced state, as shown in Figure 4.4, to confirm the site dependency of pK_a and the difference of redox potentials between two proteins. Nine SONO orbitals that have been identified correspond to ferromagnetic state of the iron-sulfur cluster. Those nine orbitals consist of an orbital that represent a mix of d_{z^2} orbital between both iron atoms,

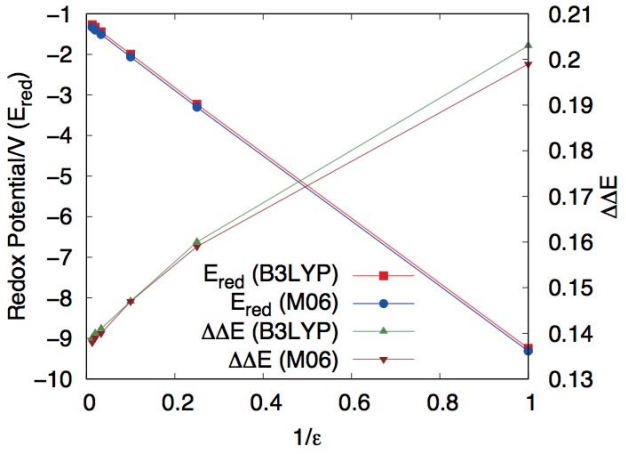

FIGURE 4.3: The dependency of absolute redox potential of feredoxin in cluster model and $\Delta\Delta E$ as a function of inverse dielectric constant by B3LYP and UM06/6-31++G(d,p).

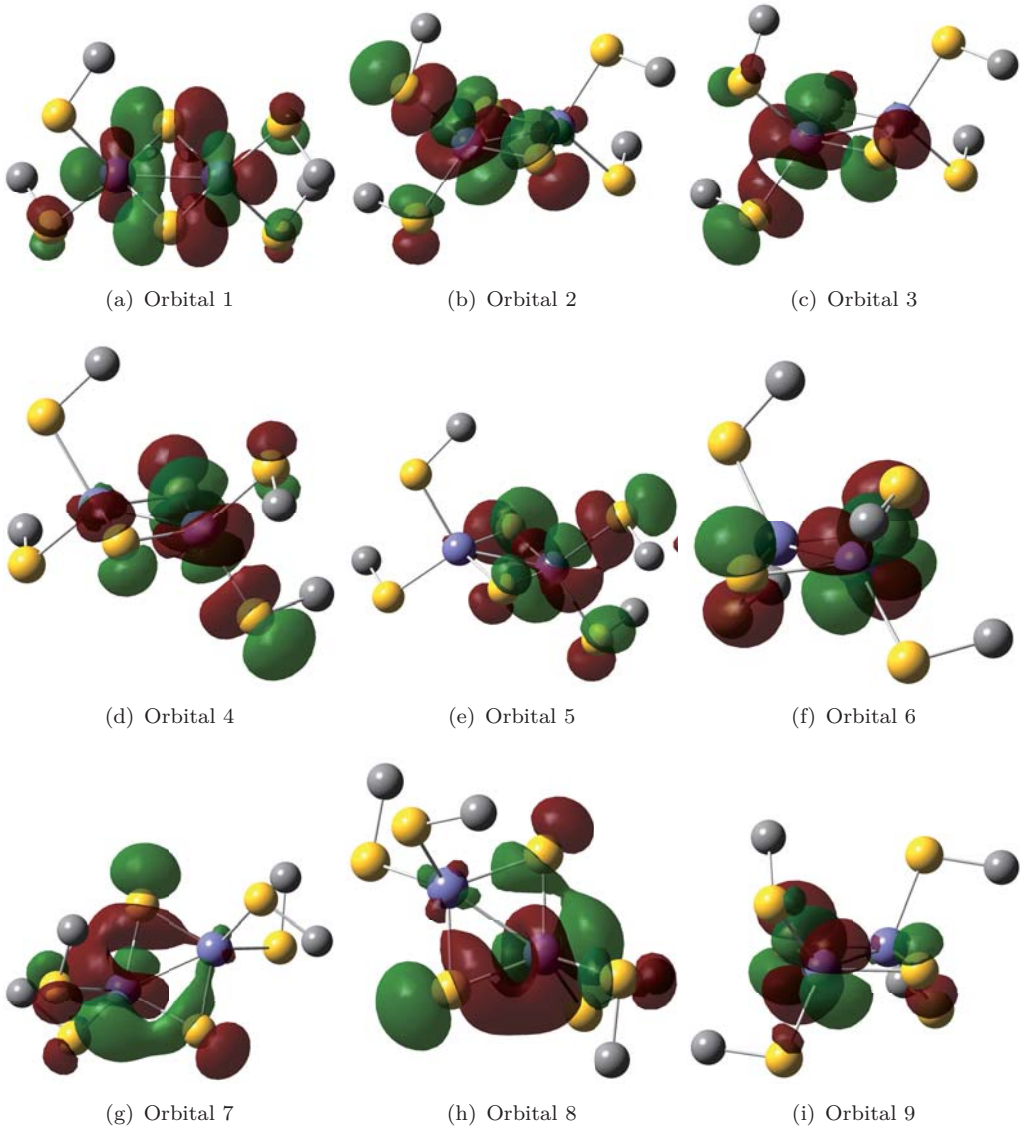

(a) Orbital 1 (b) Orbital 2 (c) Orbital 3

(d) Orbital 4 (e) Orbital 5 (f) Orbital 6

(g) Orbital 7 (h) Orbital 8 (i) Orbital 9

FIGURE 4.4: Singly occupied natural orbital (SONO) of the iron-sulfur cluster in a reduced state. Hydrogen atoms are neglected for clarity reason.

four orbitals localized around Fe^{3+} atom and four orbitals localized around Fe^{2+} atom. In orbital 1 (Figure 4.4), we identified four bonding interactions between d_{z^2} orbital of iron and σ orbital of bridging sulfur atom. We also identified anti-bonding interaction between d_{z^2} orbital of iron and σ orbital of cysteine sulfur atom. This finding confirms that the interaction between iron and bridging sulfur atom is stronger than the interaction between iron and cysteine sulfur atom. A localized d_{z^2} orbitals around each iron atom were also found in orbital 2 to 9 (Figure 4.4). In those orbitals, d_{z^2} orbitals of iron was also found to interact with cysteine sulfur atom by anti-bonding interaction.

4.3.4 Atomic Partial Charge

We presented the atomic partial charges of the iron-sulfur cluster in ferredoxin and adrenodoxin as shown in Table 4.5. As expected, the partial charge of Fe_1 (Fe3+) atom is higher than the partial charge of Fe_2 (Fe2+) atom. We found that the partial charges of both bridging sulfur atom is almost similar indicating a homogeneous charge distribution on both atoms. By evaluating the partial charges on S_3 to S_6, we also found that the averaged charge on S_3 and S_4 is larger than the averaged charge on S_5 and S_6. This correspond to the charge of iron atom where those sulfur atoms bounded and indicate the heterogeneity of charge distribution on those atoms. Bearing on the calculation method, a remarkable dependence of the exchange-correlation functional and diffuse function on the atomic partial charges were found, especially on iron atoms. This dependencies are related to the contribution of d orbitals of iron, as transition metal, to the partial charge. The inclusion of diffuse function contributes in increasing the partial charge of positively charged atom, and the decreasing of the partial charge of negatively charged atom. This indicate that the inclusion of diffuse function induced a more polarization of the electron density.

Bearing on the absolute error shown in Table 4.3, the absolute error produce by AP M06/6-31G(d) method is found to be larger than the other AP calculations. This results can be related to the tendency of partial charge shown in Table 4.5. We found that the partial charges of non-carbon atom calculated by M06/6-31G(d) method is relatively lower than another methods. This kinds of results are also reported by other group that found the error of redox calculation obtained from M06 is even worse compared to the M11 and other exchange correlation functionals upon to worth description of Fe atom.[135] Hence, the kind of the exchange correlation functional and basis set should be chosen carefully in this calculation because of their great contribution.

4.4 Conclusion

In this study, the redox potential and pK_a of iron-sulfur cluster models have been investigated. The diffuse function is found to give a contribution in improving the results that indicated by the decreasing of absolute error ($\Delta\Delta E$). Regarding DFT functional, we found that the result obtained from M06 is more accurate than those obtain from B3LYP. We also confirm that the inclusion of PCIS scheme in VIP approximation can improve the results. With the absolute error of 0.01 V, we obtain the best result from the calculation by AP UM06/6-31++G(d,p).

TABLE 4.5: The atomic partial charge of ferredoxin (adrenodoxin). The atom number refer to Figure 4.1

Atom	Method			
	1	2	3	4
Fe_1	0.98	1.06	0.94	0.97
	(1.19)	(1.64)	(1.16)	(1.55)
Fe_2	0.81	0.87	0.76	0.79
	(1.11)	(1.43)	(1.06)	(1.32)
S_1	-0.92	-0.91	-0.90	-0.86
	(-1.03)	(-1.14)	(-1.01)	(-1.09)
S_2	-0.92	-0.91	-0.90	-0.86
	(-1.06)	(-1.14)	(-1.04)	(-1.09)
S_3	-0.81	-0.90	-0.79	-0.85
	(-0.89)	(-1.12)	(-0.87)	(-1.07)
S_4	-0.78	-0.87	-0.76	-0.83
	(-0.86)	(-1.05)	(-0.84)	(-1.03)
S_5	-0.76	-0.78	-0.74	-0.74
	(-0.85)	(-1.00)	(-0.83)	(-0.96)
S_6	-0.74	-0.81	-0.71	-0.77
	(-0.85)	(-1.05)	(-0.83)	(-1.03)
C_1	0.05	0.08	0.03	0.06
	(0.08)	(0.15)	(0.07)	(0.13)
C_2	0.04	0.08	0.03	0.06
	(0.08)	(0.17)	(0.03)	(0.16)
C_3	0.03	0.01	0.02	0.00
	(0.00)	(-0.03)	(-0.01)	(-0.04)
C_4	0.03	0.05	0.01	0.03
	(0.09)	(0.14)	(0.08)	(0.14)

1: B3LYP/6-31G(d), 2: B3LYP/6-31++G(d), 3: M06/6-31G(d), 4: M06/6-31++G(d)

Chapter 5

General Conclusion

In this thesis, we presented a theoretical study on electronic structure and properties of two metalloproteins, i.e. copper protein and iron-sulfur protein. As for copper protein, we performed the investigation in two steps. Firstly, we focus in investigating the cluster of type 1 copper center (T1CC) in relation to the electronic structure and several properties. T1CC is prepared from X-ray crystal structure of a series of copper protein, consists of Azurin, Plastocyanin, Stellacyanin, and MCOs. The model cluster of T1CC comprised by a copper atom, a cysteine, two histidines and a methionine residue. Several properties of T1CC, i.e. molecular orbital, atomic partial charge, partial spin densities, ionization energy (IP) of reduced T1Cu, electron affinity (EA) of oxidized T1Cu, the bond and the angle constants, are calculated by using two typical DFT functional, i.e. B3LYP and M06.

According to the results, we presented a SOMO orbital of T1CC in oxidized state that is mainly raised from anti-bonding interaction between $d_{x^2-y^2}$ orbital of copper and π orbital of cysteine's sulfur. We also found that the shape of spin density surface is similar to the shape of SOMO. This indicate that the spin density is localized around copper and cysteine's sulfur atoms. Our results were also reveal the dependency of atomic partial charge and atomic partial spin on DFT functional, especially around the bond of copper and cysteine's sulfur. The partial charge of copper calculated by M06 is found to be less positive than those calculated by B3LYP. Meanwhile, the partial charge of cysteine's sulfur obtained from M06 calculation is less negative than those obtained from B3LYP calculation. This indicate that the negative charge of cysteine's sulfur is more distributed when calculated by M06. Regarding spin density, we found that the partial spin of copper calculated by M06 is found to be lower than those calculated by B3LYP. This suggested that M06 calculation produce a spin distribution that is more

delocalized than B3LYP does, which correspond to the increasing of t/U ratio in the simple Hubbard model.

The values of IP and EA were also found to be dependence on DFT functionals. The calculation by M06 produce those properties that is higher than those produced by B3LYP. The dependency on DFT functional is also found in the case of maximum absorption wavelength (MAW) calculation. MAW by M06 is found to be always higher than those by B3LYP. This indicate that the band gap energy between $d_{x^2-y^2}$ orbital of copper and π orbital of cysteine's sulfur is lower when one adopts M06. A significant contribution of M06 is found in bond constant calculation, especially in the case of the bond between copper (Cu) and methionine (Met). Indeed, M06 calculation produced the bond constant of Cu-Met of T1CC in Azurin that is almost three times higher than those produced by B3LYP. This indicate that M06 gives a significant contribution in bond constant calculation. However, we did not found any systematical contribution of DFT function in the calculation of angle constant due to the complexity of the calculation.

Secondly, we focus on the contribution of long-range interaction between copper and methionine residue as axial ligand to several properties of T1CC, i.e. equilibrium bond distance, bond constant, redox potential and MAW. In this part of calculation, we utilized eight DFT functionals that are represent four classes of the functional, i.e. (i) pure generalized gradient approximation (GGA) (PBE and BLYP), (ii) hybrid (B3LYP and M06), (iii) long-range corrected (LC)-GGA (LC-BLYP and LC-PBE), and (iv) LC hybrid (B97X and CAM-B3LYP). The cluster models of T1CC were prepared from X-ray crystal structure of Azurin as typical example. Similar to the first study, we prepared the model cluster of T1CC that is comprised by a copper atom, a cysteine, two histidines and a methionine residue. Since we focus to the contribution of Cu-Met interaction, we prepared several cluster by varying Cu-Met bond distance as 3.18, 3.28, 3.38, 3.48, and 3.58 .

According to the results, we found that M06 produce the equilibrium bond distance that is closer to the distance obtained from X-ray crystal structure. Furthermore, the largest bond constant value is also obtained from M06 calculation. This indicate that M06 performed better than other DFT functional in the case of equilibrium bond distance and bond constant calculation. The value of the bond constant also indicate the M06 represent a strong interaction between copper and methionine. We also found the contribution of axial ligand interaction to redox potential and MAW. The increasing of bond distance lead to the decreasing of redox potential, and the increasing of MAW.

In the case of redox potential, we found that the series of LC-DFT is more sensitive to bond distance than those of non-LC-DFT, in which the most sensitive one is presented by LC-BLYP. The series of LC-DFT were also found to be more accurate than those of

non-LC-DFT, except M06. This indicate that LC scheme in LC-DFT and hybrid scheme in M06 give positive contribution in the calculation of redox potential. In particular, the implementation of LC scheme in BLYP and B3LYP confirms the contribution of LC in improving the accuracy. In the case of MAW, M06 is found to be more sensitive to bond distance than other functionals. In this calculation, hybrid DFT produce MAW that is more accurate results than others. However, regarding LC contribution, we found that pure GGA is more accurate than LC-GGA. This correspond to the fact that short-range interaction is more dominant than long-range interaction in this calculation. Hence, hybrid DFT seems to be able to calculate both interactions in a better way.

As for iron-sulfur protein, we investigated redox potential and pK_a of iron-sulfur clusters with respect to spin structures. In this particular study, we prepared the cluster from two [2Fe-2S] iron-sulfur protein, i.e. ferredoxin and adrenodoxin. The model of iron-sulfur cluster consist of two irons, two bridging sulfur atom, and four methylthiolates as a replacement of cysteine residues. To handle the spin structure of coupled iron, we utilize several spin approximations, i.e. high spin (HS), low spin by broken symmetry technique (BS), approximated spin projected (AP), and J spin coupling (JC). The solvent environment around the cluster was approximated by using conductor-like polarizable continuum model (CPCM) with $\varepsilon = 10$. To judge the accuracy of redox potential, we calculated absolute errors toward the experimental results that is defined as a difference of relative error obtained from calculated and experimental study ($\Delta\Delta E = |\Delta E_{\mathrm{calc}} - \Delta E_{\mathrm{exp}}|$).

According to the results, we did not found any contribution of diffuse function in improving the accuracy of all B3LYP calculation, except JC approximation. In contrary, the diffuse function present a significant improvement in the calculation by M06. The most significance improvement with respect to the diffuse function was obtained from the calculation by AP UM06, which the absolute error decrease by 0.30 V. This finding confirm the contribution of diffuse function in improving the accuracy of redox potential calculation by M06. Bearing on DFT functional, we found that M06 produce a results that is more accurate than B3LYP, except for HS and AP approximation without diffuse function. This results correspond to the kind of exchange functional used in both functionals. With the absolute error of 0.01 V, we obtained the best result from the calculation by AP UM06/6-31++G(d,p).

We also calculated pK_a values on each site of sulfur of thiolate and found that those pK_as is larger than 7. This confirms that the residues were found as deprotonated state upon the reduction in vivo. The molecular orbitals of iron-sulfur cluster were investigated by approximating singly occupied natural orbital (SONO) by using linear natural orbital

(LN0) method. We found nine SONO consists of a mix of d_{z^2} orbital between both iron atoms and each four orbitals localized around Fe^{2+} and Fe^{3+} atoms.

Finally, the atomic partial charges of the cluster were investigated by using Merz-Singh-Kollman scheme. Bearing on the calculation method, a remarkable dependence of the exchange-correlation functional and diffuse function were found on the calculation of atomic partial charges, especially on iron atoms. This lead by the existence of d orbitals in iron atom and affect to calculation of atomic partial charges. The diffuse function was also contribute in increasing the partial charge of atom with positive charges, and decreasing the partial charge of atom with negative charges. This suggested that the diffuse function induced more polarization of the electron density.

Future Works A

Theoretical Study of Exit Mechanism of Water Molecule from Tri-Nuclear Copper Center of Multicopper Oxidase

A.1 Introduction

In this study, we aim to investigate the free energy of water exit pathway from tri-nuclear copper center (TNC) of multicopper oxidases (MCOs) protein by using steered molecular dynamics (SMD) simulation. The exit pathway of the water molecule has been predicted by experimental study as shown in Figure A.1.[3] In the previous report, we have presented two exit pathways through the hydrogen bond network around Glu506 and Cys500 residues. In those pathways, we assumed that the water located inside of TNC triangle ($water_{in}$) will escape from TNC site. However, after discussing with our collaborator, we change our assumption as the water located outside of TNC triangle ($water_{out}$) will escapes from TNC site in two steps (Figure A.2). Firstly, the bond between $water_{out}$ molecule and Cu_{II} atom will be broken and the water will be released. Secondly, the $water_{in}$ molecule will move to the outside and take the place of original position of $water_{out}$ molecule. As the consequence, we redefined the bond parameter in the TNC site, as shown in Figure A.3. $Water_{in}$ molecule is defined as a ligand bound to Cu_{II} atom and $water_{out}$ molecule is defined as TIP3P water.

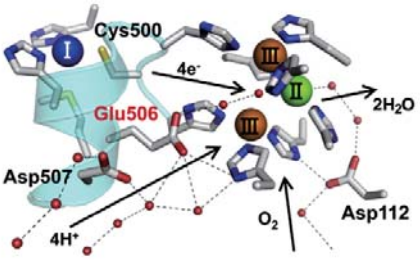

FIGURE A.1: The water exit pathway predicted by experimental study.[3]

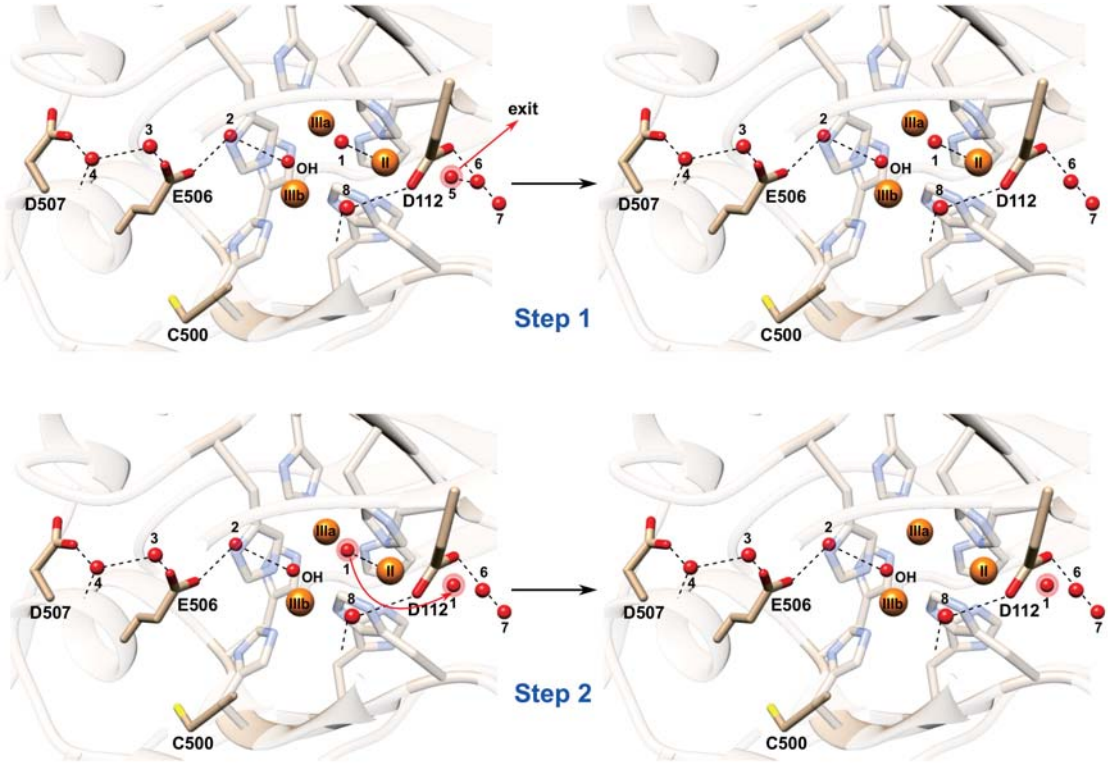

FIGURE A.2: The schematic diagram of the exit pathway.

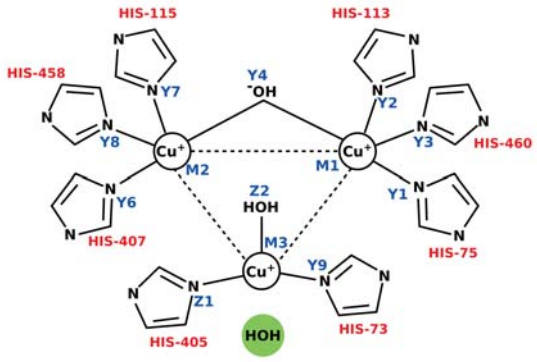

FIGURE A.3: The atomic label in the TNC site.

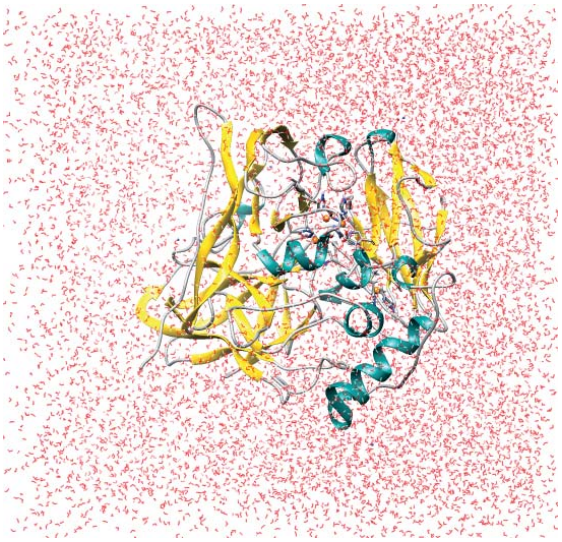

FIGURE A.4: The solvated system of Multicopper protein.

A.2 Computational Methods

We performed a SMD simulation for each step of the pathway. In these simulations, the protein molecule was prepared from X-ray crystal structure of MCOs protein (PDB ID: 4E9S)[79]. The solvated system of the protein was presented in Figure A.4. The simulation was performed by using NPT ensemble with constant temperature (300 K) and constant pressure (1 bar). The detail of simulation parameters were presented in Table A.1. For sampling purpose, we performed nine SMD simulations by varying the value of pulling force constant as 500, 1000 and 1500 kJ/mol.nm^2 and the pulling speed as 0.00050, 0.00060, 0.00070 nm/ps. The carbon α atoms were constrained during the simulation by using 1000 kJ/mol.nm^2 of weak harmonic force. All of the simulations were performed by using Gromacs 4.6 program package[136].

TABLE A.1: The parameters of steered molecular dynamics simulation

Parameter	Value
Ensemble	NPT
Non-active site FF	Amber
Active site FF	Quantum Method
Simulation time	2 ns
Time step	2 fs
Temperature	300 K
Temperature coupling	Berendsen
Pressure	1 bar
Pressure coupling	Berendsen
Cut off	10
Water type	TIP3P
Counter ion	Na^+

As for the simulation of step 1, the fluctuation of Cu_{II}-H_2O bond distance was plotted as a function of simulation time to verify the performance of pulling scheme. As shown in Figure A.5, the bond distance become larger along with the simulation time that confirm a well performance of simulation. The fluctuation difference of bond distance in each simulations related to the difference of simulation parameter. To calculate the free energy, two thousand snapshot structures were taken from each simulation and the frequency of structure with certain bond distance were calculated. By using frequency distribution, the free energy (G) was calculated as

$$G = -k_b T \ln \frac{n(r)}{N} \tag{A.1}$$

where k_b, T, $n(r)$ and N represent the Boltzmann constant, temperature, the number of snapshot structure with r bond distance, and the total number of snapshot structure, respectively.

A.3 Results and Discussions

The plot of frequency distribution and free energy as a function of bond distance for the simulation of step 1 are provided in Figure A.6(a) and A.6(b), respectively. Seven snapshot configurations on the stationary point of free energy is presented in Figure A.7. In the initial structure, we found that the $water_{out}$ molecule still interact with Cu_{II} atom and a water molecule, which the free energy of this configuration is around 1.93 kcal/mol. We also found that the initial bond distance between $water_{out}$ molecule and Cu_{II} atom is 2.10 . Meanwhile, the highest barrier energy in this step is found as around 2.62 kcal/mol (configuration 7). In this state, the bond distance between $water_{out}$ molecule and Cu_{II} atom is around 9.2 , and the $water_{out}$ molecule also interact with another water molecule by hydrogen bond interaction. The lowest free energy is presented by configuration 6 with Cu_{II}-H_2O bond distance is around 6.9 . In this state, we found that $water_{out}$ molecule interact with a water molecule and Threonine-409 residue by hydrogen bond interaction.

In the meantime, we found two local minimum and two local maximum of the free energy in this step. The free energies on those two local minimum are found as 0.82 kcal/mol (bond distance 2.40) and 0.41 kcal/mol (bond distance 4.71). The configuration of the first and second local minimum are presented by configuration 2 and 4, respectively. The free energies on those two local maximum are found as 2.03 kcal/mol (bond distance 3.91) and 1.15 kcal/mol (bond distance 6.02). The configuration of the first and second local maximum are presented by configuration 3 and 5, respectively.

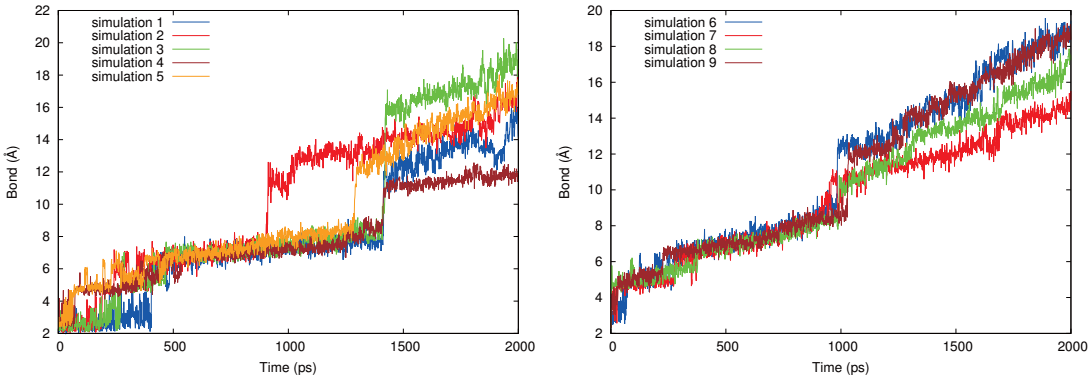

(a) (b)

FIGURE A.5: The plot of the fluctuation of Cu_{II}-H_2O bond distance in the simulation of step 1.

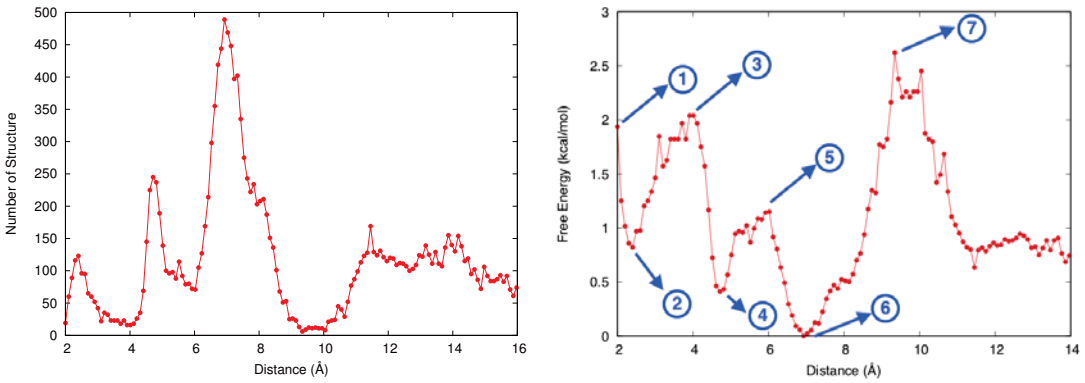

(a) (b)

FIGURE A.6: The plot of (a) frequency distribution and (b) free energy, as a function of Cu_{II}-H_2O bond distance in the simulation of step 1.

As for the simulation of step 2, we also plot the fluctuation of the bond distance between $water_{in}$ molecule and hydroxide ion to verify the performance of pulling scheme. As shown in Figure A.8, the bond distance become larger along with the simulation time, which confirm that the pulling scheme performed well. Similar to the first simulation, we use 2000 snapshot structures from each simulation to calculate the free energy and the frequency of structure. The free energy was derived from the frequency distribution by using Equation A.1.

The plot of frequency distribution and free energy as a function of bond distance for the simulation of step 2 are provided in Figure A.9(a) and A.9(b), respectively. Five snapshot configurations on the stationary point of free energy is presented in Figure A.10. In the initial structure, $water_{in}$ molecule is found inside the TNC triangle, which the free energy of this configuration is around 3.97 kcal/mol. The initial bond distance between $water_{in}$ molecule and hydroxide molecule is 2.50 . Then, the water molecule

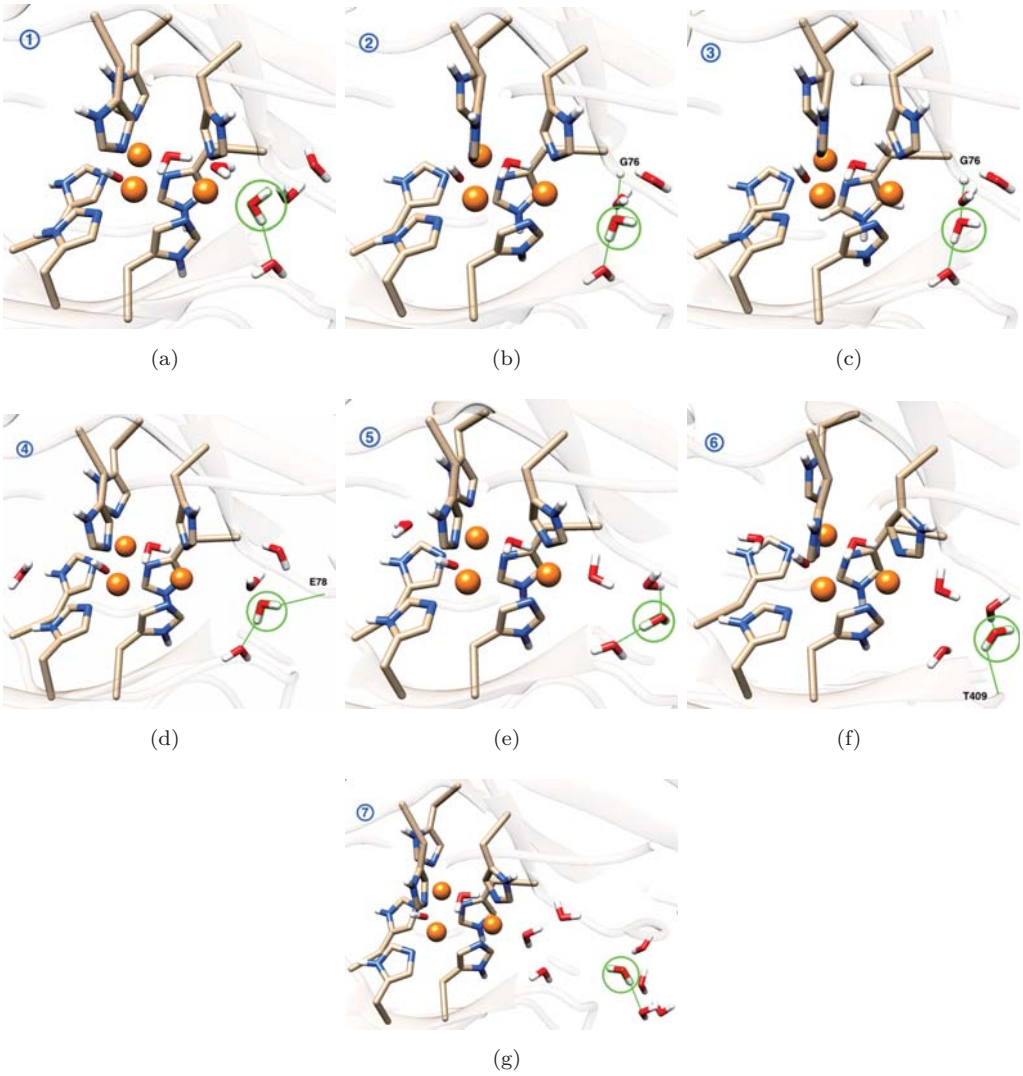

FIGURE A.7: The snapshot of the configurations captured from the simulations of step 1. The green line represent a hydrogen bond.

move to a new position located between Cu_{II} and Cu_{IIIa} ion, which the water is slightly closer to the outside. This configuration represent the lowest free energy in this step. In this state, the distance between the water molecule and hydroxide molecule become around 2.90 .

As shown in configuration 3, the water molecule move to the outside by interact with Tryptophan-74 residue by hydrogen bond interaction. The value of free energy on this state is around 1.09 kcal/mol that is higher than the previous state. In this state, the bond distance between the water and hydroxide ion become around 3.91 . The highest barrier energy in this step is found as 4.38 kcal/mol with the bond distance between the water and hydroxide molecule is 5.51 . In this state, the water molecule is found to interact with another water molecule by hydrogen bond interaction. In the final configuration, we found that $water_{in}$ molecule take a place of the original

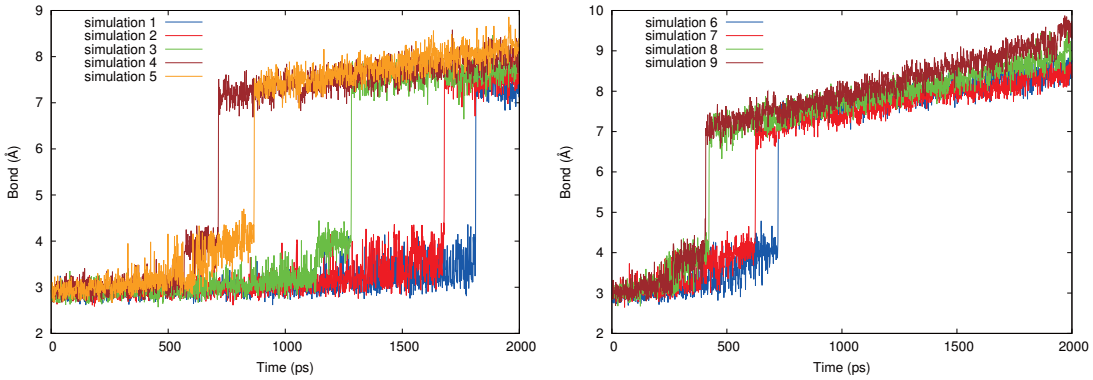

(a) (b)

FIGURE A.8: The plot of the fluctuation of OH-H_2O bond distance in the simulation of step 2.

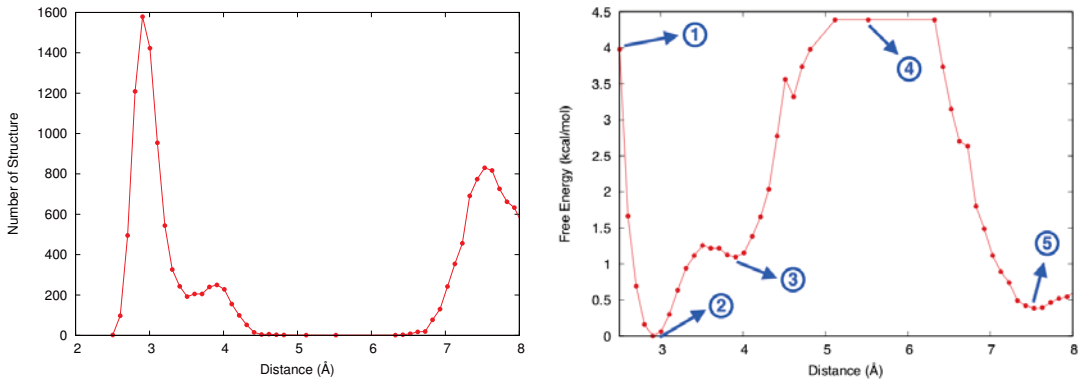

(a) (b)

FIGURE A.9: The plot of (a) frequency distribution and (b) free energy, as a function of OH-H_2O bond distance in the simulation of step 2.

position of $water_{out}$ molecule. The free energy value of this configuration is around 0.51 kcal/mol. In this configuration, we found that the water molecule interact with Leucine-77 residue, and the bond distance between the water molecule and Cu_{II} is found as 2.91 . By comparing to the initial structure, we found that the bond distance of the water molecule bound to Cu_{II} in this position become longer. This finding is in agreement with the experimental data.[2]

Finally, we compare the free energy profile between the simulation of step 1 and step 2. As for the step 1, we found that the highest barrier energy for $water_{out}$ molecule to escape from TNC site is around 2.62 kcal/mol. Meanwhile, the highest barrier energy in step 2 is found as 4.38 kcal/mol, which is almost two times of the highest barrier energy in step 1. This energy is required for $water_{in}$ molecule to move outside and take a place of original position of $water_{out}$ molecule. By comparing those barrier energies, we found that the step 2 is rate limited step due to the higher of the energy. The existence of

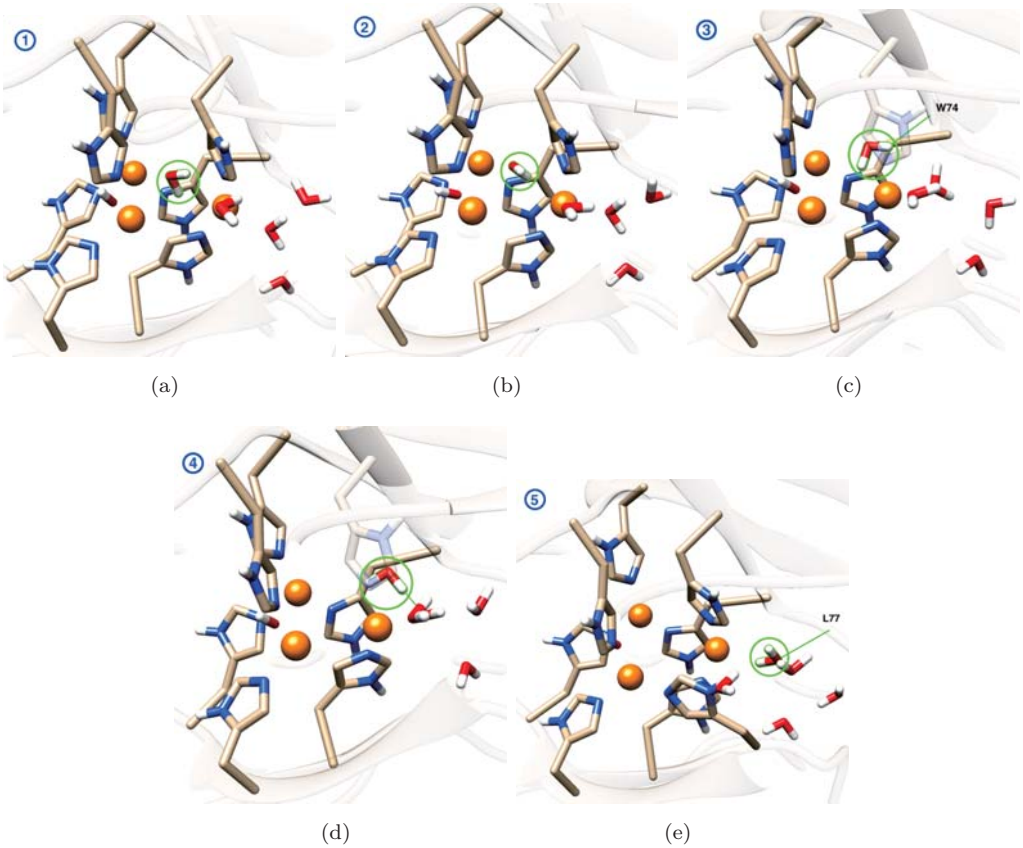

(a) (b) (c)

(d) (e)

FIGURE A.10: The snapshot of the configurations captured from the simulations of step 2. The green line represent a hydrogen bond.

several histidine residue on the vicinity of TNC triangle could be the reason of this high barrier energy, which lead to a steric effect.

Future Works B

QM/MM Study on Redox Potential of Iron-Sulfur Protein

B.1 Introduction

In this appendix, we present a study of redox potential of iron-sulfur protein by using QM/MM model. Similar to the simple cluster model, we implemented a hybrid model into two iron-sulfur protein, i.e. ferredoxin and adrenodoxin. In this model, the iron-sulfur cluster was classified as QM region, while the rest residue of protein was classified as MM region, as shown in Figure B.1. The total energy of QM/MM model is expressed as

$$E_{\text{tot}} = E_{\text{QM}} + E_{\text{MM}} + E_{\text{QM-MM}} \tag{B.1}$$

where E_{QM}, E_{MM}, and $E_{\text{QM-MM}}$ represents energies in the QM region, MM region, and QM/MM interface region, respectively. The solvent environment was approximated by using implicit solvent model, in which the dieletric constant is set to be similar to that of water. We also investigated the dependence of redox potential to dielectric constant value.

B.2 Results and Discussions

The results of redox potential calculated by QM/MM model is presented in Table B.1. In this model, we implemented the diffuse function onto non-iron atom only because of the limitation of the program package. According to the results, we found that the diffusion function in B3LYP and M06 contribute in a different way. The diffusion function improves the result of B3LYP calculation, while the implementation of the function

in M06 decrease the accuracy. The lack of diffusion function on iron atom might be the reason for this results. However, regarding DFT functional, we found that M06 calculation produce the results with the absolute error is lower than B3LYP calculation. The absolute error of B3LYP and M06 calculation without diffusion function are 2.05 and 1.90, respectively. This finding is similar to the tendency of B3LYP and M06 calculation in the cluster model. The best result by using the hybrid model was obtained from M06 calculation without diffusion function with the absolute error is 1.24 V.

In the matter of the dielectric constant, as shown in Figure B.2, we found a similar relationship of the redox potential and dielectric constant as found in the cluster model. According to the Figure, the absolute redox potential was found as inversely proportional to dielectric constant. This results point out the importance of the dielectric constant in the calculation by using hybrid model.

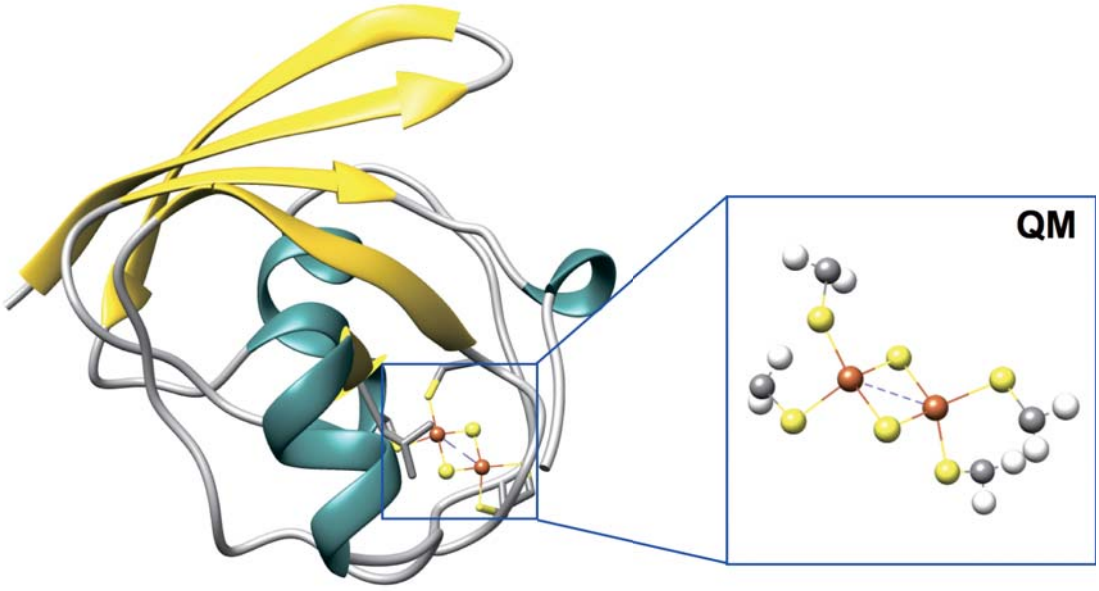

FIGURE B.1: Iron-sulfur cluster as QM region in hybrid model.

TABLE B.1: The absolute redox potential of iron-sulfur cluster in ferredoxin (adrenodoxin) protein calculated by using QM/MM model.

Method	E_{redox} (V)	ΔE (V)	$\lvert\Delta\Delta E\rvert$ (V)
1	-8.41	-2.20	2.05
	(-6.21)		
2	-8.22	-2.05	1.90
	(-6.17)		
3	-8.42	-1.39	1.24
	(-7.04)		
4	-8.24	-2.01	1.86
	(-6.23)		

1: B3LYP/6-31G(d), 2: B3LYP/6-31++G(d), 3: M06/6-31G(d), 4: M06/6-31++G(d)

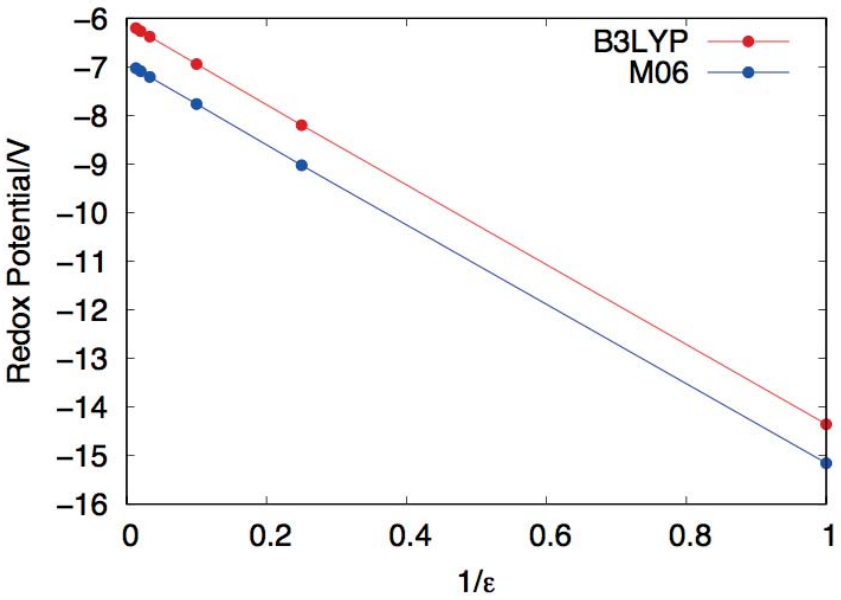

FIGURE B.2: The dependency of absolute redox potential of ferredoxin protein in hybrid model.

List of Publications

Papers as First Author

1. **I. Kurniawan**, K. Kawaguchi, M. Shoji, T. Matsui, Y. Shigeta, H. Nagao, *A Theoretical Study on Redox Potential and pKa of [2Fe-2S] Cluster Model from Iron-Sulfur Proteins.* Bulletin of the Chemical Society of Japan, 2018 (Accepted).

2. **I. Kurniawan**, T. Matsui, S. Nakagawa, K. Kawaguchi, H. Nagao. *Theoretical studies on association/dissociation process of plastocyanin and cytochrome f in photosynthesis.* Journal of Physics: Conferense Series, 2018 (Accepted).

3. **I. Kurniawan**, K. Kawaguchi, K. Sugimori, T. Sakurai, H. Nagao, *Quantum Chemical Study of Axial Ligand Effect on the Electronic Properties of Type I Copper Protein.* Chemistry Letters (Accepted).

4. **I. Kurniawan**, K. Kawaguchi, K. Sugimori, T. Sakurai, H. Nagao. *Theoretical Study on the Electronic Structure of Type I Copper Center in Copper Proteins.* Science Report of Kanazawa University (in prep).

Other Papers

1. S. Nakagawa, **I. Kurniawan**, K. Kodama, M.A. Arwansyah, K. Kawaguchi, H. Nagao. *Theoretical study on interaction of cytochrome f and plastocyanin complex by a simple coarse- grained model with molecular crowding effect.* Molecular Physics, 2018, 116 (5-6), 666 – 677.

2. K. Kawaguchi, S. Nakagawa, **I. Kurniawan**, K. Kodama, M.A. Arwansyah, H. Nagao. *A coarse-grained model of the effective interaction for charged amino acid residues and its application to formation of GCN4-pLI tetramer.* Molecular Physics, 2018, 116 (5-6), 649 – 657.

Bibliography

[1] Herbert Nar, Albrecht Messerschmidt, Robert Huber, Mart van de Kamp, and Gerard W. Canters. Crystal structure analysis of oxidized Pseudomonas aeruginosa azurin at pH $5 \cdot 5$ and pH $9 \cdot 0$: A pH-induced conformational transition involves a peptide bond flip. *Journal of Molecular Biology*, 221(3):765–772, October 1991. ISSN 0022-2836. doi: 10.1016/0022-2836(91)80173-R. URL `http://www.sciencedirect.com/science/article/pii/002228369180173R`.

[2] Hirofumi Komori, Ryosuke Sugiyama, Kunishige Kataoka, Kentaro Miyazaki, Yoshiki Higuchi, and Takeshi Sakurai. New insights into the catalytic active-site structure of multicopper oxidases. *Acta Crystallographica. Section D, Biological Crystallography*, 70(Pt 3):772–779, March 2014. ISSN 1399-0047. doi: 10.1107/S1399004713033051.

[3] Hirofumi Komori, Takao Kajikawa, Kunishige Kataoka, Yoshiki Higuchi, and Takeshi Sakurai. Crystal structure of the CueO mutants at Glu506, the key amino acid located in the proton transfer pathway for dioxygen reduction. *Biochem. Biophys. Res. Commun.*, 438(4):686–690, September 2013. ISSN 1090-2104.

[4] James A. Fee. copper proteins systems containing the "Blue" copper center. In *Biochemistry*, Structure and Bonding, pages 1–60. Springer, Berlin, Heidelberg, 1975. ISBN 978-3-540-07332-1 978-3-540-37566-1. doi: 10.1007/BFb0116549. URL `https://link.springer.com/chapter/10.1007/BFb0116549`.

[5] A. G. Sykes. Active-Site Properties Of The Blue Copper Proteins. In A. G. Sykes, editor, *Advances in Inorganic Chemistry*, volume 36, pages 377–408. Academic Press, January 1991. doi: 10.1016/S0898-8838(08)60044-6.

[6] E. T. Adman. Copper protein structures. *Advances in Protein Chemistry*, 42: 145–197, 1991. ISSN 0065-3233.

[7] Edward I. Solomon, Robert K. Szilagyi, Serena DeBeer George, and Lipika Basumallick. Electronic Structures of Metal Sites in Proteins and Models: Contributions to Function in Blue Copper Proteins. *Chemical Reviews*, 104

(2):419–458, February 2004. ISSN 0009-2665. doi: 10.1021/cr0206317. URL http://dx.doi.org/10.1021/cr0206317.

[8] Somdatta Ghosh, Abhishek Dey, Yan Sun, Charles P. Scholes, and Edward I. Solomon. Spectroscopic and Computational Studies of Nitrite Reductase: Proton Induced Electron Transfer and Backbonding Contributions to Reactivity. *Journal of the American Chemical Society*, 131(1):277–288, January 2009. ISSN 0002-7863. doi: 10.1021/ja806873e. URL https://doi.org/10.1021/ja806873e.

[9] R. K. Szilagyi and E. I. Solomon. Electronic structure and its relation to function in copper proteins. *Current opinion in chemical biology*, 6(2):250–258, April 2002. ISSN 1367-5931. doi: 10.1016/S1367-5931(02)00304-6. URL http://europepmc.org/abstract/med/12039012.

[10] Edward I. Solomon, David W. Randall, and Thorsten Glaser. Electronic structures of active sites in electron transfer metalloproteins: contributions to reactivity. *Coordination Chemistry Reviews*, 200-202(Supplement C):595–632, May 2000. ISSN 0010-8545. doi: 10.1016/S0010-8545(00)00332-5. URL http://www.sciencedirect.com/science/article/pii/S0010854500003325.

[11] Christopher Dennison. Investigating the structure and function of cupredoxins. *Coordination Chemistry Reviews*, 249(24):3025–3054, December 2005. ISSN 0010-8545. doi: 10.1016/j.ccr.2005.04.021. URL http://www.sciencedirect.com/science/article/pii/S001085450500127X.

[12] Edward I. Solomon, Paula J. Clendening, Harry B. Gray, and F. J. Grunthaner. Direct observation of sulfur coordination in bean plastocyanin by x-ray photoelectron spectroscopy. *Journal of the American Chemical Society*, 97 (13):3878–3879, June 1975. ISSN 0002-7863. doi: 10.1021/ja00846a087. URL https://doi.org/10.1021/ja00846a087.

[13] John L. Markley, Eldon L. Ulrich, Steven P. Berg, and David W. Krogmann. Nuclear magnetic resonance studies of the copper binding sites of blue copper proteins. Oxidized, reduced, and apoplastocyanin. *Biochemistry*, 14(20): 4428–4433, October 1975. ISSN 0006-2960. doi: 10.1021/bi00691a014. URL https://doi.org/10.1021/bi00691a014.

[14] Mats H.M. Olsson, Ulf Ryde, and Björn O. Roos. Quantum chemical calculations of the reorganization energy of blue-copper proteins. *Protein Science*, 7(12): 2659–2668, December 1998. ISSN 1469-896X. doi: 10.1002/pro.5560071220. URL http://onlinelibrary.wiley.com/doi/10.1002/pro.5560071220/abstract.

[15] D. R. McMillin, R. C. Rosenberg, and H. B. Gray. Preparation and spectroscopic studies of cobalt(II) derivatives of blue copper proteins. *Proceedings of the National Academy of Sciences of the United States of America*, 71(12):4760–4762, December 1974. ISSN 0027-8424.

[16] Edward I. Solomon, Michael J. Baldwin, and Michael D. Lowery. Electronic structures of active sites in copper proteins: contributions to reactivity. *Chemical Reviews*, 92(4):521–542, June 1992. ISSN 0009-2665. doi: 10.1021/cr00012a003. URL `http://dx.doi.org/10.1021/cr00012a003`.

[17] Arindam Chowdhury, Linda A. Peteanu, Patrick L. Holland, and William B. Tolman. The Electronic Properties of a Model Active Site for Blue Copper Proteins as Probed by Stark Spectroscopy. *The Journal of Physical Chemistry B*, 106 (11):3007–3012, March 2002. ISSN 1520-6106. doi: 10.1021/jp0115751. URL `https://doi.org/10.1021/jp0115751`.

[18] Ester Fraga, M. Adam Webb, and Glen R. Loppnow. Charge-Transfer Dynamics in Plastocyanin, a Blue Copper Protein, from Resonance Raman Intensities. *The Journal of Physical Chemistry*, 100(8):3278–3287, January 1996. ISSN 0022-3654. doi: 10.1021/jp9525651. URL `https://doi.org/10.1021/jp9525651`.

[19] M. Adam Webb and Glen R. Loppnow. Evidence for Anisotropic Coupling between the Protein Environment and the Copper Site in Azurin from Resonance Raman Spectroscopy. *The Journal of Physical Chemistry B*, 106(8):2102–2108, February 2002. ISSN 1520-6106. doi: 10.1021/jp013665b. URL `https://doi.org/10.1021/jp013665b`.

[20] Edward I. Solomon, Uma M. Sundaram, and Timothy E. Machonkin. Multicopper Oxidases and Oxygenases. *Chemical Reviews*, 96(7):2563–2606, November 1996. ISSN 1520-6890.

[21] Daniel J. Kosman. Multicopper oxidases: a workshop on copper coordination chemistry, electron transfer, and metallophysiology. *Journal of biological inorganic chemistry: JBIC: a publication of the Society of Biological Inorganic Chemistry*, 15(1):15–28, January 2010. ISSN 1432-1327. doi: 10.1007/s00775-009-0590-9.

[22] A. Messerschmidt, R. Ladenstein, R. Huber, M. Bolognesi, L. Avigliano, R. Petruzzelli, A. Rossi, and A. Finazzi-Agró. Refined crystal structure of ascorbate oxidase at 1.9 A resolution. *Journal of Molecular Biology*, 224(1):179–205, March 1992. ISSN 0022-2836.

[23] Nina Hakulinen, Laura-Leena Kiiskinen, Kristiina Kruus, Markku Saloheimo, Arja Paananen, Anu Koivula, and Juha Rouvinen. Crystal structure of a laccase from

Melanocarpus albomyces with an intact trinuclear copper site. *Nature Structural Biology*, 9(8):601–605, August 2002. ISSN 1072-8368. doi: 10.1038/nsb823.

[24] C. Askwith, D. Eide, A. Van Ho, P. S. Bernard, L. Li, S. Davis-Kaplan, D. M. Sipe, and J. Kaplan. The FET3 gene of S. cerevisiae encodes a multicopper oxidase required for ferrous iron uptake. *Cell*, 76(2):403–410, January 1994. ISSN 0092-8674.

[25] Sue A. Roberts, Andrzej Weichsel, Gregor Grass, Keshari Thakali, James T. Hazzard, Gordon Tollin, Christopher Rensing, and William R. Montfort. Crystal structure and electron transfer kinetics of CueO, a multicopper oxidase required for copper homeostasis in Escherichia coli. *Proceedings of the National Academy of Sciences of the United States of America*, 99(5):2766–2771, March 2002. ISSN 0027-8424. doi: 10.1073/pnas.052710499.

[26] R. A. Marcus and Norman Sutin. Electron transfers in chemistry and biology. *Biochimica et Biophysica Acta (BBA) - Reviews on Bioenergetics*, 811(3):265–322, August 1985. ISSN 0304-4173. doi: 10.1016/0304-4173(85)90014-X. URL `http://www.sciencedirect.com/science/article/pii/030441738590014X`.

[27] T. Sakurai and K. Kataoka. Structure and function of type I copper in multicopper oxidases. *Cellular and Molecular Life Sciences*, 64(19-20):2642, July 2007. ISSN 1420-682X, 1420-9071. doi: 10.1007/s00018-007-7183-y. URL `http://link.springer.com/article/10.1007/s00018-007-7183-y`.

[28] Matěj Pavelka and Jaroslav V. Burda. Computational study of redox active centres of blue copper proteins: a computational DFT study. *Molecular Physics*, 106(24): 2733–2748, December 2008. ISSN 0026-8976. doi: 10.1080/00268970802672684. URL `http://dx.doi.org/10.1080/00268970802672684`.

[29] Jacques Meyer. Iron-sulfur protein folds, iron-sulfur chemistry, and evolution. *Journal of biological inorganic chemistry: JBIC: a publication of the Society of Biological Inorganic Chemistry*, 13(2):157–170, February 2008. ISSN 0949-8257. doi: 10.1007/s00775-007-0318-7.

[30] P. J. Stephens, D. R. Jollie, and A. Warshel. Protein Control of Redox Potentials of Iron − Sulfur Proteins. *Chemical Reviews*, 96(7):2491–2514, January 1996. ISSN 0009-2665. doi: 10.1021/cr950045w. URL `https://doi.org/10.1021/cr950045w`.

[31] Helmut Beinert and R. H. Sands. Studies on succinic and DPNH dehydrogenase preparations by paramagnetic resonance (EPR) spectroscopy. *Biochemical*

and Biophysical Research Communications, 3(1):41–46, July 1960. ISSN 0006-291X. doi: 10.1016/0006-291X(60)90100-5. URL http://www.sciencedirect.com/science/article/pii/0006291X60901005.

[32] L. E. Mortenson, R. C. Valentine, and J. E. Carnahan. An electron transport factor from Clostridium pasteurianum. *Biochemical and Biophysical Research Communications*, 7:448–452, June 1962. ISSN 0006-291X.

[33] Kunio Tagawa and Daniel I. Arnon. Ferredoxins as Electron Carriers in Photosynthesis and in the Biological Production and Consumption of Hydrogen Gas. *Nature*, 195(4841):537–543, August 1962. ISSN 0028-0836. doi: 10.1038/195537a0. URL https://www.nature.com/nature/journal/v195/n4841/abs/195537a0.html.

[34] Dennis H. Flint and Ronda M. Allen. Iron − Sulfur Proteins with Nonredox Functions. *Chemical Reviews*, 96(7):2315–2334, January 1996. ISSN 0009-2665. doi: 10.1021/cr950041r. URL https://doi.org/10.1021/cr950041r.

[35] Roland Lill. Function and biogenesis of iron-sulphur proteins. *Nature*, 460(7257):831–838, August 2009. ISSN 1476-4687. doi: 10.1038/nature08301.

[36] H. Beinert, R. H. Holm, and E. Münck. Iron-sulfur clusters: nature's modular, multipurpose structures. *Science (New York, N.Y.)*, 277(5326):653–659, August 1997. ISSN 0036-8075.

[37] Kamil Brzóska, Sylwia Meczyńska, and Marcin Kruszewski. Iron-sulfur cluster proteins: electron transfer and beyond. *Acta Biochimica Polonica*, 53(4):685–691, 2006. ISSN 0001-527X.

[38] Nomenclature Committee of the International Union of Biochemistry (NC-IUB). Nomenclature of iron-sulfur proteins Recommendations, 1978. *Biochimica et Biophysica Acta (BBA) - Reviews on Bioenergetics*, 549(2):101–105, August 1979. ISSN 0304-4173. doi: 10.1016/0304-4173(79)90011-9. URL http://www.sciencedirect.com/science/article/pii/0304417379900119.

[39] Hiroshi Matsubara and Kazuhiko Saeki. Structural and Functional Diversity of Ferredoxins and Related Proteins. In Richard Cammack, editor, *Advances in Inorganic Chemistry*, volume 38, pages 223–280. Academic Press, January 1992. doi: 10.1016/S0898-8838(08)60065-3. URL http://www.sciencedirect.com/science/article/pii/S0898883808600653.

[40] H Brintzinger, G Palmer, and R H Sands. On the ligand field of iron in ferredoxin from spinach chloroplasts and related nonheme iron enzymes. *Proceedings of the*

National Academy of Sciences of the United States of America, 55(2):397–404, February 1966. ISSN 0027-8424. URL https://www.ncbi.nlm.nih.gov/pmc/articles/PMC224157/.

[41] P. J. Stephens, A. J. Thomson, J. B. R. Dunn, T. A. Keiderling, J. Rawlings, K. K. Rao, and D. O. Hall. Circular dichroism and magnetic circular dichroism of iron-sulfur proteins. *Biochemistry*, 17(22):4770–4778, October 1978. ISSN 0006-2960. doi: 10.1021/bi00615a026. URL https://doi.org/10.1021/bi00615a026.

[42] John C. M. Tsibris and Robert W. Woody. Structural studies of iron-sulfur proteins. *Coordination Chemistry Reviews*, 5(4):417–458, December 1970. ISSN 0010-8545. doi: 10.1016/S0010-8545(00)80100-9. URL http://www.sciencedirect.com/science/article/pii/S0010854500801009.

[43] P. Hohenberg and W. Kohn. Inhomogeneous Electron Gas. *Physical Review*, 136 (3B):B864–B871, November 1964. doi: 10.1103/PhysRev.136.B864. URL https://link.aps.org/doi/10.1103/PhysRev.136.B864.

[44] E. Schrödinger. Quantisierung als Eigenwertproblem. *Annalen der Physik*, 384(4): 361–376, 1926. ISSN 1521-3889. doi: 10.1002/andp.19263840404. URL https://onlinelibrary.wiley.com/doi/abs/10.1002/andp.19263840404.

[45] Paul Adrien Maurice Dirac. The quantum theory of the electron. *Proc. R. Soc. Lond. A*, 117(778):610–624, February 1928. ISSN 0950-1207, 2053-9150. doi: 10.1098/rspa.1928.0023. URL http://rspa.royalsocietypublishing.org/content/117/778/610.

[46] Attila Szabo and Neil S. Ostlund. *Modern Quantum Chemistry*. Macmillan, New York, 1982.

[47] W. Kohn and L. J. Sham. Self-Consistent Equations Including Exchange and Correlation Effects. *Physical Review*, 140(4A):A1133–A1138, November 1965. doi: 10.1103/PhysRev.140.A1133. URL https://link.aps.org/doi/10.1103/PhysRev.140.A1133.

[48] E. Fermi. Eine statistische Methode zur Bestimmung einiger Eigenschaften des Atoms und ihre Anwendung auf die Theorie des periodischen Systems der Elemente. *Zeitschrift für Physik*, 48(1-2):73–79, January 1928. ISSN 0044-3328. doi: 10.1007/BF01351576. URL https://link.springer.com/article/10.1007/BF01351576.

[49] L. H. Thomas. The calculation of atomic fields. *Mathematical Proceedings of the Cambridge Philosophical Society*, 23(5):

542–548, January 1927. ISSN 1469-8064, 0305-0041. doi: 10.1017/S0305004100011683. URL https://www.cambridge.org/core/journals/mathematical-proceedings-of-the-cambridge-philosophical-society/article/calculation-of-atomic-fields/ADCA3D21D0FACD7077B5FDBB7F3B3F3A.

[50] U. von Barth and L. Hedin. A local exchange-correlation potential for the spin polarized case. i. *Journal of Physics C: Solid State Physics*, 5(13):1629, 1972. ISSN 0022-3719. doi: 10.1088/0022-3719/5/13/012. URL http://stacks.iop.org/0022-3719/5/i=13/a=012.

[51] S. H. Vosko, L. Wilk, and M. Nusair. Accurate spin-dependent electron liquid correlation energies for local spin density calculations: a critical analysis. *Canadian Journal of Physics*, 58(8):1200–1211, August 1980. ISSN 0008-4204. doi: 10.1139/p80-159. URL http://www.nrcresearchpress.com/doi/abs/10.1139/p80-159.

[52] John P. Perdew and Yue Wang. Accurate and simple analytic representation of the electron-gas correlation energy. *Physical Review B*, 45(23):13244–13249, June 1992. doi: 10.1103/PhysRevB.45.13244. URL https://link.aps.org/doi/10.1103/PhysRevB.45.13244.

[53] John P. Perdew and Wang Yue. Accurate and simple density functional for the electronic exchange energy: Generalized gradient approximation. *Physical Review B*, 33(12):8800–8802, June 1986. doi: 10.1103/PhysRevB.33.8800. URL https://link.aps.org/doi/10.1103/PhysRevB.33.8800.

[54] John P. Perdew. Erratum: Density-functional approximation for the correlation energy of the inhomogeneous electron gas. *Physical Review B*, 34(10):7406–7406, November 1986. doi: 10.1103/PhysRevB.34.7406. URL https://link.aps.org/doi/10.1103/PhysRevB.34.7406.

[55] A. D. Becke. Density-functional exchange-energy approximation with correct asymptotic behavior. *Physical Review A*, 38(6):3098–3100, September 1988. doi: 10.1103/PhysRevA.38.3098. URL https://link.aps.org/doi/10.1103/PhysRevA.38.3098.

[56] Chengteh Lee, Weitao Yang, and Robert G. Parr. Development of the Colle-Salvetti correlation-energy formula into a functional of the electron density. *Physical Review B*, 37(2):785–789, January 1988. doi: 10.1103/PhysRevB.37.785. URL https://link.aps.org/doi/10.1103/PhysRevB.37.785.

[57] Axel D. Becke. A new mixing of Hartree – Fock and local density - functional theories. *The Journal of Chemical Physics*, 98(2):1372–1377, January 1993. ISSN

0021-9606. doi: 10.1063/1.464304. URL https://aip.scitation.org/doi/10.1063/1.464304.

[58] A. D. Becke. Correlation energy of an inhomogeneous electron gas: A coordinate - space model. *The Journal of Chemical Physics*, 88(2):1053–1062, January 1988. ISSN 0021-9606. doi: 10.1063/1.454274. URL https://aip.scitation.org/doi/10.1063/1.454274.

[59] Yan Zhao and Donald G. Truhlar. The M06 suite of density functionals for main group thermochemistry, thermochemical kinetics, noncovalent interactions, excited states, and transition elements: two new functionals and systematic testing of four M06-class functionals and 12 other functionals. *Theoretical Chemistry Accounts*, 120(1-3):215–241, July 2007. ISSN 1432-881X, 1432-2234. doi: 10.1007/s00214-007-0310-x. URL http://link.springer.com/article/10.1007/s00214-007-0310-x.

[60] John P. Perdew, Kieron Burke, and Matthias Ernzerhof. Generalized Gradient Approximation Made Simple. *Physical Review Letters*, 77(18):3865–3868, October 1996. doi: 10.1103/PhysRevLett.77.3865. URL https://link.aps.org/doi/10.1103/PhysRevLett.77.3865.

[61] P. M. Colman, H. C. Freeman, J. M. Guss, M. Murata, V. A. Norris, J. a. M. Ramshaw, and M. P. Venkatappa. X-ray crystal structure analysis of plastocyanin at 2.7 |[angst]| resolution. *Nature*, 272(5651):319–324, March 1978. ISSN 0028-0836. doi: 10.1038/272319a0. URL http://www.nature.com/nature/journal/v272/n5651/abs/272319a0.html.

[62] E. T. Adman and L. H. Jensen. Structural Features of Azurin at 2.7 Å Resolution. *Israel Journal of Chemistry*, 21(1):8–12, January 1981. ISSN 1869-5868. doi: 10.1002/ijch.198100003. URL http://onlinelibrary.wiley.com/doi/10.1002/ijch.198100003/abstract.

[63] Konstantinos Paraskevopoulos, Mahesh Sundararajan, Rajeev Surendran, Michael A. Hough, Robert R. Eady, Ian H. Hillier, and S. Samar Hasnain. Active site structures and the redox properties of blue copper proteins: atomic resolution structure of azurin II and electronic structure calculations of azurin, plastocyanin and stellacyanin. *Dalton Transactions*, 0(25):3067–3076, June 2006. ISSN 1477-9234. doi: 10.1039/B513942B. URL http://pubs.rsc.org/en/content/articlelanding/2006/dt/b513942b.

[64] Marjorie M. Harding, Matthew W. Nowicki, and Malcolm D. Walkinshaw. Metals in protein structures: a review of their principal features. *Crystallography Reviews*,

16(4):247–302, October 2010. ISSN 0889-311X. doi: 10.1080/0889311X.2010.485616. URL http://dx.doi.org/10.1080/0889311X.2010.485616.

[65] David E. Heppner, Christian H. Kjaergaard, and Edward I. Solomon. Mechanism of the Reduction of the Native Intermediate in the Multicopper Oxidases: Insights into Rapid Intramolecular Electron Transfer in Turnover. *Journal of the American Chemical Society*, 136(51):17788–17801, December 2014. ISSN 0002-7863. doi: 10.1021/ja509150j. URL http://dx.doi.org/10.1021/ja509150j.

[66] R A Holwerda, S Wherland, and and H. B. Gray. Electron Transfer Reactions of Copper Proteins. *Annual Review of Biophysics and Bioengineering*, 5(1):363–396, 1976. doi: 10.1146/annurev.bb.05.060176.002051. URL http://dx.doi.org/10.1146/annurev.bb.05.060176.002051.

[67] Edward I. Solomon, Jeffrey W. Hare, David M. Dooley, John H. Dawson, Philip J. Stephens, and Harry B. Gray. Spectroscopic studies of stellacyanin, plastocyanin, and azurin. Electronic structure of the blue copper sites. *Journal of the American Chemical Society*, 102(1):168–178, January 1980. ISSN 0002-7863. doi: 10.1021/ja00521a029. URL http://dx.doi.org/10.1021/ja00521a029.

[68] David R. McMillin and Margaret C. Morris. Further perspectives on the charge transfer transitions of blue copper proteins and the ligand moieties in stellacyanin. *Proceedings of the National Academy of Sciences of the United States of America*, 78(11):6567–6570, November 1981. ISSN 0027-8424. URL http://www.ncbi.nlm.nih.gov/pmc/articles/PMC349088/.

[69] E. Bouwman, W. L. Driessen, and J. Reedijk. Model systems for type I copper proteins: structures of copper coordination compounds with thioether and azole-containing ligands. *Coordination Chemistry Reviews*, 104(1):143–172, July 1990. ISSN 0010-8545. doi: 10.1016/0010-8545(90)80042-R. URL http://www.sciencedirect.com/science/article/pii/001085459080042R.

[70] Di Qiu, Shoulian Dong, Joel Ybe, Michael Hecht, and Thomas G. Spiro. Variations in the Type I Copper Protein Coordination Group: Resonance Raman Spectrum of 34s-, 65cu-, and 15n-Labeled Plastocyanin. *Journal of the American Chemical Society*, 117(24):6443–6446, June 1995. ISSN 0002-7863. doi: 10.1021/ja00129a005. URL http://dx.doi.org/10.1021/ja00129a005.

[71] Edward I. Solomon, Peng Chen, Markus Metz, Sang-Kyu Lee, and Amy E. Palmer. Oxygen Binding, Activation, and Reduction to Water by Copper Proteins. *Angewandte Chemie (International Ed. in English)*, 40(24):4570–4590, December 2001. ISSN 1521-3773.

[72] Klaus Piontek, Matteo Antorini, and Thomas Choinowski. Crystal Structure of a Laccase from the FungusTrametes versicolor at 1.90-Å Resolution Containing a Full Complement of Coppers. *Journal of Biological Chemistry*, 277 (40):37663–37669, October 2002. ISSN 0021-9258, 1083-351X. URL `http://www.jbc.org/content/277/40/37663`.

[73] Sergey Shleev, Jan Tkac, Andreas Christenson, Tautgirdas Ruzgas, Alexander I. Yaropolov, James W. Whittaker, and Lo Gorton. Direct electron transfer between copper-containing proteins and electrodes. *Biosensors and Bioelectronics*, 20(12): 2517–2554, June 2005. ISSN 0956-5663. doi: 10.1016/j.bios.2004.10.003. URL `http://www.sciencedirect.com/science/article/pii/S0956566304004580`.

[74] Marta Ferraroni, Nina M. Myasoedova, Vadim Schmatchenko, Alexey A. Leontievsky, Ludmila A. Golovleva, Andrea Scozzafava, and Fabrizio Briganti. Crystal structure of a blue laccase from Lentinus tigrinus: evidences for intermediates in the molecular oxygen reductive splitting by multicopper oxidases. *BMC Structural Biology*, 7:60, 2007. ISSN 1472-6807. doi: 10.1186/1472-6807-7-60. URL `http://dx.doi.org/10.1186/1472-6807-7-60`.

[75] Takeshi Sakurai and Kunishige Kataoka. Basic and applied features of multicopper oxidases, CueO, bilirubin oxidase, and laccase. *The Chemical Record*, 7(4):220–229, January 2007. ISSN 1528-0691. doi: 10.1002/tcr.20125. URL `http://onlinelibrary.wiley.com/doi/10.1002/tcr.20125/abstract`.

[76] Jungjoo Yoon and Edward I. Solomon. Electronic structures of exchange coupled trigonal trimeric Cu(II) complexes: Spin frustration, antisymmetric exchange, pseudo-A terms, and their relation to O2 activation in the multicopper oxidases. *Coordination Chemistry Reviews*, 251(3 – 4):379–400, February 2007. ISSN 0010-8545. doi: 10.1016/j.ccr.2006.04.012. URL `http://www.sciencedirect.com/science/article/pii/S0010854506001172`.

[77] Liliana Quintanar, Christopher Stoj, Alexander B. Taylor, P. John Hart, Daniel J. Kosman, and Edward I. Solomon. Shall We Dance? How A Multicopper Oxidase Chooses Its Electron Transfer Partner. *Accounts of Chemical Research*, 40(6): 445–452, June 2007. ISSN 0001-4842. doi: 10.1021/ar600051a. URL `http://dx.doi.org/10.1021/ar600051a`.

[78] Jungjoo Yoon, Barry D. Liboiron, Ritimukta Sarangi, Keith O. Hodgson, Britt Hedman, and Edward I. Solomon. The two oxidized forms of the trinuclear Cu cluster in the multicopper oxidases and mechanism for the decay of the native intermediate. *Proceedings of the National Academy of Sciences*, 104(34):13609–13614,

August 2007. ISSN 0027-8424, 1091-6490. doi: 10.1073/pnas.0705137104. URL http://www.pnas.org/content/104/34/13609.

[79] Kunishige Kataoka, Hirofumi Komori, Yusaku Ueki, Yusuke Konno, Yuji Kamitaka, Shinji Kurose, Seiya Tsujimura, Yoshiki Higuchi, Kenji Kano, Daisuke Seo, and Takeshi Sakurai. Structure and Function of the Engineered Multicopper Oxidase CueO from Escherichia coli—Deletion of the Methionine-Rich Helical Region Covering the Substrate-Binding Site. *Journal of Molecular Biology*, 373(1): 141–152, October 2007. ISSN 0022-2836. doi: 10.1016/j.jmb.2007.07.041. URL http://www.sciencedirect.com/science/article/pii/S0022283607009692.

[80] Karrera Y. Djoko, Lee Xin Chong, Anthony G. Wedd, and Zhiguang Xiao. Reaction Mechanisms of the Multicopper Oxidase CueO from Escherichia coli Support Its Functional Role as a Cuprous Oxidase. *Journal of the American Chemical Society*, 132(6):2005–2015, February 2010. ISSN 0002-7863. doi: 10.1021/ja9091903. URL http://dx.doi.org/10.1021/ja9091903.

[81] Anthony J. Augustine, Christian Kjaergaard, Munzarin Qayyum, Lynn Ziegler, Daniel J. Kosman, Keith O. Hodgson, Britt Hedman, and Edward I. Solomon. Systematic Perturbation of the Trinuclear Copper Cluster in the Multicopper Oxidases: The Role of Active Site Asymmetry in Its Reduction of O2 to H2o. *Journal of the American Chemical Society*, 132(17):6057–6067, May 2010. ISSN 0002-7863. doi: 10.1021/ja909143d. URL http://dx.doi.org/10.1021/ja909143d.

[82] Isabel Pardo and Susana Camarero. Laccase engineering by rational and evolutionary design. *Cellular and Molecular Life Sciences*, 72(5):897–910, 2015. ISSN 1420-682X. doi: 10.1007/s00018-014-1824-8. URL http://www.ncbi.nlm.nih.gov/pmc/articles/PMC4323517/.

[83] David Robinson and Nicholas A. Besley. Modelling the spectroscopy and dynamics of plastocyanin. *Physical chemistry chemical physics: PCCP*, 12(33):9667–9676, September 2010. ISSN 1463-9084. doi: 10.1039/c001805h.

[84] Stefano Corni, Francesca De Rienzo, Rosa Di Felice, and Elisa Molinari. Role of the electronic properties of azurin active site in the electron-transfer process. *International Journal of Quantum Chemistry*, 102(3):328–342, January 2005. ISSN 1097-461X. doi: 10.1002/qua.20374. URL http://onlinelibrary.wiley.com/doi/10.1002/qua.20374/abstract.

[85] Yan Zhao and Donald G. Truhlar. Computational characterization and modeling of buckyball tweezers: density functional study of concave – convex π π interactions. *Physical Chemistry Chemical Physics*, 10(19):2813–2818, May 2008. ISSN

1463-9084. doi: 10.1039/B717744E. URL http://pubs.rsc.org/en/content/articlelanding/2008/cp/b717744e.

[86] Umesh Warde, Lydia Rhyman, Ponnadurai Ramasami, and Nagaiyan Sekar. DFT Studies of the Photophysical Properties of Fluorescent and Semiconductor Polycyclic Benzimidazole Derivatives. *Journal of Fluorescence*, 25(3):685–694, March 2015. ISSN 1053-0509, 1573-4994. doi: 10.1007/s10895-015-1554-9. URL http://link.springer.com/article/10.1007/s10895-015-1554-9.

[87] Yury Minenkov, Åsmund Singstad, Giovanni Occhipinti, and Vidar R. Jensen. The accuracy of DFT-optimized geometries of functional transition metal compounds: a validation study of catalysts for olefin metathesis and other reactions in the homogeneous phase. *Dalton Transactions*, 41(18):5526–5541, April 2012. ISSN 1477-9234. doi: 10.1039/C2DT12232D. URL http://pubs.rsc.org/en/content/articlelanding/2012/dt/c2dt12232d.

[88] Dilek Coskun, Steven V. Jerome, and Richard A. Friesner. Evaluation of the Performance of the B3lyp, PBE0, and M06 DFT Functionals, and DBLOC-Corrected Versions, in the Calculation of Redox Potentials and Spin Splittings for Transition Metal Containing Systems. *Journal of Chemical Theory and Computation*, 12(3):1121–1128, March 2016. ISSN 1549-9618. doi: 10.1021/acs.jctc.5b00782. URL http://dx.doi.org/10.1021/acs.jctc.5b00782.

[89] Tomofumi Shuku, Kimikazu Sugimori, Ayumu Sugiyama, Hidemi Nagao, Takeshi Sakurai, and Kiyoshi Nishikawa. Molecular orbital analysis of active site of oxidized azurin: Dependency of electronic properties on molecular structure. *Polyhedron*, 24(16 – 17):2665–2670, November 2005. ISSN 0277-5387. doi: 10.1016/j.poly.2005.03.141. URL http://www.sciencedirect.com/science/article/pii/S0277538705003281.

[90] Ayumu Sugiyama, Kimikazu Sugimori, Tomofumi Shuku, Taichi Nakamura, Hiroaki Saito, Hidemi Nagao, Hiroyuki Kawabe, and Kiyoshi Nishikawa. Electronic structure of the active site with two configurations of azurin. *International Journal of Quantum Chemistry*, 105(6):588–595, January 2005. ISSN 1097-461X. doi: 10.1002/qua.20783. URL http://onlinelibrary.wiley.com/doi/10.1002/qua.20783/abstract.

[91] Kimikazu Sugimori, Tomofumi Shuku, Ayumu Sugiyama, Hidemi Nagao, Takeshi Sakurai, and Kiyoshi Nishikawa. Solvent effects on electronic structure of active site of azurin by polarizable continuum model. *Polyhedron*, 24(16 – 17):2671–2675, November 2005. ISSN 0277-5387. doi: 10.1016/j.poly.2005.03.140. URL http://www.sciencedirect.com/science/article/pii/S027753870500327X.

[92] M. J. Frisch, G. W. Trucks, H. B. Schlegel, G. E. Scuseria, M. A. Robb, J. R. Cheeseman, G. Scalmani, V. Barone, B. Mennucci, G. A. Petersson, H. Nakatsuji, M. Caricato, X. Li, H. P. Hratchian, A. F. Izmaylov, J. Bloino, G. Zheng, J. L. Sonnenberg, M. Hada, M. Ehara, K. Toyota, R. Fukuda, J. Hasegawa, M. Ishida, T. Nakajima, Y. Honda, O. Kitao, H. Nakai, T. Vreven, J. A. Montgomery, J. E. Peralta, F. Ogliaro, M. Bearpark, J. J. Heyd, E. Brothers, K. N. Kudin, V. N. Staroverov, R. Kobayashi, J. Normand, K. Raghavachari, A. Rendell, J. C. Burant, S. S. Iyengar, J. Tomasi, M. Cossi, N. Rega, J. M. Millam, M. Klene, J. E. Knox, J. B. Cross, V. Bakken, C. Adamo, J. Jaramillo, R. Gomperts, R. E. Stratmann, O. Yazyev, A. J. Austin, R. Cammi, C. Pomelli, J. W. Ochterski, R. L. Martin, K. Morokuma, V. G. Zakrzewski, G. A. Voth, P. Salvador, J. J. Dannenberg, S. Dapprich, A. D. Daniels, O. Farkas, J. B. Foresman, J. V. Ortiz, J. Cioslowski, and D. J. Fox. Gaussian 09, Revision E.01, 2009.

[93] U. Chandra Singh and Peter A. Kollman. An approach to computing electrostatic charges for molecules. *Journal of Computational Chemistry*, 5(2): 129–145, April 1984. ISSN 1096-987X. doi: 10.1002/jcc.540050204. URL `http://onlinelibrary.wiley.com/doi/10.1002/jcc.540050204/abstract`.

[94] Benedetta Mennucci. Polarizable continuum model. *Wiley Interdisciplinary Reviews: Computational Molecular Science*, 2(3):386–404, May 2012. ISSN 1759-0884. doi: 10.1002/wcms.1086. URL `http://onlinelibrary.wiley.com/doi/10.1002/wcms.1086/abstract`.

[95] Travis V. Harris and Robert K. Szilagyi. Protein environmental effects on iron-sulfur clusters: A set of rules for constructing computational models for inner and outer coordination spheres. *Journal of Computational Chemistry*, 37(18): 1681–1696, July 2016. ISSN 1096-987X. doi: 10.1002/jcc.24384. URL `http://onlinelibrary.wiley.com/doi/10.1002/jcc.24384/abstract`.

[96] Chunmei Liu, Bin Zhang, Yanyan Zhu, and Mingsheng Tang. Evaluations of AMBER force field parameters by MINA approach for copper-based nucleases. *Structural Chemistry*, pages 1–16, May 2016. ISSN 1040-0400, 1572-9001. doi: 10.1007/s11224-016-0764-3. URL `http://link.springer.com/article/10.1007/s11224-016-0764-3`.

[97] Timothy E. Machonkin, Liliana Quintanar, Amy E. Palmer, Richard Hassett, Scott Severance, Daniel J. Kosman, and Edward I. Solomon. Spectroscopy and Reactivity of the Type 1 Copper Site in Fet3p from Saccharomyces cerevisiae: Correlation of Structure with Reactivity in the Multicopper Oxidases. *Journal of the American Chemical Society*, 123(23):5507–5517, June 2001. ISSN 0002-7863. doi: 10.1021/ja003975s. URL `http://dx.doi.org/10.1021/ja003975s`.

[98] Harry B. Gray, Bo G. Malmström, and R. J. P. Williams. Copper coordination in blue proteins. *JBIC Journal of Biological Inorganic Chemistry*, 5(5):551–559, October 2000. ISSN 0949-8257, 1432-1327. doi: 10.1007/s007750000146. URL https://link.springer.com/article/10.1007/s007750000146.

[99] Angel J. Di Bilio, Michael G. Hill, Nicklas Bonander, B. Göran Karlsson, Randy M. Villahermosa, Bo G. Malmström, Jay R. Winkler, and Harry B. Gray. Reorganization Energy of Blue Copper: Effects of Temperature and Driving Force on the Rates of Electron Transfer in Ruthenium- and Osmium-Modified Azurins. *Journal of the American Chemical Society*, 119(41):9921–9922, October 1997. ISSN 0002-7863. doi: 10.1021/ja971518e. URL http://dx.doi.org/10.1021/ja971518e.

[100] Michael D. Lowery and Edward I. Solomon. Axial ligand bonding in blue copper proteins. *Inorganica Chimica Acta*, 198-200(Supplement C):233–243, August 1992. ISSN 0020-1693. doi: 10.1016/S0020-1693(00)92365-X. URL http://www.sciencedirect.com/science/article/pii/S002016930092365X.

[101] Hui Li, Simon P. Webb, Joseph Ivanic, and Jan H. Jensen. Determinants of the relative reduction potentials of type-1 copper sites in proteins. *Journal of the American Chemical Society*, 126(25):8010–8019, June 2004. ISSN 0002-7863. doi: 10.1021/ja049345y.

[102] Dewain K. Garner, Mark D. Vaughan, Hee Jung Hwang, Masha G. Savelieff, Steven M. Berry, John F. Honek, and Yi Lu. Reduction Potential Tuning of the Blue Copper Center in Pseudomonas aeruginosa Azurin by the Axial Methionine as Probed by Unnatural Amino Acids. *Journal of the American Chemical Society*, 128(49):15608–15617, December 2006. ISSN 0002-7863. doi: 10.1021/ja062732i. URL http://dx.doi.org/10.1021/ja062732i.

[103] Yuji Kamitaka, Seiya Tsujimura, Kunishige Kataoka, Takeshi Sakurai, Tokuji Ikeda, and Kenji Kano. Effects of axial ligand mutation of the type I copper site in bilirubin oxidase on direct electron transfer-type bioelectrocatalytic reduction of dioxygen. *Journal of Electroanalytical Chemistry*, 601(1):119–124, March 2007. ISSN 1572-6657. doi: 10.1016/j.jelechem.2006.10.035. URL http://www.sciencedirect.com/science/article/pii/S0022072806006140.

[104] Sandra J. Kroes, Carla W. G. Hoitink, Colin R. Andrew, Jingyuan Ai, Joann Sanders-Loehr, Albrecht Messerschmidt, Wilfred R. Hagen, and Gerard W. Canters. The Mutation Met121 → His Creates a Type-1.5 Copper Site in Alcaligenes denitrificans Azurin. *European Journal of Biochemistry*, 240(2): 342–351, September 1996. ISSN 1432-1033. doi: 10.1111/j.1432-1033.1996.0342h.

x. URL http://onlinelibrary.wiley.com/doi/10.1111/j.1432-1033.1996.0342h.x/abstract.

[105] Serena DeBeer, David W. Randall, Aram M. Nersissian, Joan Selverstone Valentine, Britt Hedman, Keith O. Hodgson, and Edward I. Solomon. X-ray Absorption Edge and EXAFS Studies of the Blue Copper Site in Stellacyanin: Effects of Axial Amide Coordination. *The Journal of Physical Chemistry B*, 104(46): 10814–10819, November 2000. ISSN 1520-6106. doi: 10.1021/jp001334d. URL http://dx.doi.org/10.1021/jp001334d.

[106] Ole Farver, Lars K. Skov, Torbjoern Pascher, B. Goeran Karlsson, Margareta Nordling, Lennart G. Lundberg, Tore Vaenngaard, and Israel Pecht. Intramolecular electron transfer in single-site-mutated azurins. *Biochemistry*, 32 (28):7317–7322, July 1993. ISSN 0006-2960. doi: 10.1021/bi00079a031. URL http://dx.doi.org/10.1021/bi00079a031.

[107] S. Trasatti. The absolute electrode potential: an explanatory note (Recommendations 1986). *Pure and Applied Chemistry*, 58(7):417–428, January 1986. ISSN 1365-3075, 0033-4545. doi: 10.1351/pac198658070955. URL http://www.degruyter.com/view/j/pac.1986.58.issue-7/pac198658070955/pac198658070955.xml.

[108] Wen-Ge Han and Louis Noodleman. Quantum cluster size and solvent polarity effects on the geometries and Mössbauer properties of the active site model for ribonucleotide reductase intermediate X: a density functional theory study. *Theoretical Chemistry Accounts*, 125(3-6):305–317, April 2009. ISSN 1432-881X, 1432-2234. doi: 10.1007/s00214-009-0566-4. URL http://link.springer.com/article/10.1007/s00214-009-0566-4.

[109] Jing Liu, Saumen Chakraborty, Parisa Hosseinzadeh, Yang Yu, Shiliang Tian, Igor Petrik, Ambika Bhagi, and Yi Lu. Metalloproteins Containing Cytochrome, Iron – Sulfur, or Copper Redox Centers. *Chemical Reviews*, 114(8):4366–4469, April 2014. ISSN 0009-2665. doi: 10.1021/cr400479b. URL http://dx.doi.org/10.1021/cr400479b.

[110] Jeverson Frazzon and Dennis R Dean. Formation of iron – sulfur clusters in bacteria: an emerging field in bioinorganic chemistry. *Current Opinion in Chemical Biology*, 7(2):166–173, April 2003. ISSN 1367-5931. doi: 10.1016/S1367-5931(03)00021-8. URL http://www.sciencedirect.com/science/article/pii/S1367593103000218.

[111] Y. I. Shethna, P. W. Wilson, Raymond E. Hansen, and Helmut Beinert. IDENTIFICATION BY ISOTOPIC SUBSTITUTION OF THE EPR SIGNAL AT g =

1.94 IN A NON-HEME IRON PROTEIN FROM AZOTOBACTER*. *Proceedings of the National Academy of Sciences of the United States of America*, 52(5): 1263–1271, November 1964. ISSN 0027-8424. URL http://www.ncbi.nlm.nih.gov/pmc/articles/PMC300434/.

[112] D. C. Yoch and R. P. Carithers. Bacterial iron-sulfur proteins. *Microbiological Reviews*, 43(3):384–421, September 1979. ISSN 0146-0749.

[113] Walter Lovenberg, Bob B. Buchanan, and Jesse C. Rabinowitz. Studies on the Chemical Nature of Clostridial Ferredoxin. *Journal of Biological Chemistry*, 238 (12):3899–3913, December 1963. ISSN 0021-9258, 1083-351X. URL http://www.jbc.org/content/238/12/3899.

[114] Bob B. Buchanan, Walter Lovenberg, and Jesse C. Rabinowitz. A COMPARISON OF CLOSTRIDIAL FERREDOXINS*. *Proceedings of the National Academy of Sciences of the United States of America*, 49(3):345–353, March 1963. ISSN 0027-8424. URL http://www.ncbi.nlm.nih.gov/pmc/articles/PMC299830/.

[115] Kunio Tagawa and Daniel I. Arnon. Oxidation-reduction potentials and stoichiometry of electron transfer in ferredoxins. *Biochimica et Biophysica Acta (BBA) - Bioenergetics*, 153(3):602–613, April 1968. ISSN 0005-2728. doi: 10.1016/0005-2728(68)90188-6. URL http://www.sciencedirect.com/science/article/pii/0005272868901886.

[116] Louis Noodleman, Joe G. Norman, Joseph H. Osborne, Arie Aizman, and David A. Case. Models for ferredoxins: electronic structures of iron-sulfur clusters with one, two, and four iron atoms. *Journal of the American Chemical Society*, 107 (12):3418–3426, June 1985. ISSN 0002-7863. doi: 10.1021/ja00298a004. URL http://dx.doi.org/10.1021/ja00298a004.

[117] Louis. Noodleman, David A. Case, and Arie. Aizman. Broken symmetry analysis of spin coupling in iron-sulfur clusters. *Journal of the American Chemical Society*, 110(4):1001–1005, February 1988. ISSN 0002-7863. doi: 10.1021/ja00212a003. URL http://dx.doi.org/10.1021/ja00212a003.

[118] Jean-Marie Mouesca, Jun L. Chen, Louis Noodleman, Donald Bashford, and David A. Case. Density Functional/Poisson-Boltzmann Calculations of Redox Potentials for Iron-Sulfur Clusters. *Journal of the American Chemical Society*, 116 (26):11898–11914, December 1994. ISSN 0002-7863. doi: 10.1021/ja00105a033. URL http://dx.doi.org/10.1021/ja00105a033.

[119] Lucia Banci, Ivano Bertini, Giovanni Gori Savellini, and Claudio Luchinat. Individual Reduction Potentials of the Iron Ions in Fe2s2 and High-Potential Fe4s4

Ferredoxins. *Inorganic Chemistry*, 35(14):4248–4253, January 1996. ISSN 0020-1669. doi: 10.1021/ic960051q. URL http://dx.doi.org/10.1021/ic960051q.

[120] Jian Li, Melanie R. Nelson, Chun Y. Peng, Donald Bashford, and Louis Noodleman. Incorporating Protein Environments in Density Functional Theory: A Self-Consistent Reaction Field Calculation of Redox Potentials of [2fe2s] Clusters in Ferredoxin and Phthalate Dioxygenase Reductase. *The Journal of Physical Chemistry A*, 102(31):6311–6324, July 1998. ISSN 1089-5639. doi: 10.1021/jp980753w. URL http://dx.doi.org/10.1021/jp980753w.

[121] Toru Matsui, Yasutaka Kitagawa, Mitsutaka Okumura, Yasuteru Shigeta, and Shigeyoshi Sakaki. Consistent scheme for computing standard hydrogen electrode and redox potentials. *Journal of Computational Chemistry*, 34(1):21–26, January 2013. ISSN 1096-987X. doi: 10.1002/jcc.23100. URL http://onlinelibrary.wiley.com/doi/10.1002/jcc.23100/abstract.

[122] Toru Matsui, Yasutaka Kitagawa, Yasuteru Shigeta, and Mitsutaka Okumura. A Density Functional Theory Based Protocol to Compute the Redox Potential of Transition Metal Complex with the Correction of Pseudo-Counterion: General Theory and Applications. *Journal of Chemical Theory and Computation*, 9(7):2974–2980, July 2013. ISSN 1549-9618. doi: 10.1021/ct4002653. URL http://dx.doi.org/10.1021/ct4002653.

[123] Toru Matsui, Yasutaka Kitagawa, Mitsutaka Okumura, and Yasuteru Shigeta. Accurate Standard Hydrogen Electrode Potential and Applications to the Redox Potentials of Vitamin C and NAD/NADH. *The Journal of Physical Chemistry A*, 119(2):369–376, January 2015. ISSN 1089-5639. doi: 10.1021/jp508308y. URL http://dx.doi.org/10.1021/jp508308y.

[124] C. Binda, A. Coda, A. Aliverti, G. Zanetti, and A. Mattevi. Structure of the mutant E92k of [2fe-2s] ferredoxin I from Spinacia oleracea at 1.7 A resolution. *Acta Crystallographica. Section D, Biological Crystallography*, 54(Pt 6 Pt 2):1353–1358, November 1998. ISSN 0907-4449.

[125] Holger Webert, Sven-Andreas Freibert, Angelo Gallo, Torsten Heidenreich, Uwe Linne, Stefan Amlacher, Ed Hurt, Ulrich Mühlenhoff, Lucia Banci, and Roland Lill. Functional reconstitution of mitochondrial Fe/S cluster synthesis on Isu1 reveals the involvement of ferredoxin. *Nature Communications*, 5:5013, October 2014. ISSN 2041-1723. doi: 10.1038/ncomms6013.

[126] K. Yamaguchi, Y. Takahara, T. Fueno, and K. N. Houk. Extended Hartree-Fock (EHF) theory of chemical reactions. *Theoretica chimica acta*, 73(5):337–364, 1988.

ISSN 1432-2234. doi: 10.1007/BF00527740. URL http://dx.doi.org/10.1007/BF00527740.

[127] K. Yamaguchi, F. Jensen, A. Dorigo, and K. N. Houk. A spin correction procedure for unrestricted Hartree-Fock and Møller-Plesset wavefunctions for singlet diradicals and polyradicals. *Chemical Physics Letters*, 149:537–542, September 1988. ISSN 0009-2614. doi: 10.1016/0009-2614(88)80378-6. URL http://adsabs.harvard.edu/abs/1988CPL...149..537Y.

[128] K. Yamaguchi, M. Okumura, W. Mori, J. Maki, K. Takada, T. Noro, and K. Tanaka. Comparison between spin restricted and unrestricted post-Hartree —Fock calculations of effective exchange integrals in Ising and Heisenberg models. *Chemical Physics Letters*, 210(1):201–210, July 1993. ISSN 0009-2614. doi: 10.1016/0009-2614(93)89124-Z. URL http://www.sciencedirect.com/science/article/pii/000926149389124Z.

[129] Howard Reiss and Adam Heller. The absolute potential of the standard hydrogen electrode: a new estimate. *The Journal of Physical Chemistry*, 89(20):4207–4213, September 1985. ISSN 0022-3654. doi: 10.1021/j100266a013. URL http://dx.doi.org/10.1021/j100266a013.

[130] Casey P. Kelly, Christopher J. Cramer, and Donald G. Truhlar. Aqueous Solvation Free Energies of Ions and Ion − Water Clusters Based on an Accurate Value for the Absolute Aqueous Solvation Free Energy of the Proton. *The Journal of Physical Chemistry B*, 110(32):16066–16081, August 2006. ISSN 1520-6106. doi: 10.1021/jp063552y. URL http://dx.doi.org/10.1021/jp063552y.

[131] Dhammike P. Dissanayake and Rajendram Senthilnithy. Thermodynamic cycle for the calculation of ab initio pKa values for hydroxamic acids. *Journal of Molecular Structure: THEOCHEM*, 910(1):93–98, September 2009. ISSN 0166-1280. doi: 10.1016/j.theochem.2009.06.021. URL http://www.sciencedirect.com/science/article/pii/S0166128009004047.

[132] Bishnu Thapa and H. Bernhard Schlegel. Density Functional Theory Calculation of pKa' s of Thiols in Aqueous Solution Using Explicit Water Molecules and the Polarizable Continuum Model. *The Journal of Physical Chemistry A*, 120(28):5726–5735, July 2016. ISSN 1089-5639. doi: 10.1021/acs.jpca.6b05040. URL http://dx.doi.org/10.1021/acs.jpca.6b05040.

[133] Mitsuo Shoji, Yasunori Yoshioka, and Kizashi Yamaguchi. An efficient initial guess formation of broken-symmetry solutions by using localized natural orbitals. *Chemical Physics Letters*, 608:50–54, July 2014. ISSN 0009-2614. doi: 10.1016/

j.cplett.2014.05.063. URL http://www.sciencedirect.com/science/article/pii/S0009261414004382.

[134] R. H. Sands and W. R. Dunham. Spectroscopic studies on two-iron ferredoxins. *Quarterly Reviews of Biophysics*, 7(4):443–504, November 1974. ISSN 0033-5835.

[135] Ruifang Li, Roberto Peverati, Miho Isegawa, and Donald G. Truhlar. Assessment and Validation of Density Functional Approximations for Iron Carbide and Iron Carbide Cation. *The Journal of Physical Chemistry A*, 117(1):169–173, January 2013. ISSN 1089-5639. doi: 10.1021/jp3079106. URL https://doi.org/10.1021/jp3079106.

[136] Mark James Abraham, Teemu Murtola, Roland Schulz, Szilárd Pall, Jeremy C. Smith, Berk Hess, and Erik Lindahl. GROMACS: High performance molecular simulations through multi-level parallelism from laptops to supercomputers. *SoftwareX*, 1−2:19–25, September 2015. ISSN 2352-7110. doi: 10.1016/j.softx.2015.06.001.